

University of Windsor

## Scholarship at UWindor

---

Electronic Theses and Dissertations

Theses, Dissertations, and Major Papers

---

2003

### A biomechanical model of the spine to predict trunk muscle forces: Optimizing the relationship between spinal stability and spinal loading.

Stephen Hadley Morgan Brown  
*University of Windsor*

Follow this and additional works at: <https://scholar.uwindsor.ca/etd>

---

#### Recommended Citation

Brown, Stephen Hadley Morgan, "A biomechanical model of the spine to predict trunk muscle forces: Optimizing the relationship between spinal stability and spinal loading." (2003). *Electronic Theses and Dissertations*. 519.

<https://scholar.uwindsor.ca/etd/519>

This online database contains the full-text of PhD dissertations and Masters' theses of University of Windsor students from 1954 forward. These documents are made available for personal study and research purposes only, in accordance with the Canadian Copyright Act and the Creative Commons license—CC BY-NC-ND (Attribution, Non-Commercial, No Derivative Works). Under this license, works must always be attributed to the copyright holder (original author), cannot be used for any commercial purposes, and may not be altered. Any other use would require the permission of the copyright holder. Students may inquire about withdrawing their dissertation and/or thesis from this database. For additional inquiries, please contact the repository administrator via email ([scholarship@uwindsor.ca](mailto:scholarship@uwindsor.ca)) or by telephone at 519-253-3000ext. 3208.

**A BIOMECHANICAL MODEL OF THE SPINE TO PREDICT TRUNK  
MUSCLE FORCES: OPTIMIZING THE RELATIONSHIP BETWEEN  
SPINAL STABILITY AND SPINAL LOADING**

**by**

**Stephen H. M. Brown**

**A Thesis**

**Submitted to the Faculty of Graduate Studies and Research  
through Human Kinetics  
in Partial Fulfillment of the Requirements for the  
Degree of Masters of Human Kinetics at the  
University of Windsor**

**Windsor, Ontario, Canada**

**2003**

**© 2003 Stephen H. M. Brown**

National Library  
of Canada

Bibliothèque nationale  
du Canada

Acquisitions and  
Bibliographic Services

Acquisitions et  
services bibliographiques

395 Wellington Street  
Ottawa ON K1A 0N4  
Canada

395, rue Wellington  
Ottawa ON K1A 0N4  
Canada

*Your file* *Votre référence*

*ISBN: 0-612-82859-X*

*Our file* *Notre référence*

*ISBN: 0-612-82859-X*

The author has granted a non-exclusive licence allowing the National Library of Canada to reproduce, loan, distribute or sell copies of this thesis in microform, paper or electronic formats.

L'auteur a accordé une licence non exclusive permettant à la Bibliothèque nationale du Canada de reproduire, prêter, distribuer ou vendre des copies de cette thèse sous la forme de microfiche/film, de reproduction sur papier ou sur format électronique.

The author retains ownership of the copyright in this thesis. Neither the thesis nor substantial extracts from it may be printed or otherwise reproduced without the author's permission.

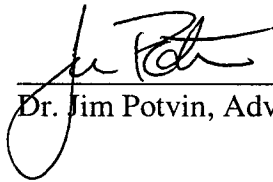
L'auteur conserve la propriété du droit d'auteur qui protège cette thèse. Ni la thèse ni des extraits substantiels de celle-ci ne doivent être imprimés ou autrement reproduits sans son autorisation.

# Canada

983501

A Biomechanical Model of the Spine to Predict  
Trunk Muscle Forces: Optimizing the Relationship  
Between Spinal Stability and Spinal Loading

APPROVED BY:



---

Dr. Jim Potvin, Advisor



---

Dr. Dave Andrews, Kinesiology



---

Dr. Bill Altenhof, Mechanical, Automotive & Materials  
Engineering

## ABSTRACT

### A BIOMECHANICAL MODEL OF THE SPINE TO PREDICT TRUNK MUSCLE FORCES: OPTIMIZING THE RELATIONSHIP BETWEEN SPINAL STABILITY AND SPINAL LOADING

Stephen H. M. Brown  
University of Windsor, 2003

The purpose of this study was to develop an optimization model of the spine that, incorporating a measure of spinal stability as a constraint, allowed for realistic predictions of trunk muscle and spine compression forces. A 3-dimensional, 52 muscle, single joint model of the lumbar spine was developed and tested in situations of pure trunk flexor and lateral bend moments. Spinal stability, about each anatomical axis, was calculated at the L4/L5 spinal joint. Estimates of the optimal level of spinal stability, in a given loading situation, obtained through the use of regression equations developed from experimental findings, were utilized as constraints in the optimization model. Two separate optimization cost functions were tested: 1) minimization of the sum of the cubed trunk muscle forces; 2) minimization of the intervertebral force at the L4/L5 joint level. The addition of spinal stability measures, about each anatomical axis, as constraints in the optimization model, caused significantly improved estimates of the compressive forces acting on the spine, as well as improved prediction of trunk muscle forces as a whole. Furthermore, the addition of stability constraints allowed the model to predict activity in muscles functioning as pure antagonists to the applied external moment, a first for optimization models of the spine. Thus, it is concluded that spinal stability plays a vital role in dictating the recruitment patterns of trunk muscles.

## ACKNOWLEDGEMENTS

First, I would like to thank my advisor, Dr. Jim Potvin. I truly appreciate all of your time and effort, and I would like to say that, without a doubt, if it were not for your encouragement years ago, I would not be doing anything near what I'm doing today, and since I love what I'm doing, I am very grateful (how's that for a convoluted sentence!).

Next, to my committee members, Dr. Bill Altenhof and Dr. Dave Andrews, thank-you for all of your help, and especially for the enthusiasm you've shown me throughout the course of this thesis.

I would also like to thank all of the friends that I've made during the last three (three??) years, especially Monica, Mike, Diane and Jon. You guys have made this a fantastic experience, and I look forward to many more fantastic years ahead.

To all of my other friends, thanks for not thinking it too weird that I'm still in school after all these years (with no end in sight?); and thanks especially for allowing me to have a life outside of school (and a pretty fun one at that!).

Finally, to my family, Mom, Dad and Eric; there's only one word that encompasses all for which I would like to say thanks...**EVERYTHING!**

“all of us in the car knew a poem when we saw one,  
and were grateful”

Raise High the Roof Beam, Carpenters  
J. D. Salinger

## TABLE OF CONTENTS

<b>ABSTRACT</b>	iii
<b>ACKNOWLEDGEMENTS</b>	iv
<b>LIST OF TABLES</b>	ix
<b>LIST OF FIGURES</b>	x
<b>LIST OF ABBREVIATIONS</b>	xiii
<b>CHAPTER 1: INTRODUCTION</b>	1
1.1 Purpose	4
1.2 Hypotheses	4
<b>CHAPTER 2: REVIEW OF LITERATURE</b>	7
2.1 Anatomy of the Trunk	7
2.1.1 Passive Tissues	7
2.1.2 Muscles of the Trunk	8
2.1.2.1 Abdominal Musculature	9
2.1.2.1.1 Rectus Abdominus	9
2.1.2.1.2 External Oblique	9
2.1.2.1.3 Internal Oblique	9
2.1.2.2 Posterior Musculature	9
2.1.2.2.1 Lumbar Erector Spinae	9
2.1.2.2.2 Thoracic Erector Spinae	10
2.1.2.2.3 Multifidus	10
2.1.2.2.4 Latissimus Dorsi	10
2.1.2.2.5 Quadratus Lumborum	11
2.2 Trunk Muscle Recruitment Patterns	11
2.2.1 Flexion-extension	11
2.2.2 Lateral Bend	12
2.2.3 Axial Twist	12
2.3 EMG-Force Relationship	13
2.4 Biomechanical Modeling of the Spine	14
2.4.1 EMG-assisted Models	15
2.4.2 Optimization Models	16
2.4.3 EMG-assisted with Optimization Models	19
2.5 Spinal Stability	20
2.5.1 Role of Muscles in Spinal Stability	22
2.5.2 Co-activation of Trunk Musculature	23
2.5.3 Stability in the Modeling of the Spine	26
2.5.4 Measuring Spinal Stability	27



<b>CHAPTER 3: METHODOLOGY</b>	29
3.1 Model Development	29
3.1.1 Anatomical Representation	29
3.1.2 Optimization Technique	34
3.1.3 Calculation of Spinal Stability	36
3.2 Experimental Validation of the Model	43
3.2.1 Subjects	43
3.2.2 Experimental Conditions	43
3.2.2.1 Anterior (Flexion) Moment Condition	44
3.2.2.2 Lateral Bend Moment Condition	46
3.2.2.3 Isometric Ramped Force Exertions	46
3.2.3 Data Acquisition	49
3.2.4 Gain Adjustment for EMG to Force Conversion	51
3.2.4.1 Flexion Trials	52
3.2.4.2 Lateral Bend Trials	53
3.2.5 Force Data	53
3.2.6 Calculation of Experimental Moments	54
3.2.7 Data Analysis	54
3.2.7.1 Examination of Stability Values	54
3.2.7.2 Statistics	54
<b>CHAPTER 4: RESULTS</b>	57
4.1 Experimental Stability Values	57
4.2 Optimization Model Performance	61
4.2.1 Definition of Cost Functions Used in Optimization	62
4.2.2 Flexion Moment Model	62
4.2.2.1 Stability Levels	69
4.2.3 Lateral Bend Moment Model	71
4.2.3.1 Stability Levels	79
<b>CHAPTER 5: DISCUSSION</b>	81
5.1 Hypotheses Revisited	81
5.2 Model Performance	84
5.2.1 Flexion Moment Trials	86
5.2.1.1 Antagonist Muscles	87
5.2.1.1.1 Rectus Abdominus	88
5.2.1.1.2 External Oblique	89
5.2.1.1.3 Internal Oblique	89
5.2.1.2 Agonist Muscles	91
5.2.1.2.1 Lumbar Erector Spinae	91
5.2.1.2.2 Thoracic Erector Spinae	92
5.2.1.2.3 Multifidus	94
5.2.1.2.4 Latissimus Dorsi	95
5.2.1.2.5 Quadratus Lumborum	95
5.2.2 Lateral Bend Moment Trials	96
5.2.2.1 Antagonist Muscles	98

5.2.2.2 Agonist Muscles	99
5.2.2.3 Rectus Abdominus	99
5.2.2.4 External Oblique	101
5.2.2.5 Internal Oblique	101
5.2.2.6 Lumbar Erector Spinae	102
5.2.2.7 Thoracic Erector Spinae	104
5.2.2.8 Multifidus	105
5.2.2.9 Latissimus Dorsi	106
5.2.2.10 Quadratus Lumborum	106
5.2.3 Examination of the Robustness of the Model	108
5.2.3.1 Static versus Ramped	108
5.2.3.2 Two Load Heights	110
5.3 Insights into Stability Modeling	112
5.4 Insights into Spinal Stability	114
5.5 Limitations	118
5.5.1 Lateral Bend Experimental Data	118
5.5.2 Use of Regression Equations	119
5.5.3 Stability Measures	120
5.6 Conclusions	122
5.7 Recommendations for Future Research	123
<b>REFERENCES</b>	126
<b>APPENDIX A</b>	133
<b>APPENDIX B</b>	134
<b>APPENDIX C</b>	139
<b>VITA AUCTORIS</b>	142

## LIST OF TABLES

Table 1. Summary of static flexion moment trials.	45
Table 2. Summary of static lateral bend moment trials.	46
Table 3. Summary of ramped flexion and lateral bend moment trials.	47
Table 4. Average muscle activation levels (% MVC) for static and ramped Flexion Moment trials, in which external moments were identical.	61
Table 5. Average muscle activation levels (% MVC) for static and ramped Lateral Bend Moment trials, in which external moments were identical.	61
Table 6. Anatomical muscle coordinates	135
Table 7. Additional nodal points for the TES muscle fascicles	136
Table 8. Normalized moment and stabilizing potentials for each individual muscle	136
Table 9. Absolute moment and stabilizing potentials, and ratios of moment to stabilizing potentials for each individual muscle	137
Table 10. Individual muscle fascicle 3-dimensional moment arm, 2-dimensional moment arm, full fascicle length, and length of the fascicle vector where it crosses L4/L5	138
Table 11. Standard errors (N) for individual muscle forces for the Flexion Moment conditions	140
Table 12. Standard errors (N) for the RMS errors between model predicted and experimentally determined muscle forces for the Flexion Moment conditions	140
Table 13. Standard errors for individual muscle forces for the Lateral Bend Moment Conditions	141
Table 14. Standard errors for the RMS errors between model predicted and experimentally determined muscle forces for the Lateral Bend Moment conditions	141

## LIST OF FIGURES

Figure 1. Functioning of the Spinal Stability System.	22
Figure 2. Hypothetical Model of Injury Risk to the Spine due to Spinal Instability.	24
Figure 3. Antero-posterior view of approximate modeled right side muscle fascicle locations.	30-31
Figure 4. Side view of approximate modeled right side muscle fascicle locations.	32-33
Figure 5. Example of a generic trunk muscle with nodal points.	34
Figure 6. Right side two-dimensional representation of the model, for flexion moments, with two muscles being shown.	37
Figure 7. Two-dimensional inverted pendulum model for one muscle.	38
Figure 8. Components of the energy stored within a muscle.	39
Figure 9. Front-side two-dimensional representation of the model, for lateral bend moments, with two muscles being shown.	42
Figure 10. View of the four main experimental conditions.	48
Figure 11. EMG and force data from a sample ramped contraction trial.	50
Figure 12. Schematic of the 2 X 2 Repeated Measures ANOVA model used for the statistical analysis.	56
Figure 13. Relationship between external flexion moment and stability about each of the three anatomical axes.	58-59
Figure 14. Relationship between external lateral bend moment and stability about each of the three anatomical axes.	59-60
Figure 15. RMS error between model predicted and experimental muscle forces (Flexion Moment) for each individual muscle.	62
Figure 16. RMS error between model predicted and experimental compressive forces, agonist muscle forces, antagonist muscle forces, and all muscle forces combined (Flexion Moment).	63

- Figure 17. Model predicted muscle forces, using the InterForce cost function, and experimentally found muscle forces (Flexion Moment), for each individual muscle. **64**
- Figure 18. Model predicted muscle forces, using the SumCubed cost function, and experimentally found muscle forces (Flexion Moment), for each individual muscle. **65**
- Figure 19. Model predicted and experimentally found compressive forces (Flexion Moment). **65**
- Figure 20. RMS percent error between model predicted and experimentally found compressive forces (Flexion Moment), collapsed across static and ramped conditions. **67**
- Figure 21. RMS percent error between model predicted and experimentally found compressive forces (Flexion Moment), for the static condition alone. **67**
- Figure 22. Average experimental and model predicted (with stability) compression Levels (Flexion Moment), comparing the two experimental load heights: L4/L5 height and chest height. **68**
- Figure 23. Average stability values (Flexion Moment) calculated about each axis, collapsed across static and ramped conditions. Stability values were calculated for experimental trials, predictions from regression equations, and in each of the four optimization schemes. **69**
- Figure 24. Average experimental stability levels (Flexion Moment), about each axis, comparing between the two external load heights: L4/L5 height and chest height. **70**
- Figure 25. RMS error between model predicted and experimental muscle forces (Lateral Bend Moment) for each individual muscle. **71**
- Figure 26. RMS error between model predicted and experimental compressive forces, agonist muscle forces, antagonist muscle forces, and all muscle forces combined (Lateral Bend Moment). **72**
- Figure 27. Model predicted muscle forces, using the InterForce cost function, and experimentally found muscle forces (Lateral Bend Moment), for each individual muscle. **73**

- Figure 28. Model predicted muscle forces, using the SumCubed cost function, and experimentally found muscle forces (Lateral Bend Moment), for each individual muscle. **74**
- Figure 29. Model predicted and experimentally found compressive forces (Lateral Bend Moment). **75**
- Figure 30. RMS percent error between model predicted and experimentally found compressive forces (Lateral Bend Moment), collapsed across static and ramped conditions. **76**
- Figure 31. RMS percent error between model predicted and experimentally found compressive forces (Lateral Bend Moment), for the static condition alone. **77**
- Figure 32. Average experimental and model predicted (with stability) compression Levels (Lateral Bend Moment), comparing the two experimental load heights: L4/L5 height and chest height. **78**
- Figure 33. Average stability values (Lateral Bend Moment) calculated about each axis, collapsed across static and ramped conditions. Stability values were calculated for experimental trials, predictions from regression equations, and in each of the four optimization schemes. **79**
- Figure 34. Average experimental stability levels (Lateral Bend Moment), about each axis, comparing between the two external load heights: L4/L5 height and chest height. **80**

## LIST OF ABBREVIATIONS

CNS: central nervous system

EMG: electromyography

EO: external oblique

InterForce: optimization cost function to minimize the intervertebral force at the L4/L5 disc level

IO: internal oblique

LBP: low back pain

LD: latissimus dorsi

LES: lumbar erector spinae

L4/L5: joint between the 4<sup>th</sup> and 5<sup>th</sup> lumbar vertebrae

MULT: multifidus

MVC: maximum voluntary contraction

QL: quadratus lumborum

RA: rectus abdominus

RMS error: root-mean-square error

sEMG: surface electromyography

SumCubed: optimization cost function to minimize the sum of the cubed muscle forces

TES: thoracic erector spinae

## *Chapter 1*

### **INTRODUCTION**

Back injury and low back pain (LBP) have become major issues within industry and society in general. By 1981 it had been estimated that 70 million Americans had suffered back injuries and that the number would increase by 7 million annually (Caillet, 1981). Furthermore, it has been shown that 27% of all injuries in the U.S. private sector involve the back (Mital and Pennathur 1999). In fact, Leamon (1994) has stated that LBP is the most expensive injury with occupational origins. With the enormous amount of money being lost and pain being suffered due to this problem, it is essential that better understanding of the mechanisms of LBP and injury be attained.

Trunk muscle recruitment patterns have long been studied for various postures and under various loading conditions. Knowledge of how and why muscles are recruited in a particular manner, and also of the disc compressive and shear forces produced in such instances, provide insight into the development of LBP and injury. Biomechanical modeling of the spinal system can allow researchers to study these mechanisms in an attempt to gain further knowledge into the function and integration of the spine and its components.

In general, models of the spine attempt to predict forces being generated by muscles under various loading conditions. However, the majority of these models consist of a higher number of unknown muscles forces than there are equations of equilibrium.



To solve for this problem of static indeterminacy, two major types of models have been developed: 1) EMG-assisted and 2) optimization.

Electromyography (EMG) analysis of a muscle can be utilized to indicate the force being produced by said muscle (DeLuca, 1995). Thus, EMG-assisted models monitor EMG recordings of trunk muscles in order to estimate the force being generated by each muscle.

A major drawback to EMG-assisted models is that they do not allow for the balancing of moment equations about all three axes simultaneously. Optimization models balance these moment equations by predicting appropriate muscles forces that, at the same time, optimize some objective function. A variety of objective functions have been incorporated into optimization models of the spine, such as minimizing the sum of the cubed muscle forces (Crowninshield & Brand, 1981), minimizing the compressive forces on the spine (Schultz, Andersson, Haderspeck, Ortengren, Nordin, & Bjork, 1982), and minimizing the sum of the squared intervertebral forces (Stokes & Gardner-Morse, 2001). However, to this day, none of these methods of optimization accurately predict trunk muscle co-activity, which, in experimental research, has repeatedly been shown to exist (Pope, Andersson, Browman, Svensson, & Zetterberg, 1986; McGill, 1991; McGill, 1992; Lavender, Trafimow, Andersson, Mayer, & Chen, 1994; Granata & Marras, 1995; Thelen, Schultz, & Ashton-Miller, 1995; Cholewicki, Panjabi, & Khachatryan, 1997; Gardner-Morse & Stokes, 1998).

To gain a full understanding into the workings of the spinal system, co-activation of trunk muscles must be accurately represented. Recently, spinal stability has been examined as a benefit of muscular co-activation, and has been defined as the ability of the

spine to limit patterns of displacement to prevent damage or irritation of spinal structures and the spinal cord (White & Panjabi, 1990). As muscle activity increases, so to does the compressive force acting on the spine. While high compressive forces have been identified as a risk factor for the development of LBP (Chaffin & Andersson, 1984), they have also been shown to increase the level of spinal stability (Cholewicki & McGill, 1996). Moreover, Panjabi (1992) has identified spinal instability as another risk factor for the development of LBP. Thus, a hypothetical relationship may be drawn where injury can result from excessive loads on the spine causing damage to tissues, as well as from loads that are too low and thus insufficient to stabilize the spine.

The spine has been shown to be in a stable state when the second derivative of the potential energy of the spinal system is greater than zero (Hunt & Thompson, 1973). Employing this measure of stability as an objective function in an optimization model of the spine may allow the true nature of the co-activity in the muscle recruitment patterns to be represented. To this date, only one attempt has been made to include a measure of stability in an optimization model of the spine. Stokes and Gardner-Morse (2001) maximized spinal stability levels and showed poor representation of actual experimental muscle forces. However, as indicated by the previously mentioned hypothetical relationship between stability and compressive forces, an optimum level of stability probably exists in conjunction with moderate levels of compression on the spine. A model that successfully predicts muscle forces and recruitment patterns through the optimization of spinal stability has the potential to provide further understanding into how and why muscles are recruited in a particular fashion.

To summarize, EMG-assisted models are, to this point, the only models of the spine that accurately represent realistic muscle co-activation patterns. However, these models do not allow for equilibrium conditions to be satisfied, and can be time consuming and overly complex to utilize in industry. Optimization models have the advantage of solving equilibrium constraints quickly and relatively simply, but to this point do so at the expense of poor representation of muscle co-activation patterns. Spinal stability has been shown to increase with muscle activation and be important in the prevention of injury. It is therefore reasonable to hypothesize that stability may play a role in dictating muscle recruitment patterns in the trunk. Thus, a spine model that incorporates this idea of an optimal relationship existing between compression and stability may provide further insight into the nature of muscle recruitment, as well as accurately representing and predicting muscular actions of the trunk.

### **1.1 Purpose**

The purpose of this study was to develop and validate an optimization model of the spine that incorporates, as a primary constraint, a measure of optimum stability, with one of two cost functions: 1) minimize the sum of the cubed trunk muscle forces; 2) minimize the sum of the squared intervertebral forces at the L4/L5 joint level. This model will allow for a more accurate prediction of the recruitment of trunk musculature and, hence, spinal loading during various tasks.

## 1.2 Hypotheses

1. An optimal level of spinal stability exists somewhere between the maximum and minimum levels possible for a given loading situation. It is predicted that this optimum level of stability will occur at a stability level that is marginally above the minimum possible level. A minimum level of stability is simply that level at which the spine will not buckle in its current state, but does not allow for a “margin of safety” which will prevent damage from occurring in higher loading situations. Maximum stability would require excessively high levels of compression on the spine, as well as limit mobility, and would thus put the spine in a high degree of risk for injury. In the current model, the stability constraint will be set at an “optimal level” as determined through analyses of experimental data.
2. The optimal level of spinal stability will show a positive non-linear relationship with the moment demand of the task. As tasks become more difficult, the spinal system will adopt a more stable state to decrease the likelihood of the spine buckling. A high positive correlation will thus be found between the level of optimal stability and the moment demand of the task.
3. An optimization model of the spine, with a constraint being a measure of optimal spinal stability, will accurately predict and reproduce muscle recruitment patterns in the trunk. More specifically, the model will predict opposing muscle groups to be active simultaneously during the tasks examined. Co-activation of the trunk musculature is necessary to stabilize

the spine. Hence, optimizing a measure of spinal stability will require co-activity to be present in the model. Root-mean-square (RMS) errors and correlations will be calculated between predicted forces from the model and actual forces obtained through experimentation.

## *Chapter 2*

### **REVIEW OF LITERATURE**

To begin to understand the complex nature of the human trunk, it is probably best to first undertake a brief look at its anatomical structure.

#### **2.1 *Anatomy of the Trunk***

##### **2.1.1 *Passive Tissues***

The information in this section has been adapted from Tortora (1995). The human spine is made up of 26 vertebrae which are distributed as follows: 7 cervical vertebrae (neck region); 12 thoracic vertebrae (upper back); 5 lumbar vertebrae (lower back); 5 sacral vertebrae fused into one bone called the sacrum; 4 coccygeal vertebrae fused into two bones called the coccyx. Although vertebrae located in separate regions do differ from one another, the similarities are numerous enough that one typical vertebra can be described.

The body, or centrum, is the thick anterior portion of a vertebra. The superior and inferior surfaces attach to intervertebral discs. The anterior and lateral surfaces contain nutrient foramina for blood vessels. The vertebral (neural) arch is the posterior extension of the body. The spinal cord runs through the vertebral foramen, which is formed between the body and vertebral arch. The vertebral arch actually consists of structures called pedicles and laminae. The pedicles are two short, thick processes that project posteriorly from the body and unite with the laminae. The laminae join to form the posterior portion of the arch. The vertebral arch also gives rise to seven processes: two

transverse and one spinous process which serve as points of attachment to muscles; and two superior and two inferior articular processes which serve to form joints with immediately adjacent vertebrae. The articulating surfaces of the articular processes are referred to as facets.

An intervertebral disc lies between each vertebra from C1 to the sacrum. The discs are composed of an outer ring made up of fibrocartilage called the annulus fibrosus, and a soft, elastic inner structure called the nucleus pulposus. The discs function as joints between adjacent vertebrae and shock absorbers to vertically applied forces.

Joints between adjacent vertebrae are termed cartilaginous due to the fact that they are tightly connected by cartilage. More specifically, each joint is known as a symphysis. The joint capsule surrounds the joint and is made up of dense irregular connective tissue. The tensile strength of the capsule prevents joint dislocation and the flexibility of the capsule allows for movement.

Ligaments are tightly bunched fibres running parallel to one another and which are highly resistant to strain. They span the joint capsule and attach to adjacent vertebrae. Spinal ligaments have been shown to contribute very little in the way of moment restoration in static postures (Anderson, Chaffin, Herrin and Matthews, 1985) and in lifting (McGill and Norman, 1986). Potvin, McGill and Norman (1991) demonstrated that ligament moment contribution increases with higher degrees of trunk flexion, but never to levels greater than 16% of the total moment. However, ligaments, combined with the other passive tissues of the trunk, have been proposed to play a crucial role in stabilizing the spine during tasks requiring low muscular activation (Cholewicki and McGill, 1996).

## **2.1.2 *Muscles of the Trunk***

Muscular activation produces movement at the joints and is the primary means of stabilizing the spine. It is thus necessary to examine the muscles that will be examined in this thesis. Information in the following section has been integrated from Tortora (1995) and Stone & Stone (1990).

### **2.1.2.1 *Abdominal Musculature***

#### **2.1.2.1.1 Rectus Abdominus**

The rectus abdominus (RA) originates from the pubic crest and pubic symphysis. It inserts on the cartilage of the 5<sup>th</sup>, 6<sup>th</sup>, and 7<sup>th</sup> ribs as well as on the xiphoid process. Actions of the RA include flexing the vertebral column and compressing the abdomen. Fibres of the RA run parallel to the midline of the trunk. The RA is the most superficial of the anterior abdominal muscles.

#### **2.1.2.1.2 External Oblique**

The external oblique (EO) originates from the inferior eight ribs and inserts on the iliac crest and linea alba. Contraction of both EOs at the same time compresses the abdomen, while contraction of one side will laterally flex and rotate the vertebral column ipsilaterally. Fibres of the EO run anteriorly and inferiorly across the anterolateral abdominal wall.

#### **2.1.2.1.3 Internal Oblique**

The internal oblique (IO) originates from the iliac crest, inguinal ligament, and thoracolumbar fascia. It inserts on the cartilage of the last three or four ribs, and the linea alba. The IO is responsible for compressing the abdomen, laterally bending and rotating the vertebral column. Rotation due to IO occurs to the side contralateral to the muscle.



### **2.1.2.2 *Posterior Musculature***

#### **2.1.2.2.1 Lumbar Erector Spinae**

The lumbar erector spinae (LES) consists of the iliocostalis lumborum and the longissimus thoracis. The iliocostalis lumborum originates from the iliac crest and inserts on the inferior six ribs. The iliocostalis lumborum acts to extend and laterally flex the lumbar portion of the vertebral column. The longissimus thoracis originates from the transverse processes of lumbar vertebrae and inserts on the transverse processes of all thoracic and upper lumbar vertebrae as well as the ninth and tenth ribs. Actions of the longissimus thoracis include extending and laterally flexing the vertebral column.

#### **2.1.2.2.2 Thoracic Erector Spinae**

The thoracic erector spinae (TES) consists of the iliocostalis thoracis, longissimus thoracis, and the spinalis thoracis. The iliocostalis thoracis originates from the inferior six ribs and inserts on the superior six ribs. The iliocostalis thoracis acts to extend and laterally flex the vertebral column as well as to maintain the erect position of the spine. The longissimus thoracis has previously been described above as part of the LES. The spinalis thoracis originates from the spinous processes of upper lumbar and lower thoracic vertebrae and inserts on the spinous processes of the upper thoracic vertebrae. Actions of the spinalis thoracis include extending the vertebral column.

### **2.1.2.2.3 Multifidus**

The multifidus muscles originate from the sacrum, ilium, and the transverse processes of the lumbar, thoracic, and lower four cervical vertebrae. They insert on the spinous processes of two to four vertebrae superior to the origin. The multifidus acts to extend the vertebral column and rotate it to the opposite side.

### **2.1.2.2.4 Latissimus Dorsi**

The latissimus dorsi (LD) originates from the iliac crest, and the spines of the sacrum, lumbar, and six lower thoracic vertebrae. It inserts on the intertubercular sulcus of the humerus. The LD is responsible for extending, adducting, and rotating the arm medially, as well as drawing the arm inferiorly and posteriorly. It may also play a role in rotating the vertebral column (McGill, 1991).

### **2.1.2.2.5 Quadratus Lumborum**

The quadratus lumborum originates from the iliac crest and transverse processes of the lower three lumbar vertebrae. It inserts on the twelfth rib and the transverse processes of the first four lumbar vertebrae. Actions of the quadratus lumborum include extending and laterally bending the vertebral column.

## **2.2 *Trunk Muscle Recruitment Patterns***

Numerous studies have examined patterns of muscular recruitment in the trunk. This review will focus on three major movement patterns: flexion-extension; lateral bend; and axial twist. However, it must be noted that none of the muscles to be discussed in this section produce movement about only one of these axes. The LES and TES contribute to movement in both extension and lateral bend of the trunk. The RA is involved in flexing and laterally bending the trunk. The EO and IO produce movement

of the trunk in flexion, lateral bend, and axial twist. Thus, when any of these muscles are activated, they inevitably cause moments about more than one axis. This in turn creates the need for opposing muscles to activate to counteract these new moments.

### *2.2.1 Flexion-extension*

When looking at muscle activation patterns in response to applied pure flexion moments, Lavender, Trafimow, Andersson, Mayer, & Chen (1994) found that highest levels of activation were exhibited in the erector spinae muscles (greater than 15% maximum voluntary contraction) or, in other words, muscles that directly oppose the applied moment. The LD, EO, and RA were all active at levels of less than 5% of maximum voluntary contraction (MVC).

Krajcarski, Potvin, & Chiang (1999) made similar findings that the LES was most active (20 – 25% MVC) when subjects were loaded with an external flexion moment, followed by the TES (15 – 20% MVC), and the IO (approximately 15% MVC). EO and RA both displayed activity levels of less than 5% MVC.

### *2.2.2 Lateral Bend*

Various studies have examined the activity of trunk muscles under isometric, lateral bend exertions. Both McGill (1992) and Lavender, Tsuang, Andersson, Hafezi, & Shin (1992) determined that, in general, agonist muscles with the longest lateral moment arms were most active in these situations. More specifically, McGill (1992) found that the ipsilateral EO was most active (25 – 55% MVC), followed by ipsilateral LES (10 – 30% MVC), ipsilateral IO (> 15% MVC), ipsilateral TES (5 – 25% MVC), and ipsilateral RA (5 – 15% MVC). Contralateral (antagonist) muscles also displayed levels of

activation (8% MVC or lower) that would effectively contribute to the compressive forces on the spine. The LD was shown to have slightly higher levels of activity on its contralateral side, which was hypothesized to be due to its acting to stabilize the load supporting shoulder.

### **2.2.3 Axial Twist**

Various studies have examined muscular contributions to isometric axial twist exertions. In torques to the left, the right EO and left IO have been shown to provide the dominant contributions (Pope et al., 1986; McGill, 1991), with McGill (1991) finding average activity levels peaking at 52% MVC in the EO and 55% MVC in the IO. McGill (1991) also showed the left LD to contribute significantly (74% MVC) to this axial torque effort. TES activity also demonstrated a strong link to axial torque (56% MVC left side activity versus 12% MVC right side activity). This muscle does not, however, have the potential to contribute to axial torque and has thus been hypothesized to activate in a balancing and stabilizing role (McGill, 1991). Other monitored trunk muscles, RA and LES, have not shown a strong link to axial torque (Pope et al., 1986; McGill, 1991), yet still exhibit peak activity levels of 21% MVC for the RA and 33% MVC for the LES (McGill, 1991). This activity may be responsible for counterbalancing flexion and lateral bend moments that are also produced by the active axial torque producing muscles (Schultz et al., 1983). High levels of antagonistic activity have also been demonstrated in these type of torque exertions (Pope, Svensson, Andersson, Broman, & Zetterberg 1987; McGill, 1991; Thelen et al., 1995). Specifically, McGill (1991) found peak average levels of antagonistic activity of 16% MVC in the IO, 28% MVC in the EO, and 23% MVC in the LD.

### 2.3 EMG-Force Relationship

The surface electromyogram (sEMG) records the sum of motor unit action potentials as a means of indicating the tension developed in a muscle and the degree to which a muscle is fatigued. Furthermore, sEMG analyses of a rested muscle provides a good indication of force generation by the muscle in question (DeLuca, 1995). Bigland-Ritchie (1981) indicates that, in general, the best relationship between EMG and force occurs under isometric conditions. This is due to the absence of a change in muscle length. Furthermore, Bigland-Ritchie (1981) states that EMG-force relationships differ in their degree of linearity depending on the physiological properties of the individual muscles involved. Muscles of mixed fibre composition (Type I and Type II) tend to result in non-linear relationships whereas muscles composed predominantly of Type I fibres tend to produce linear relationships.

Force of a particular muscle,  $j$ , can be derived from the surface EMG signal using the product of normalized EMG (EMG level at a particular point in time/ Maximum EMG level), muscle cross-sectional area, a gain factor which represents maximum muscle force per unit area, and modulation factors which describe EMG and force behaviour as a function of muscle length and muscle velocity (Marras & Sommerich, 1991a):

$$\text{Force}_j = \text{Gain} * \text{EMG}_j(t)/\text{EMGmax}_j * \text{Area}_j * v(\text{Vel}_j) * l(\text{length}_j).$$

### 2.4 Biomechanical Modeling of the Spine

Biomechanical modeling of the lumbar spine allows for further understanding of the function and integration of the various mechanisms of the spinal system. Knowledge of muscle recruitment patterns and activity levels, as well as disc compressive and shear forces provide insights into the development and progression of LBP and injury.

Early work on whole-body modeling by Chaffin (1969) focused on computing reactive forces and torques at major articulations of the extremities during various materials handling tasks. Furthermore, his model was significant in being one of the first to provide estimates of compressive and shear forces acting on the lower lumbar spine.

Static biomechanical models on the lumbar spine are far ranging in their complexity in terms of number of muscles incorporated in the model. The majority of models, however, consist of a higher number of unknown muscle forces than there are equations of equilibrium (three force equations and three moment equations). This presents a problem of static indeterminacy. Two general approaches exist to solve for this problem: 1) EMG-assisted modeling; 2) Optimization modeling.

#### **2.4.1** *EMG-assisted Models*

Morris, Lucas, Bresler (1961) was the first to employ surface EMG recording in the prediction of muscle stress in the trunk musculature. The use of individual subject EMG recordings also allowed for the individual differences that have been reported in muscular activation patterns (Cholewicki et al., 1997) to be accounted for. Furthermore, maximum muscle stress potential ( $40 \text{ N/cm}^2$ ) was incorporated in their model to allow for the prediction of muscle forces from EMG recordings.

Marras and Sommerich (1991) developed a model utilizing EMG recordings to describe muscle activity and its influence on spinal loading during trunk motion. Anthropometric data, trunk flexion angle, angular velocity, and trunk torque were also included as inputs into the model. Static moment and force equations were calculated throughout trunk motion to provide a dynamic estimate of spinal loading. This model

provided the advantage of allowing for both the collective influence of muscle activity, as well as peak activity, on spinal loading to be addressed.

Another major step in the development of EMG-assisted models of the spine was made by the work of McGill (1992). This model was the first to incorporate extensive anatomical detail of the musculo-ligamentous-skeletal system in the prediction of spinal loading. The model was composed of two parts: 1) a 3-dimensional linked-segment representation of the body linkage; 2) a 3-dimensional representation of the trunk tissues. Sources of input into the model included 3-D joint coordinates taken from video records, the load magnitude in the hands, and 12 channels of trunk muscle EMG recordings. Muscle and ligament lengths, as well as velocity of change, were calculated based on the orientation of the skeletal components of the model. This allowed for the moment about the L4-L5 disc to be calculated, which along with the EMG recordings, enabled the restorative moment allocated to each muscle to be estimated. Restorative moments produced by the ligaments were also calculated utilizing stress-strain relationships reported in the literature.

#### ***2.4.2 Optimization Models***

The main advantage of optimization modeling is that it allows for muscle forces to be estimated while at the same time allowing for the moment equations to be satisfied through a process in which some objective function is optimized. A number of different functions have been employed over the years in an attempt to predict muscle forces that best represent the actual muscle recruitment patterns of the trunk.

In general, some main criterion is selected to be minimized (or possibly maximized), while at the same time satisfying various other criteria. For example, Bean & Chaffin (1988) explain that an optimization model can be stated in the following form:

$$\begin{aligned} \text{minimize} \quad & \sum_{j=1}^n c_j x_j \quad (\text{the objective function}) \\ \text{subject to:} \quad & \\ & \sum_{j=1}^n a_{ij} x_j \geq b_i, \quad i = 1, 2, \dots, m \quad (\text{the constraints}) \\ & x_j \geq 0, \quad j = 1, 2, \dots, n \end{aligned}$$

where  $c_j$ ,  $b_i$  and  $a_{ij}$  are known parameters and  $x_j$  are the unknown variables.

Crowninshield and Brand (1981) hypothesized that muscular activation patterns of many normal physical activities, especially prolonged and repetitive activities, are selected to maximize activity endurance. In order to optimize this objective, they chose to minimize the sum of the cubed muscle forces involved in the task. In the study of gait, this non-linear optimization approach showed relatively good correlations between predicted temporal muscle patterns and experimental patterns obtained through the use of EMG. However, magnitude of the predicted forces and the EMG were not closely examined and were considered only intuitively reasonable.

Schultz et al. (1982) looked at the ability to predict trunk muscle recruitment patterns in situations involving upright standing with and without twist; lateral bend; and combinations of lateral bend and twist. They compared the results stemming from two



different objective functions: 1) minimizing the compressive forces on the L3 motion segment; 2) minimizing muscular intensity (stress) levels. The function of minimizing the muscular intensity levels was found to produce better agreement with actual experimental findings than did minimizing the compressive forces. However, neither method produced very high correlations between the six predicted muscle forces and the actual activity levels: 0.67 to 0.88 for minimizing muscular intensity; and 0.34 to 0.92 for minimizing compression. Particular problems were experienced in tasks involving extension, lateral bend, and twist. This was theorized to be because these tasks tend to recruit a larger number of trunk muscles, including the LD and obliques, muscles with more variable and less defined lines of action. This variability makes it more difficult to represent these muscles as single equivalent muscles.

Shultz et al. (1983) were the first to attempt to model the human spinal system by employing a double linear optimization method. To do this they minimized spinal compressive forces while at the same time minimizing maximum muscle contraction intensity. This model produced results that were in better agreement with experimental measurements than previous models. Bean et al. (1988) further modified the optimization methods of Shultz et al. (1983b) by solving the two separate linear problems sequentially. Their first linear program determined the lowest muscular intensity level that produced feasible equilibrium solutions. The second linear program then selected which of these solutions would minimize spinal compression. This method allowed for reduced computational requirements and more stable solutions than the previous method proposed by Schultz et al. (1983b).

In comparing the ability of the various optimization objective functions to predict actual EMG data collected in the lab, Hughes (2000) determined that significant differences do not exist between the double linear method of Bean et al. (1988) and the non-linear method of Crowninshield and Brand (1981) when analyzing tasks in which extension moments predominate.

While the methods of optimization modeling presented so far provide the advantage of solving for equilibrium in the moment equations, they do so without accurately accounting for the co-activation of musculature that has often been reported in the literature (Pope et al., 1986; McGill, 1991; McGill, 1992; Lavender et al., 1994; Granata and Marras, 1995; Thelen et al., 1995; Cholewicki et al., 1997; Gardner Morse and Stokes, 1998).

#### **2.4.3** *EMG-assisted with Optimization Modeling*

Despite the anatomical detail and complexity of the model developed by McGill (1992), it still did not allow for the balancing of moment equations simultaneously about all three axes. This problem was addressed through the work of Cholewicki and McGill (1996). The anatomical representation and calculation of external loads in their model expanded on that of McGill (1992) to include 90 muscle fascicles and 18 degrees of freedom (6 joints x 3 dof each). Similar methods to those of McGill (1992) were followed in the calculation of muscular forces in the trunk. However, once these forces were estimated based on the EMG recordings, they were adjusted with an optimization algorithm to satisfy the external moment requirements. The objective was set to balance the 3 moment equations while minimizing the adjustment to the muscle forces. Thus, this

model successfully combined the advantages of both EMG-assisted and optimization modeling techniques discussed earlier.

While the EMG-based models of McGill (1992) and Cholewicki and McGill (1996) are very successful in describing muscle activation patterns and their influence on spinal loading, they are far too complex to be used outside of the lab or in industry. Thus, alternate methods for modeling the spinal system need to be examined. Furthermore, continued examination of modeling methods will help expand the understanding of the manner in which muscles are recruited. Incorporating other objective functions into optimization techniques may provide more of a window onto how muscles work and the ultimate goal of muscle recruitment in control of the spinal system.

Muscular activation has been shown to play an important role in the stabilization of the spine (Bergmark, 1989; Crisco and Panjabi, 1991). It is thus reasonable to hypothesize that spinal stability may be crucial in determining the patterning of muscular activation. Hence, the spinal system may recruit muscles in an attempt to optimize the stability of the spine. As a result, including a measure of stability as a constraint in an optimization model of the spine may provide a more accurate representation, and hence understanding, of trunk muscle recruitment strategies.

## ***2.5 Spinal Stability***

To best understand the role of stability in the human spinal system, it is easiest to first look at the spine in purely mechanical terms. In a static mechanical system it is necessary for equations of equilibrium to always be fulfilled. Thus, the sum of all forces

acting on the system as a whole, or any one part of the system, must equal zero. This state of static equilibrium does not, however, imply that stability is present. From a mechanical point of view, Bergmark (1989) defines stability as “the ability of a loaded structure to maintain static equilibrium even at small fluctuations around the equilibrium position”. Crisco and Panjabi (1992) provide an illustrative example of a column that returns to its vertical position after it has been perturbed by some force. The load at which the column buckles is said to be its buckling, or critical, load. Thus, a mechanical system is inherently unstable to loads greater than the buckling load of the system. The spine, of course, is not a typical mechanical structure. The biological nature of the spinal system presents a more complex view of stability. In clinical terms, spinal stability has been described as the ability of the spine to limit patterns of displacement to prevent damage or irritation of spinal structures and the spinal cord (White and Panjabi, 1978). Thus, as pointed out by Bergmark (1989), the clinical stability of the spine is a continuously variable phenomenon; whereas the mechanical stability of an engineering structure does not vary in such a manner. Spinal instability has been identified as a major risk factor for LBP and injury, thus illuminating the importance of continuous stabilization of the spine (Panjabi, 1992).

Panjabi (1992) conceptualized the spinal stabilizing system as being composed of three interdependent subsystems: the passive musculoskeletal system, the active musculoskeletal system, and the neural and feedback system. Each subsystem plays an important role in maintaining a stable environment. The interactions between and amongst the components of the three subsystems are crucial in maintaining the proper functioning of the system as a whole. First, the passive subsystem is made up of the

vertebrae, facet articulations, intervertebral discs, spinal ligaments, joint capsules, and the passive mechanical properties of the muscles. Next, the active subsystem consists of the muscles and tendons of the trunk. Finally, the neural and feedback (neural control) subsystem includes the various force and motion transducers located in ligaments, tendons, muscles, and the neural control subsystems. Figure 1 shows how these subsystems interact to achieve spinal stability.

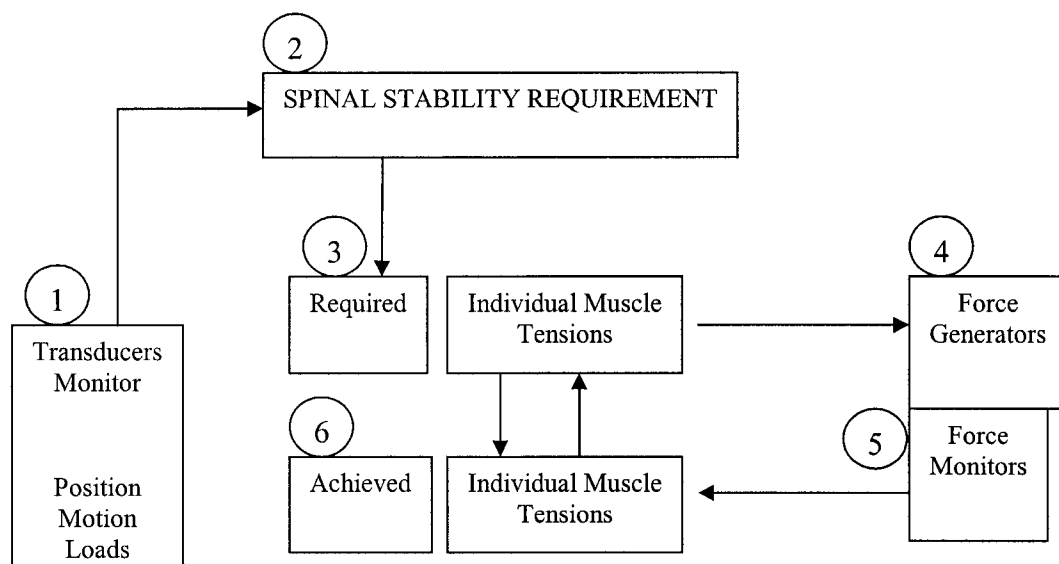


**Figure 1.** Functioning of the spinal stability system. (1) Passive subsystem provides information which determines (2) the requirements of spinal stability. (3) Neural control unit determines individual muscle tensions and sends this message to (4) the force generators (active subsystem). (5) Force monitors provide feedback by comparing the (6) achieved and (3) required muscle tensions. (Panjabi, 1992).

### 2.5.1 Role of Muscles in Spinal Stability

In vitro studies have shown the ligamentous lumbar spine to be unstable at compressive loads of only 90N (Crisco, Panjabi, Yamamoto, & Oxland, 1992). However, NIOSH has set an action limit (AL) for compression of 3400N (Waters, Putz-

Anderson, Garg, & Fine, 1993) and it has been estimated that compressive loads of up to 18,000N can be reached in competitive power lifting (Cholewicki, McGill, & Norman, 1991). Thus, the active forces within the trunk must be operating to stabilize the spine.

It is known that as muscles increase activation, they also increase their stiffness. Muscle stiffness has been defined as the ratio of the change in passive force to the change in length (Gajdosik, 2001). In fact, it has been demonstrated that muscle stiffness increases proportionately with muscle force, and it is this increased stiffness that aids in stabilizing the spine. The critical stiffness is the lowest possible stiffness of the muscle at which the spinal system is still stable (Bergmark, 1989). Bergmark (1989) further proposed that numerically, muscle stiffness could be described by the equation:

$$k = q * F/L$$

where k: the muscle stiffness (N/m)  
q: the muscle stiffness coefficient  
F: the muscle force (N)  
L: the muscle length (m).

The value of q was deemed to be approximately 40 and assumed to be approximately equal for all skeletal muscles. However, Crisco and Panjabi (1991), after performing calculations based on data collected from an extensive review of literature, found values for q ranging from 0.5 to 42 with an average of 10. Thus, they concluded that the current extent of knowledge of muscle mechanics is insufficient to establish a simple relationship for muscle stiffness such as the one presented by Bergmark (1989).

### **2.5.2 Co-activation of Trunk Musculature**

Increased muscular activation not only increases muscle stiffness but also causes a rise in compressive forces acting on the spine. High compressive forces on the L5-S1

disk have been implicated as a risk factor for the development of LBP (Chaffin & Andersson, 1984).

In the studies mentioned earlier concerning the muscle recruitment patterns of the trunk, antagonist muscle activation was evident in each. This is seemingly an inefficient and potentially harmful way of utilizing the muscles of the trunk. The action of antagonist muscles would create an additional moment that would have to be counteracted by further activating agonist muscles. The metabolic cost would, of course, now increase, as would the compression on the spine. However, Cholewicki and McGill (1996) demonstrated that increased moment demand and increased joint compression on the trunk lead to greater stability. This indicates that compressive forces on the spine play a role in both the development of injury as well as stability (see Figure 2).

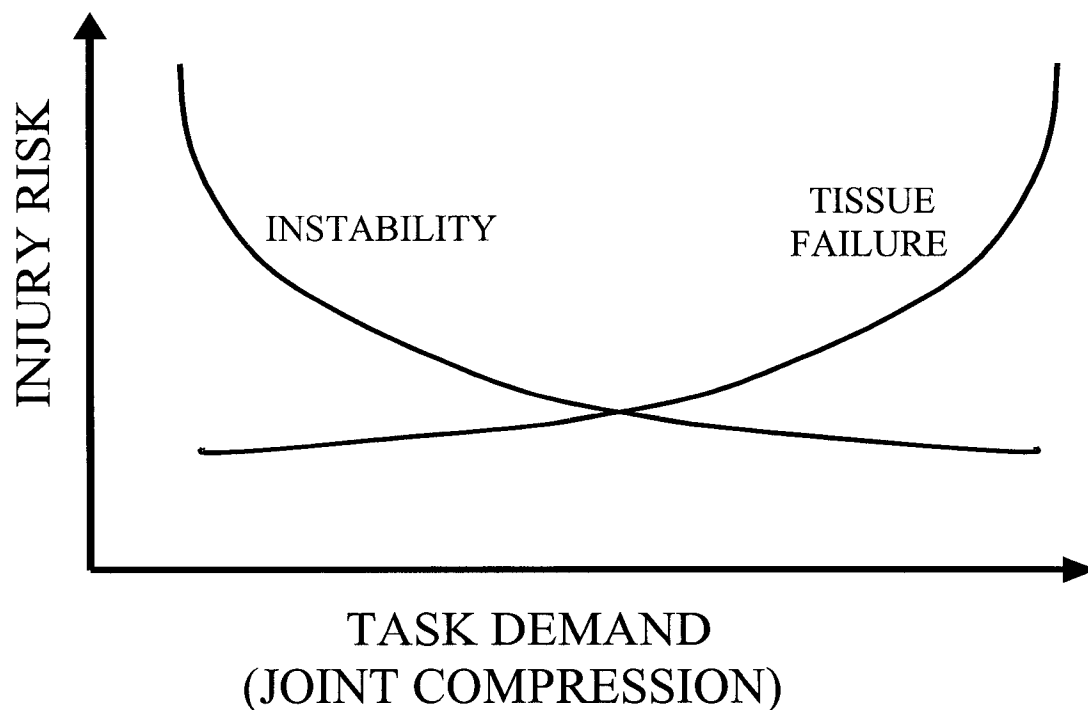


Figure 2. Hypothetical model for injury risk to the spine due to tissue failure and spine instability (Cholewicki and McGill, 1996).

This hypothetical relationship indicates that injury can occur due to high loads causing tissue disruption, or due to low loads resulting in instability. A non-biological parallel can be drawn to a column of soda cans arranged one on top of another. With insufficient compressive forces acting on the column, the column is unstable and will buckle easily; while with overly high compressive forces acting on the column, the individual cans in the column will deform and fail. In a biological sense, this trade-off indicates that it is likely that some ideal relationship exists between spinal stability and compressive forces that would reduce the likelihood of injury and LBP. A number of studies have examined the extent to which muscular co-activation acts in stabilizing the lumbar spine.

Granata and Marras (1995) monitored muscle activity levels in subjects performing lifts from a 45 degree trunk angle to an upright posture at varying speeds and with different loads. They determined that extensor muscles generated lifting moments as much as 47% greater than the moment due to the static load in the hands. At least part of this excess extensor moment was necessary to counterbalance the increased flexion moment produced by the active antagonistic flexor muscles. Furthermore, muscle coactivity increased as either lifting load and/or trunk extension velocity increased. In addition to this, Cholewicki et al. (1997) investigated the stabilizing role of co-activation around a neutral posture. They found that low levels of muscle co-activity existed during the execution of trunk flexion-extension tasks. Moreover, as lifting loads were incorporated, co-activity of antagonistic muscles increased. These studies lead to the conclusion that co-activation of trunk muscles serve to improve the stability of the spine.



This view was reinforced by the work of Gardner-Morse and Stokes (1998). Using a biomechanical model, they calculated spinal loads and stability for maximal and submaximal extension and lateral bending tasks. They too found that the antagonistic coactivation of abdominal muscles increased the stability of the lumbar spine. When modeled without the effect of coactivation, spinal stability decreased as bending effort increased. When coactivation of the internal and external obliques was considered, spinal stability increased. Furthermore, as bending effort increased so did the level of activation of both obliques. It was also found that the external obliques provided the greater overall gains in stability, while the internal obliques produced the larger gains in stability relative to the increase in muscle fatigue rate.

Recently, Cholewicki and Van Vliet IV (2002) concluded that all trunk muscles are involved in stabilizing the spine, and that no single muscle group contributes more than 30% to the overall stability of the lumbar spine. Furthermore, they determined that relative contributions of each muscle to spine stability are dependent on the direction and magnitude of trunk loading, as well as the different recruitment patterns of the other trunk muscles.

### *2.5.3 Stability in the Modeling of the Spine*

Clearly, muscular co-activation is a very real and important aspect of trunk muscle recruitment. Co-activation can be recruited as a means of balancing the risk of tissue overload and spinal instability, both of which can lead to injury (Granata and Marras, 2000). Furthermore, it was determined that muscle recruitment patterns could be better predicted when considering spinal stability than when satisfying equilibrium alone

(Granata and Wilson, 2001). Thus, it is essential that co-activation be incorporated into models of the human spine if a realistic representation of the workings of the muscles is to be presented.

One of the major drawbacks to optimization models that have been previously developed is that, due to the nature of their objective functions, they do not exhibit muscular co-activation. Employing a measure of spinal stability as a constraint in an optimization model can potentially allow for muscular co-activation to be represented.

Up to this point, Stokes and Gardner-Morse (2001) have made the only attempt to incorporate spinal stability as a cost function in an optimization model of the spine. In their model, they maximized spinal stability by maximizing the smallest eigenvalues of buckling modes of the trunk. It was found that maximizing spinal stability, in conjunction with various other objective functions, actually reduced the agreement between muscle activation in the model and that found experimentally. This finding is to be expected because maximum stability would require unreasonably high levels of muscular activation, which would in turn create tremendous levels of compressive forces on the spine. As mentioned earlier, it is more likely that muscles are recruited to optimize a trade-off between spinal compressive forces and spinal stability.

#### ***2.5.4 Measuring Spinal Stability***

Bergmark (1989) was the first to attempt to calculate the stability of the spine. He states that a system will be in stable equilibrium when the potential energy ( $V$ ) of that system is at a minimum.

Static equilibrium of the spinal system is satisfied by the first partial derivative of the  $V$  of the system, with respect to the coordinates of the lumbar vertebrae, being equal to zero. In order for this system to be considered stable, the second partial derivative of this system must be greater than zero (positive definite) (Hunt & Thompson, 1973).

## Chapter 3

# METHODOLOGY

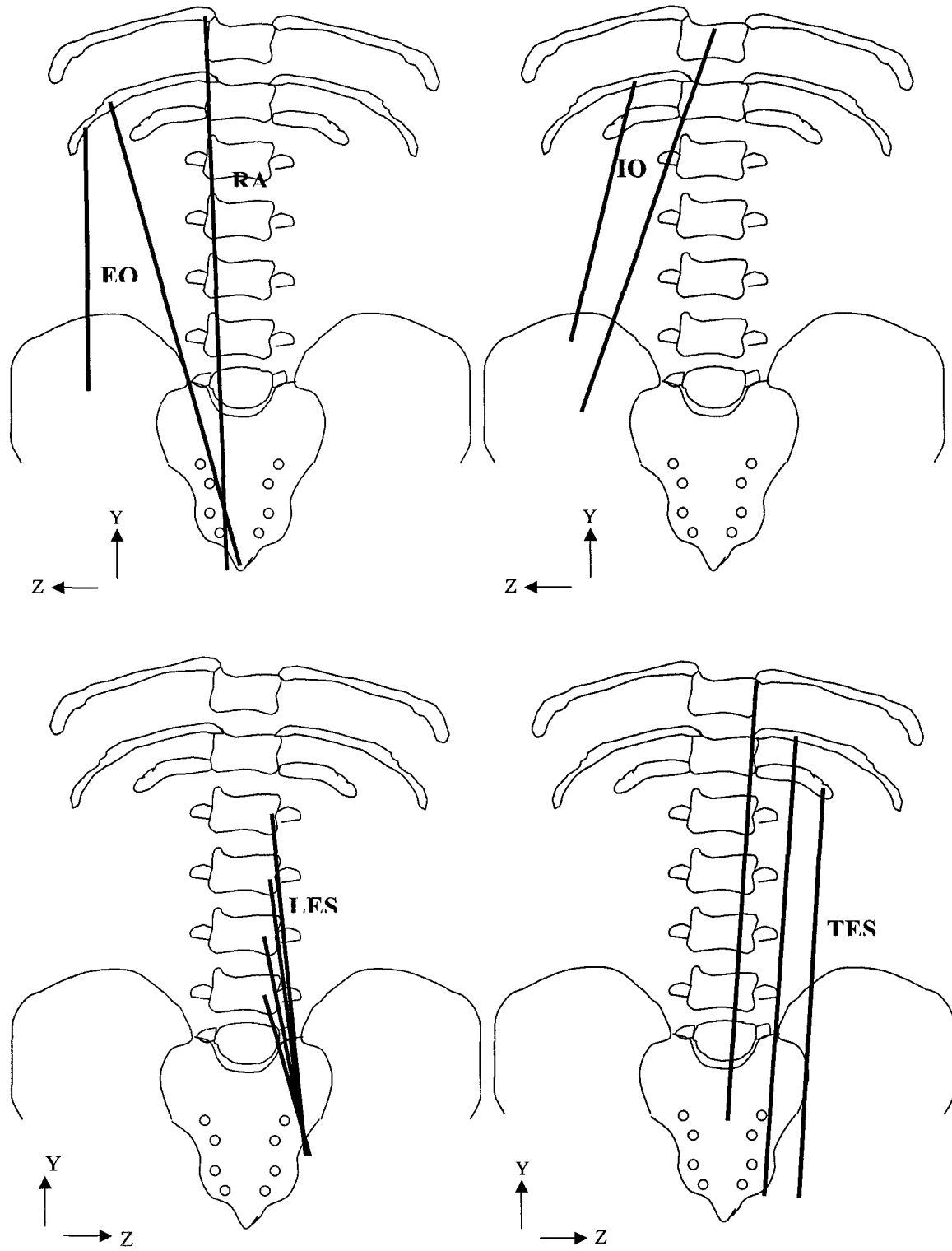
The scope of this project consisted of three parts: 1) the development of a three-dimensional model of the spine and its corresponding musculature; 2) the establishment of an optimization method to predict muscle forces by simultaneously optimizing stability about three axes and minimizing an objective function; 3) the validation of this optimization strategy using EMG data collected from empirical tests of various trunk exertions.

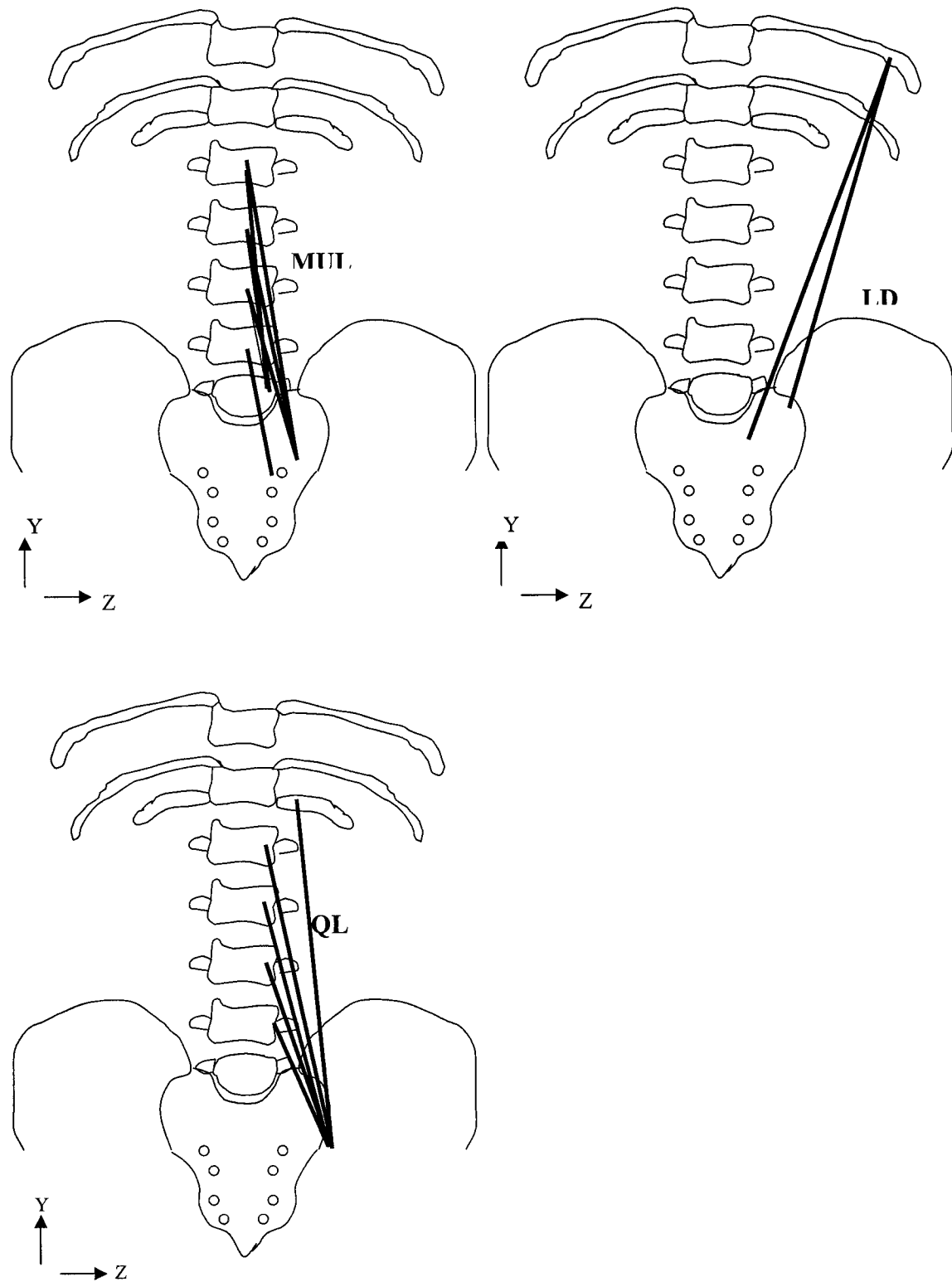
### 3.1 *Model Development*

#### 3.1.1 *Anatomical Representation*

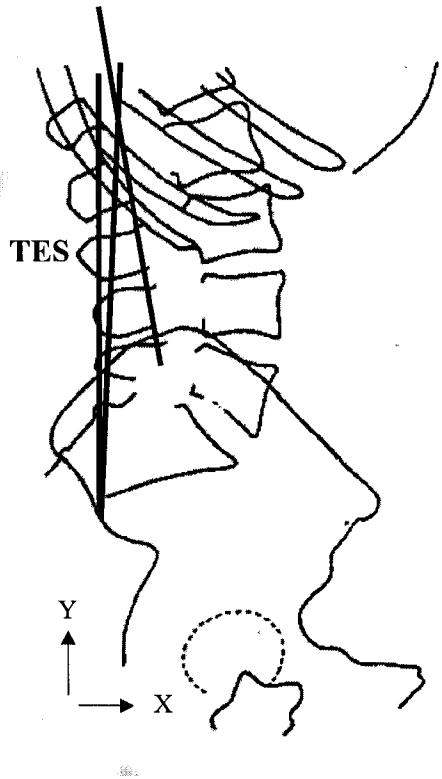
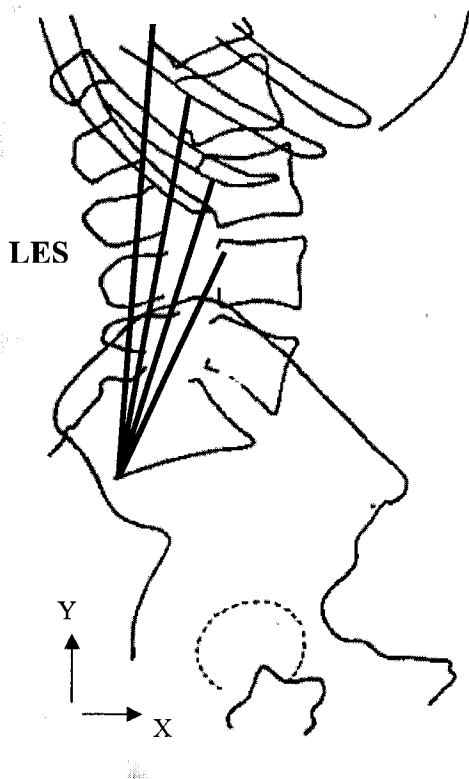
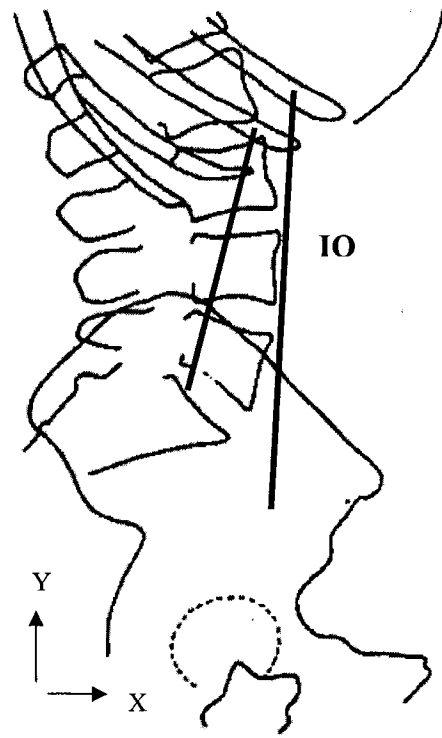
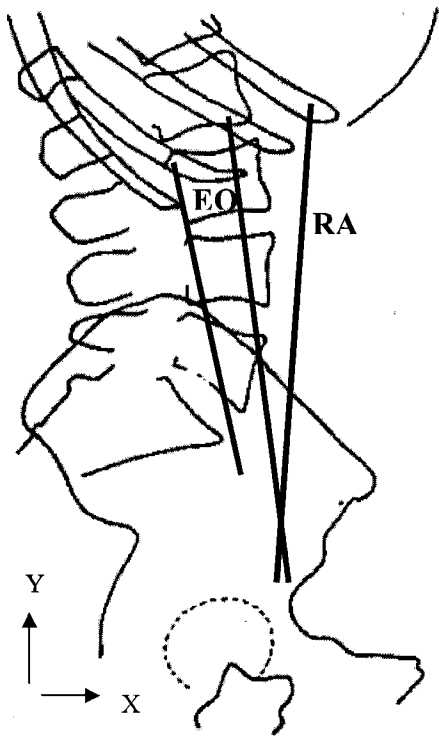
The anatomical model was formulated as a simplified version of the model of Cholewicki and McGill (1996). A single centre of rotation existed at the L4-L5 disc level. Therefore, muscle fascicles were only included in the model if they crossed, and thus created a moment about, the L4-L5 joint. This reduced the number of muscle fascicles from 90 in Cholewicki and McGill (1996) to 52 in the present model. Certain muscle fascicles were represented as having one or more nodal points, which alter the muscle line-of action, to make for a more realistic representation of muscle function. All other muscles were represented as having straight lines-of-action. Table 1 in Appendix B displays the cross-sectional areas, origin and insertion, and nodal points of each muscle fascicle in the model. Furthermore, all rotations were considered to occur about the fixed L4-L5 disc.

Figures 3 and 4 show the approximate locations, without nodal points, of all of the muscle fascicles in the present model. Figure 5 presents a view of a generic muscle with two nodal points.





**Figure 3.** Antero-posterior views of right side muscle fascicles in the current model. RA, EO and IO are shown from anterior view; LES, TES, MUL, LD and QL are shown from posterior view.



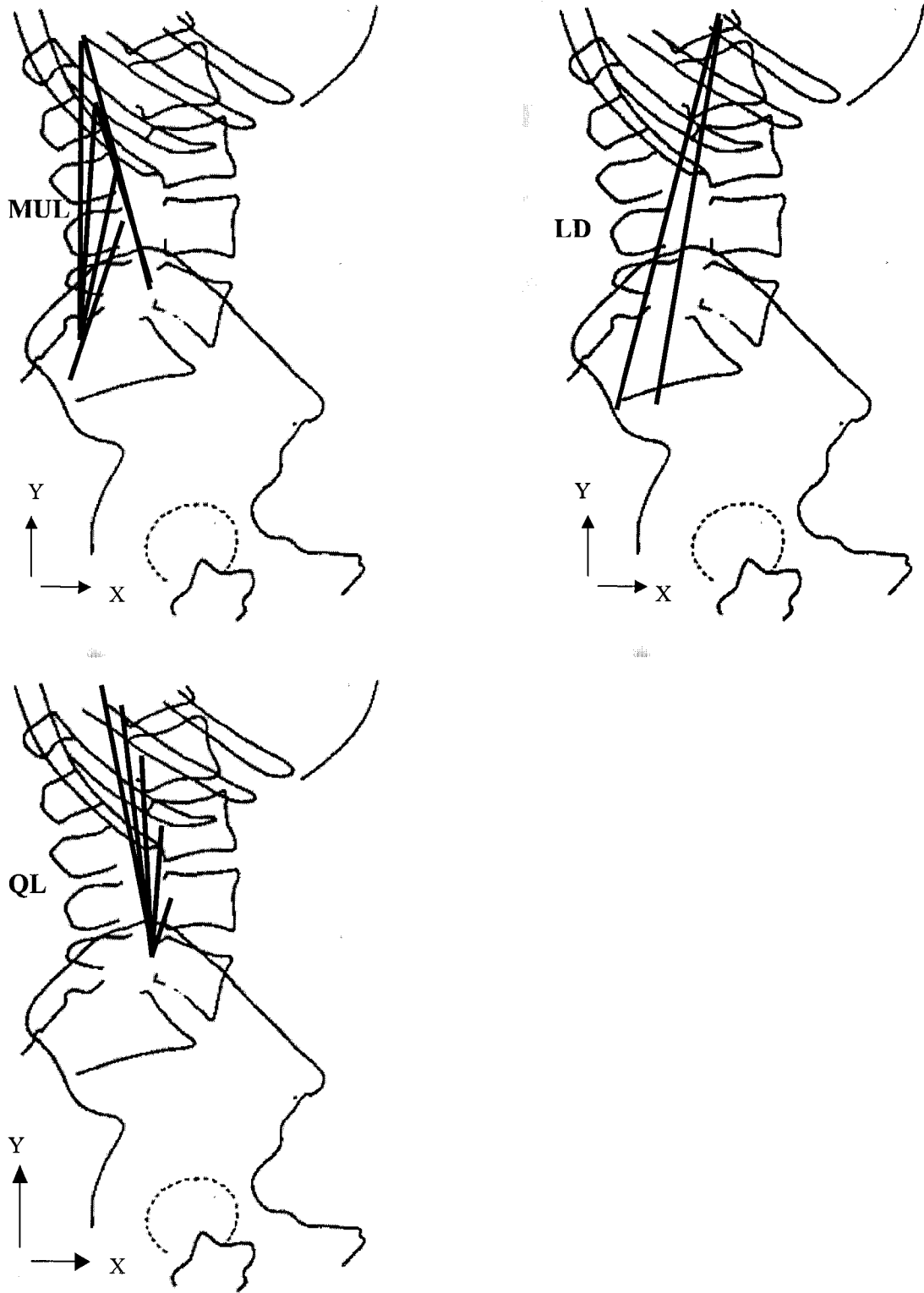


**Figure 4.** Side views of right side muscle fascicles in the current model.



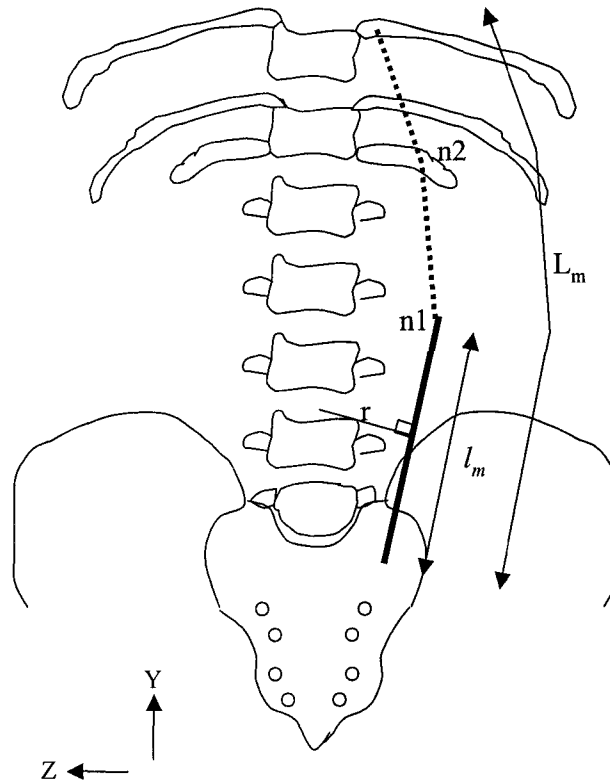


Figure 5. Example of a muscle with two nodal points (n1 and n2).  $r$  is the muscle moment arm at the L4/L5 joint;  $l_m$  is the length of the muscle vector crossing L4/L5;  $L_m$  is the total length of the muscle.

### 3.1.2 Optimization Technique

Various optimization techniques were utilized and compared. In all cases an initial constraint was set to simultaneously balance the net moments about each axis to zero. Two cost functions were then tested separately: 1) minimization of the sum of the cubed muscle forces (SumCubed); 2) minimization of the sum of the squared intervertebral forces at the L4-L5 disc level (InterForce). The method of calculation of the intervertebral force was incorporated from Stokes and Gardner-Morse (2001) where the relative subweighting of intervertebral forces and moments were such that 333 N of force and 1 Nm of moment were equally weighted. The logic of this method stems from presumed safe limits of intervertebral loads being 3000 N of force and 9 Nm of moment

(333 to 1 ratio). Values were squared so as to treat positive and negative values the same. The two cost functions were then tested again adding a second constraint of a measure of spinal stability about each of the three anatomical axes.

Potential muscle forces were given maximum constraints determined by muscle fascicle cross-sectional areas multiplied by an assumed maximum isometric muscle stress of 50 N/cm<sup>2</sup>. This value was selected based on reports in the literature of the maximum strength of erector spinae muscles of 48 N/cm<sup>2</sup> (Reid and Costigan, 1987) and trunk muscles in general of approximately 50 N/cm<sup>2</sup> (McGill and Norman, 1986). Minimum potential muscle force was set at 0 N.

The stability constraint was determined using a regression equation to predict the optimal stability level about each axis, from model inputs. A zero band was set around the predicted stability levels, thus forcing them to be met exactly. However, only the predicted stability level of the dominant axis, in which the external moment was applied, was set as an equality constraint. The stability levels about the other two axes were set as inequality constraints. Equality constraints force the independent variable in question to be met exactly to a target level (ie.  $a = b$ ); whereas inequality constraints force the independent variable to fall within a specified range of the target level (ie.  $a > b$ ). Preliminary testing showed that solutions to the optimization problem were considered unfeasible if stability about all three axes were set as equality constraints. Therefore, stability levels about the two non-dominant axes were set as inequality constraints, but were still forced to be met exactly to target levels in the following manner:  $\text{TargetStability} - \text{ModeledStability} > \text{Zero}$ ;  $\text{TargetStability} - \text{ModeledStability} < \text{Zero}$ . The optimization program solves for the cost function while satisfying the most

constraints possible in order of importance; equality constraints first (in this case the moment and dominant axis stability constraints), followed by inequality constraints (stability levels about the additional two axes). In the event that the optimization is having difficulty satisfying all constraints, the program will abandon inequality constraints one by one until the problem is solved. This results in the possibility that inequality constraints may not be met exactly, and that they will only be forced as close as possible to the desired level. The development of the regression equation will be discussed later.

The optimization model was run using the Optimization Toolbox of the MATLAB software program (The MathWorks, Inc., 1984-2000). The `fmincon` function, employing a medium-scale algorithm, was used to perform the minimization in the simulations.

Inputs to the optimization model were subject mass, subject height, load mass, load height, and external moment.

### **3.1.3** *Calculation of Spinal Stability*

Spinal stability was measured as the second derivative of the potential energy ( $V$ ) of the system. To take the second derivative of  $V$ , two simplified two-dimensional versions of the model were utilized (Figures 6 and 9).

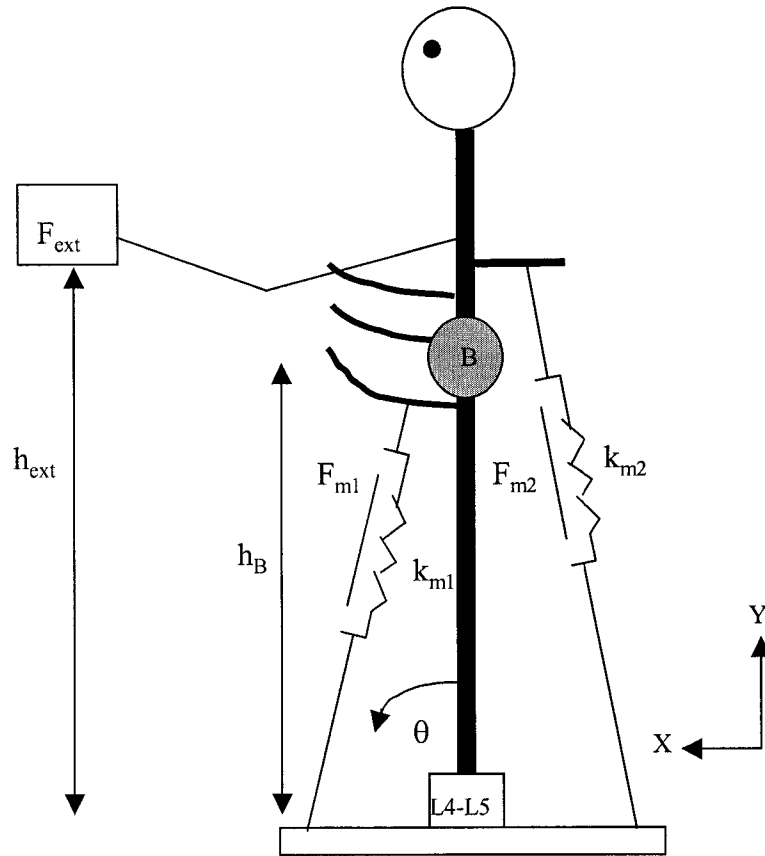


Figure 6. Right side two-dimensional representation of the model, for flexion moments, with two muscles being shown as a representation of all muscles.

The V of the system will be calculated as follows:

$$V_T = U_M + V_P - W \quad (1)$$

Where  $V_T$  = the total potential energy of the entire system

$W$  = the work done by the external forces acting on the body

$U_M$  = the work done by the muscles (described in detail later)

$V_P$  = the strain energy stored within the passive structures of the spine, ie. the potential of the deformed elastic structures to do work

$$W = F_{ext} (h_{ext} - h_{ext} \cos \theta) + B (h_B - h_B \cos \theta) \quad (2)$$

where:  $B$  = body weight above L4-L5

$h_B$  = height of center-of-mass above L4-L5 (cm)

$F_{ext}$  = external force acting on body (N)  
 $h_{ext}$  = height of external force above L4-L5 (cm)

The  $V_P$  was calculated (in Nm) as per McGill, Seguin and Bennett (1994), as follows, using male coefficients:

$$V_P = \lambda/\beta * e^{\beta\theta} \quad (3)$$

where:  $\lambda = 2.12$  (flexion); 2.44 (lateral bend)  
 $\beta = 0.11$  (flexion); 0.11 (lateral bend)  
 $\theta$  = trunk angle  
 $e = 2.7182818$

For flexion trials, it was necessary to adjust trunk angle from zero to  $-28.4$ , as McGill et al. (1994) collected data with subjects in a semi-seated position with knees bent, as position which produces 28.4 degrees of trunk flexion (Andersson, Murphy, Ortengren and Nachemson, 1979).

A simple inverted pendulum model will first be used to demonstrate the relationships involved in the calculation of the muscular contribution to Potential Energy ( $V$ ) about a joint (Fig. 7).

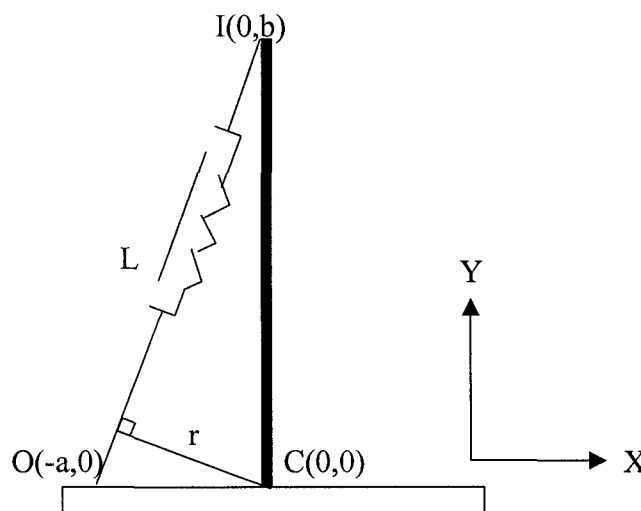
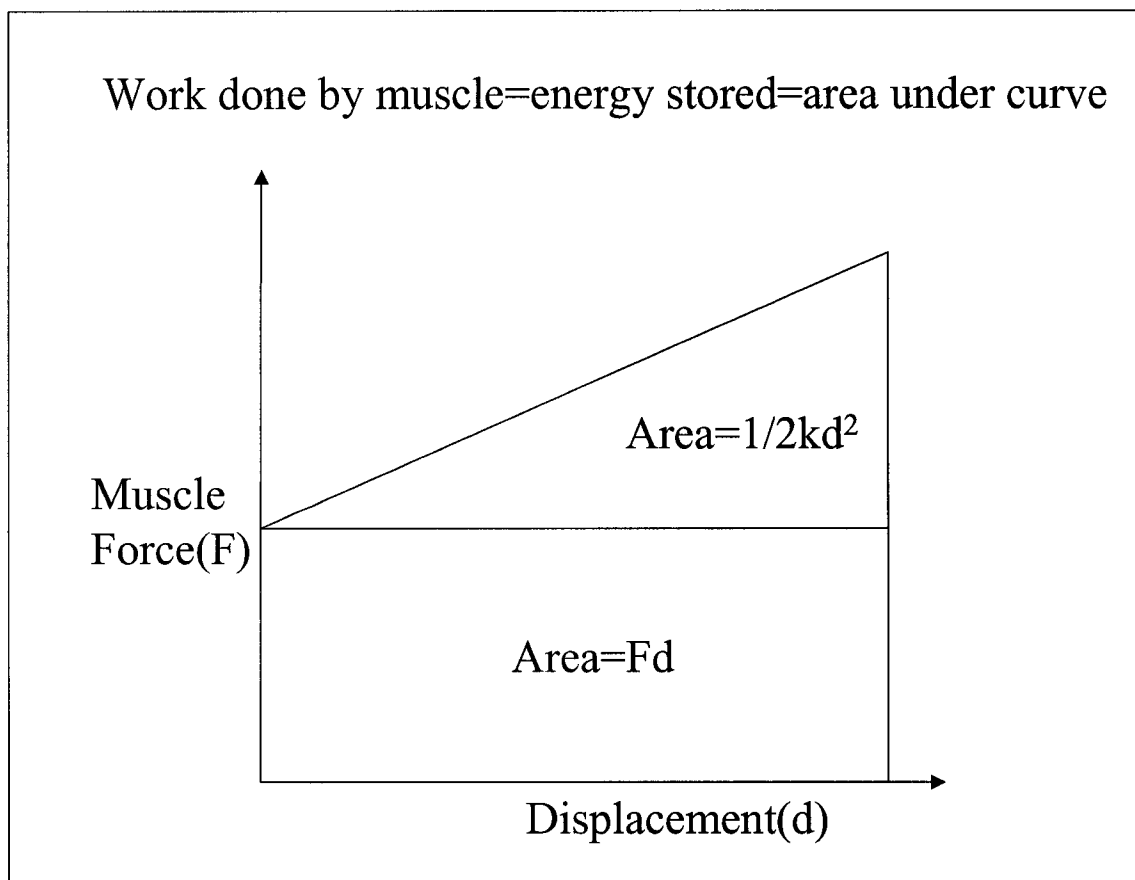


Figure 7. Two-dimensional inverted pendulum model for one muscle. (C: center of rotation, I: muscle insertion, O: muscle origin, r: muscle moment arm, L: muscle length).

The 2-dimensional moment arm ( $r$ ) is calculated by the cross-product of the muscle's position vector ( $\vec{p} = 0i + bj$ ) by its unit vector ( $\vec{u} = \frac{-ai - bj}{l}$ ), yielding:

$$r = \frac{ab}{l} \quad (4) \quad \text{where } l = \sqrt{a^2 + b^2} \quad (5)$$

Figure 8 presents the concept behind the calculation of the energy stored within a muscle.



**Figure 8.** Components of the energy stored within a muscle.  $F$  is the muscle Force;  $d$  is the change in length of the muscle.

Based on Figure 8, the elastic energy ( $U_m$ ) stored in a muscle (m) is calculated as

follows: 
$$U_m = F_m \Delta l + \frac{1}{2} k_m \Delta l^2 \quad (6)$$

Where  $dl$  is the change in the length of the muscle vector, as it crosses L4/L5, between the initial and final in the system:

$$dl = \sqrt{(b^2 \cos^2 \theta) + (a + b \sin \theta)^2} - l_m \quad (7)$$

where:  $F_m$  = initial force (N) for an individual muscle (m)

$k_m$  = stiffness of an individual muscle (m)

$a$  = horizontal (x) distance between the center of rotation and the intersection of the muscle vector (cm).

$b$  = vertical (y) distance between the center of rotation and the intersection of the muscle vector (cm)

$l_m$  = hypotenuse of the triangle formed by  $a$  and  $b$  (cm)

$r_m$  = 2-dimensional moment arm of hypotenuse (cm)

Substituting (7) into (6), simplifying and applying a Taylor Series expansion to the second order yields:

$$U_m = \left( \frac{1}{2} \frac{k_m a^2 b^2}{l_m^2} - \frac{1}{2} \frac{F_m a^2 b^2}{l_m^3} \right) \theta^2 \quad (8)$$

Substituting (4) into (8) and applying to the more generalized muscle model in

Figure 5 gives:

$$U_m = \left( \frac{1}{2} k r^2 - \frac{1}{2} \frac{F r^2}{l} \right) \theta^2 \quad (9)$$

where  $l$  is the 2-dimensional length of the muscle fascicle as it crosses L4/L5. Everything below the squared term will be eliminated through the first and second differentiation.

Higher order terms have been neglected as they were shown to produce negligible effects (less than 0.01%) on the final calculation.

Thus:

$$\frac{dU_m}{d\theta} = 2 \left( \frac{1}{2} k r^2 - \frac{1}{2} \frac{F_m r^2}{l_m} \right) \theta \quad (10)$$

$$\frac{d^3 U_m}{d\theta^2} = k_m r_m^2 - \frac{F_m r_m^2}{l_m} \quad (11)$$

Bergmark (1989) states that muscle stiffness can be calculated as:

$$k_m = \frac{q F_m}{L_m} \quad (12)$$

Substituting (12) into (11) and simplifying gives:

$$\frac{d^2 U_m}{d\theta^2} = q \frac{F_m r_m^2}{L_m} - \frac{F_m r_m^2}{l_m} \quad (13)$$

$L_m$  and  $l_m$  differ only in muscles in which nodal points are present. Figure 5 displays such differences in the two variables.

Differentiating  $V_p$ :

$$\begin{aligned} \frac{dV_p}{d\theta} &= \lambda e^{\beta\theta} \\ \frac{d^2 V_p}{d\theta^2} &= \lambda \beta e^{\beta\theta} \end{aligned} \quad (14)$$

Applying a Taylor Series expansion to the second order to  $W$  and differentiating:

$$\begin{aligned} W &= \left( \frac{1}{2} F_{ext} h_{ext} + B h_B \right) \theta^2 \\ \frac{dW}{d\theta} &= (F_{ext} h_{ext} + B h_B) \theta \\ \frac{dW^2}{d^2 \theta} &= F_{ext} h_{ext} + B h_B \end{aligned} \quad (15)$$



Therefore the overall second derivative of V becomes:

$$\frac{d^2V_T}{d\theta^2} = \sum_{m=1}^M \left( q \frac{F_m r_m^2}{L_m} - \frac{F_m r_m^2}{l_m} \right) + \lambda \beta e^{\beta \theta} - F_{ext} h_{ext} - B h_B = S \quad (16)$$

where  $S$  is the value for stability about a single axis at the L4/L5 joint.

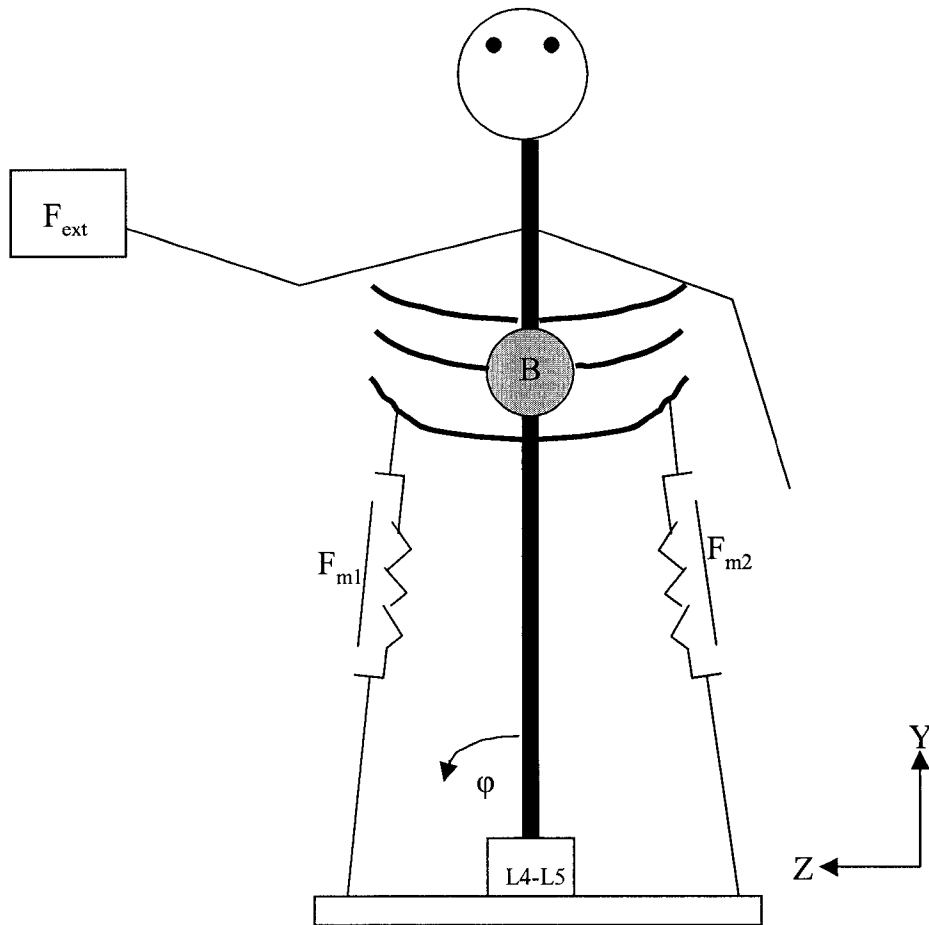


**Figure 9.** Front-side two-dimensional representation of the model, for lateral bend moments, with two muscles being shown to represent all of the muscles.

The same formulae, as used above for calculating stability about the flexion/extension axis, can be applied to the lateral axis, in Figure 9 with:

$\varphi$  replacing  $\theta$

$a_m$  = z-direction difference between origin and insertion (cm).

The L4-L5 disc will be fixed, therefore compression at this joint will be calculated simply as the sum of the forces acting in the y-axis.

### ***3.2 Experimental Validation of Model***

#### ***3.2.1 Subjects***

Eleven healthy males volunteers with no history of back pain were obtained from the university population. Subject mean (standard deviation) anthropometric data was as follows: age 24.2 (2.2) years, height 181.5 (5.8) cm, mass 84.6 (9.1) kg.

#### ***3.2.2 Experimental Conditions***

Upon arrival in the lab subjects were explained the experimental protocol and given the opportunity to familiarize themselves with the equipment and experimental set-up. Next, bipolar Ag/AgCl surface electrodes (Medi-trace disposable electrodes, Graphic Controls) were attached over the belly of seven muscles bilaterally. The muscles examined were as follows (Cholewicki and McGill, 1996): lumbar erector spinae (LES), thoracic erector spinae (TES), multifidus (MULT), latissimus dorsi (LD), rectus abdominus (RA), internal oblique (IO), external oblique (EO), and quadratus lumborum (QL). Locations of electrode placement will be as follows: LES (3 cm lateral to L3 spinous process, TES (5 cm lateral to T9 spinous process), MULT (2 cm lateral to L4-L5 spinous process), LD (lateral to T9 over the muscle belly), RA (3 cm lateral to the umbilicus), IO (approximately midway between the anterior superior iliac spine and symphysis pubis, above the inguinal ligament), and EO (approximately 15 cm lateral to the umbilicus). QL activity was estimated from the LES electrode location, based on the

data of McGill, Juker and Kropf (1996a), who demonstrated the ability to predict QL activity from this electrode site with RMS errors of less than 6% Maximum Voluntary Contraction (MVC). Intra-electrode distance was 2.5 cm.

MVCs were obtained for each of the 14 muscle sites for the purpose of normalization of experimental EMG data. For posterior muscle MVCs, subjects lay prone on a table with their hips and legs secured to the table. A series of back extensions was then performed, against resistance, which allowed for varying degrees of extension to occur. For anterior muscle MVCs, subjects sat, with feet flat and knees up, on a table with their ankles secured. A series of isometric trunk curls (to the left, right, and directly anterior to the body) was then performed against resistance. MVC trials were continued until both the researcher and subject were satisfied that maximum activity levels had been attained. Adequate rest was given in between trials to allow for full subject recovery.

Four separate experimental conditions were examined for each subject: 1) subject statically resists an applied anterior moment; 2) subject statically resists an applied lateral bend moment; 3) subject isometrically ramps force over time to create an anterior moment; 4) subject isometrically ramps force over time to create a lateral bend moment. Examples of each of the four main conditions are shown in Figure 10.

#### **3.2.2.1 Anterior (Flexion) Moment Condition**

Subjects were instructed to stand statically in an upright position with feet separated by approximately shoulder width. Subjects were instructed to hold a load with both hands directly anterior to the body. The load was held at a horizontal distance from the ankle to the center of the load of either 30 cm or 50 cm, thus creating flexion moment

arms of 30 or 50 cm. At each of these moment arm positions, the subject held the load at two separate heights: 1) L4-L5; 2) 50% of the distance between L4-L5 and shoulder.

Two separate masses were utilized at each of the two horizontal distances: 4.7 and 13.8 kg (30 cm moment arm); 3.2 and 9.3 kg (50 cm moment arm). Thus, a total of 8 separate flexion conditions were tested (Table 1). Three trials of each condition were collected. Each trial lasted two seconds.

Table 1. Summary of static flexion moment trials.

Moment Arm	30 cm				50 cm			
Load Height	L4-L5		50% between		L4-L5		50% between	
Load Mass (kg)	4.7	13.8	4.7	13.8	3.2	9.3	3.2	9.3

### 3.2.2.2 Lateral Bend Moment Condition

Subjects were instructed to stand statically in an upright position with feet separated by approximately shoulder width. Subjects were instructed to hold a load with their right hand directly lateral to the body. The load was held at a horizontal distance from the body midline to the centre of the load of either 40 cm or 60 cm, thus creating lateral bend moment arms of 40 or 60 cm. At each of these moment arm positions, the subject held the load at two separate heights: 1) L4-L5; 2) 50% of the distance between L4-L5 and shoulder.

Two separate masses were utilized at each of the two horizontal distances: 3.4 and 9.1 kg (40 cm moment arm); 2.3 and 5.7 kg (60 cm moment arm). Thus, a total of 8 separate lateral bend conditions were tested (Table 2). Three trials of each condition were collected. Each trial lasted two seconds.

Table 2. Summary of static lateral bend moment trials.

Moment Arm	40 cm				60 cm			
Load Height	L4-L5		50% between		L4-L5		50% between	
Load Mass (kg)	3.4	9.1	3.4	9.1	2.3	5.7	2.3	5.7

### 3.2.2.3 Isometric ramped force exertions

Subjects were instructed to stand statically in an upright position with feet separated by approximately shoulder width. Their ankles were positioned at a distance equivalent to the short horizontal moment arm in the static trials, either posterior (30 cm) or lateral (40 cm) to a chain apparatus that will be fastened to the floor. The chain was

instrumented with a force transducer that recorded the force being exerted by the subject. The length of the chain was adjusted to reach either L4-L5 height or a height of 50 percent of the distance between L4-L5 and shoulder. Subjects grasped a handle at the end of the chain. They then isometrically pulled directly up on the chain, slowly ramping their force to a level that exceeded the highest moment produced in the static trials by 10 percent and then slowly down to zero. Subjects were given a total of 10 seconds to complete each trial.

For both anterior and lateral bend conditions, subjects performed two trials at each of the two heights, for a total of eight trials.

A sample ramped contraction trial is shown later in Figure 11.

Table 3. Summary of ramped flexion and lateral bend moment trials.

Moment Arm	30 cm (flexion)				40 cm (lateral bend)			
Load Mass (kg)	4.7		13.8		3.4		9.1	
Ramp direction	up	down	up	down	up	down	up	down

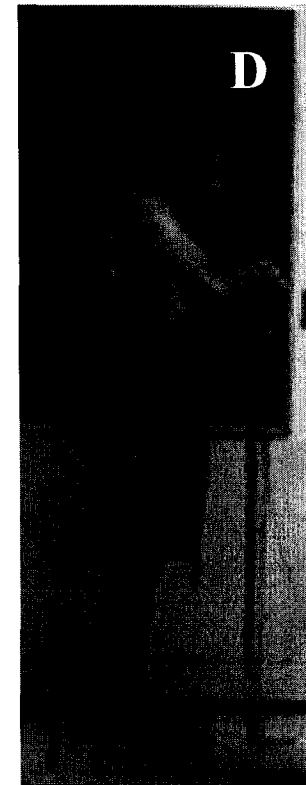
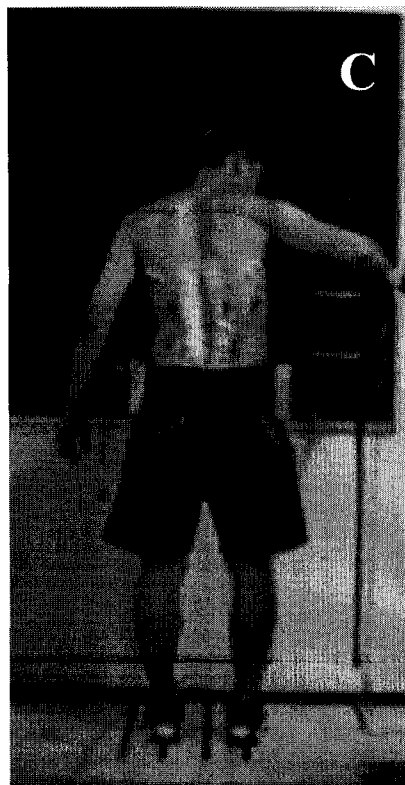
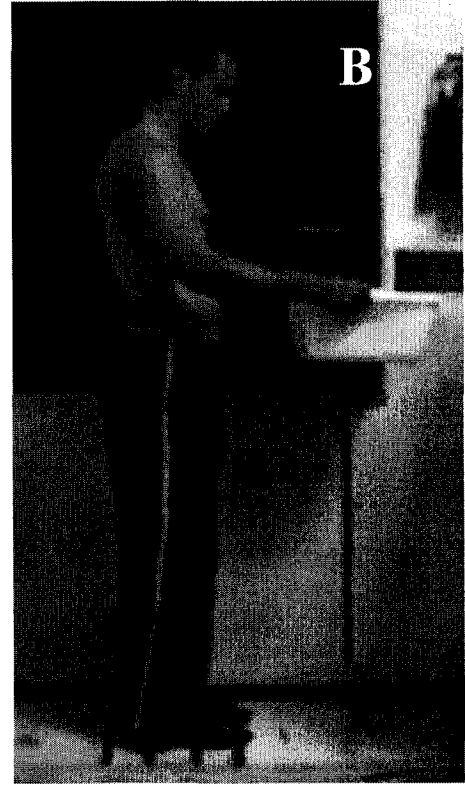


Figure 10. Examples of the four main experimental conditions. A) Static Lateral Bend Moment; B) Static Flexion Moment; C) Ramped Lateral Bend Moment; D) Ramped Flexion Moment. Static are shown in the far moment arm, low load height position; Ramped are shown in the close moment arm, high load height position.

All static and ramped flexion trials were performed prior to any lateral bend trials. This was done to prevent the development of any asymmetrical muscle activity patterns in flexion trials that might have resulted due to fatigue or recruitment preferences in lateral bend trials.

Sub-conditions within each of the flexion and lateral bend conditions were presented randomly.

### **3.2.3 Data Acquisition**

EMG and force data were collected with LabVIEW software (National Instruments, Austin Tx.) using a PC compatible computer and converted by a 12-bit A/D card (National Instruments, Austin Tx.).

EMG signals were amplified (1000 to 5000 times) prior to sampling, digitized at 1000 Hz, bandpass filtered (20-490 Hz), full-wave rectified, and low-pass filtered using a first order Butterworth filter with a cut-off of 10 Hz.

For static trials a half-second window was visually selected for analysis by the researcher for each individual trial. The window was selected over the period in which the EMG signals appeared to maintain the most static level.

For ramped force trials, a quarter-second window was selected at four instances per trial. These instances were the points at which force of pull equaled each of the low and high forces held in the static trials, both during the ramp up and ramp down phase of the trial. The point at which the force of pull exactly achieved this force goal was considered to be the middle point of the window.



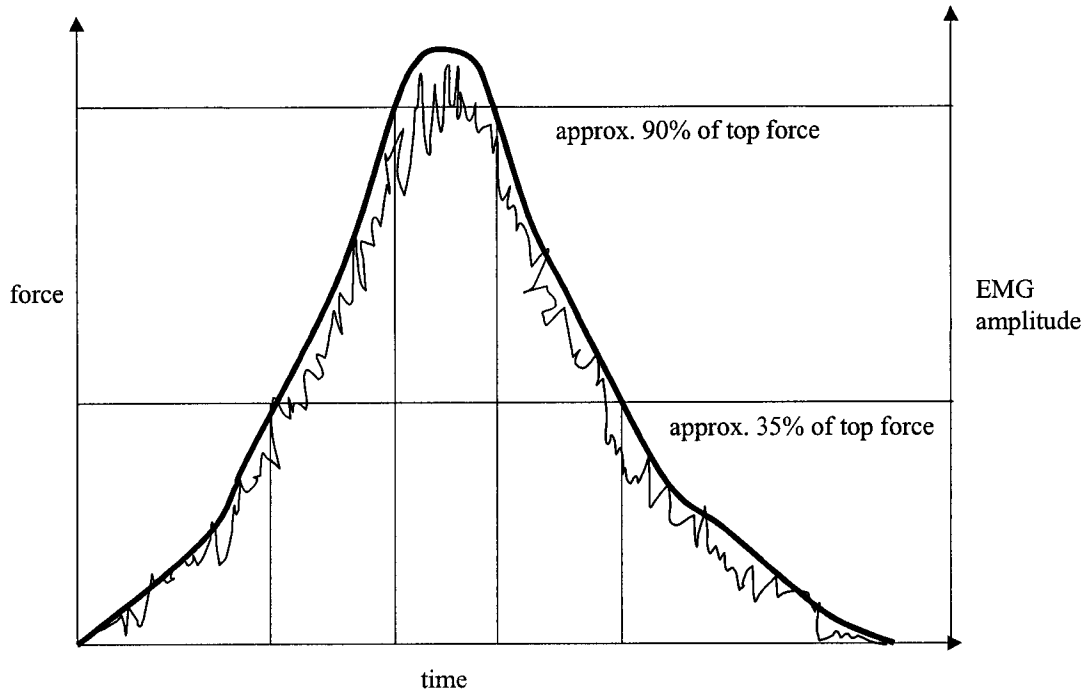


**Figure 11.** Sample ramped contraction trial. Dark smooth line represents force at the hands; lighter jagged line represents EMG activity; straight horizontal lines represent force level for high and low moment conditions; straight vertical lines represent midpoint of quarter-second window in which EMG was examined.

EMG data was filtered again with a first order Butterworth filter at a low-pass cutoff of 10 Hz, averaged over each of these half-second and quarter-second windows, and used to derive the average force that each muscle produces over this period in each trial. To do this the following formula was utilized:

$$F_j = G * \frac{EMG_j(t)}{EMG \max_j} * A_j * \delta \quad (17)$$

where:  $F_j$  = the force in a particular muscle, j,  
 $G$  = (gain) maximum muscle force per unit area  
 $EMG_j(t)$  = measured EMG level at a particular point in time, t,  
 $EMG \max_j$  = MVC level  
 $A_j$  = cross-sectional area  
 $\delta$  = active length coefficient

The active length coefficient is responsible for modulating the force output to correspond to muscle length. Every muscle has an optimal length at which it is best capable of generating force. As the muscle deviates from this optimal length, its force generating capacity diminishes. Trunk flexor muscles are at a resting length when the trunk is in approximately 10 degrees of extension, while trunk extensor muscles are at a resting length when the trunk is flexed approximately 40 degrees. In upright standing, each of the trunk muscles is in a shortened position. In such situations, the active length coefficient, as taken from McGill (1992), can be calculated as follows:

$$\delta = \sin(\pi[(L/L_0) - 0.5]) \quad (18)$$

where: L = current muscle length  
 $L_0$  = resting muscle length

The EMG-force relationship for both the LES and TES muscle groups has been shown to be non-linear in nature (Potvin, Norman and McGill, 1996). Thus, EMG data for these two muscles was non-linearly normalized in the following manner, taken from Potvin, Norman and McGill (1996):

$$EMG_N = 100 * e^{(-EMGL * \alpha)} - 1 / e^{(-100 * \alpha)} - 1 \quad (19)$$

where:  $EMG_N$  = EMG non-linearly normalized to 100% of maximum  
 $EMGL$  = EMG linearly normalized to 100% of maximum  
 $\alpha$  = 17 (TES); 12 (LES)

### 3.2.4 Gain adjustment for EMG to Force conversion

For the calculation of stability about each axis it was essential that the net moment about each axis be balanced to zero. Thus, gains and in some cases muscle activation levels had to be adjusted to ensure equilibrium about each axis. This was accomplished in different ways for the flexion and lateral bend data.

In instances of pure flexion or extension spinal loading, muscles, due to their bilateral nature, and under the assumption of symmetry in such instances, can be viewed purely as acting as flexors or extensors of the trunk, without creating moments about the other two axes. In such conditions, it is relatively simple to adjust the gain level to balance the moment about a single axis. However, in conditions of pure lateral bend loading, muscles produce net moments about all three axes simultaneously. This creates a need for a more complex method of adjusting gain levels to create equilibrium in all three axes.

#### **3.2.4.1 *Flexion Trials***

To ensure that moments would balance about the lateral bend and axial twist axes, muscle activation levels were taken as the average of right and left EMG values for each muscle. Gain was initially set at a value of 1 N/cm<sup>2</sup>, and then adjusted to balance the net moment about each axis to zero. The adjusted gain was set to a value that would force the sum of the moments due to muscle and passive tissue to equal the dominant external moment. This was accomplished by dividing the net internal moment (muscle moment + passive moment) by the dominant external moment, and then multiplying each muscle force by the result. Trials in which the gain factor fell outside of the physiological range for human muscle of 30 – 100 N/cm<sup>2</sup> (McGill and Norman, 1987; Reid and Costigan, 1987) were then subjected to an additional method of muscle activation adjustment to be described in the next section.

### 3.2.4.2 *Lateral Bend Trials*

Cholewicki and McGill (1994) developed what has been termed a “hybrid” method of combining EMG data with an optimization technique to achieve moment equilibrium. A version of this method was used in this study. Gain was initially determined as the numerical value between 30 and 100 N/cm<sup>2</sup> (based on the physiological range of human muscle (Reid and Costigan, 1987; McGill and Norman, 1987) that resulted in the lowest RMS error of the net moments derived solely from the EMG-based method. The error of the dominant moment (moment in the direction of the external load) was given additional weighting by being cubed, while the errors of the other two moments were squared. Next, an optimization technique was used that minimized the RMS change in the muscle activation levels necessary to balance each moment to zero. The following equation was utilized:

$$RMSchange = \sqrt{\frac{\sum_{i=1}^{n=52} (EMGO_i - EMGA_i)^2}{n}} \quad (20)$$

where:  $EMGO_i$  = original EMG activation level (%MVC) for each muscle  $i$   
 $EMGA_i$  = adjusted EMG activation level (%MVC) for each muscle  $I$

What will be termed the *PercentRMSchange* was also calculated, for errors in compression estimates, for comparison to other data in the literature:

$$PercentRMSchange = \sqrt{\frac{1}{N} \sum_{i=1}^{n=52} \left( \frac{EMGO_i - EMGA_i}{EMGO_i} \right)^2} \quad (21)$$

### 3.2.5 *Force Data*

Force data was digitized at 1000 Hz, calibrated to Newtons, and lowpass filtered using a first order Butterworth filter with a cut-off of 20 Hz.

### **3.2.6 *Calculation of Experimental Moments***

Video (30 Hz) of each subject was taken for each condition. GOBER software (Copyright Dr. J.P. Callaghan) was used to digitize the video and output the net moment acting at L4-L5, as well.

### **3.2.7 *Data Analysis***

#### **3.2.7.1 Examination of Stability Values**

EMG data were first run through the biomechanical model to determine stability values about all three axes for each condition. Next, the data were collapsed across subject, load mass, load height, and horizontal moment arm, and separate stepwise regression analyses, using StatView (SAS Institute Inc., 1992-1998) software, were conducted for the flexion and lateral bend (combining static and ramped data) conditions to determine the ability to predict stability based on model inputs. Independent variables entered into the regression were: external moment, subject height, subject mass, external load height, external load mass, and the combined potential energy due to the external load and upper body mass.

#### **3.2.7.2 Statistics**

For each muscle, predicted forces obtained from the each of the four optimization schemes were compared to the actual experimental forces. Root Mean Square errors (RMS error) were calculated to determine the difference between the predicted and experimentally obtained muscle forces.

$$RMSError = \sqrt{\frac{\sum_1^n (F_{mod\ i} - F_{exp\ i})^2}{n}} \quad (22)$$

This was done for each individual muscle, collapsed across agonist and antagonist muscle groups, and collapsed across all muscles. Also, an RMS error was calculated between the compressive force predicted in each of the four optimization schemes and that determined by the experimental data.

Furthermore, a percent RMS error between the modeled and experimental compressive forces was calculated as follows:

$$PercentError = \sqrt{\frac{1}{n} \sum_i^n \left( \frac{F_{mod\ i} - F_{exp\ i}}{F_{exp\ i}} \right)^2} \quad (23)$$

where:  $n = 88$

$F_{mod}$  = compression force at L4/L5 predicted by the optimization model (N)

$F_{exp}$  = true compression force at L4/L5 (N)

For significance testing, data were collapsed across static and ramped trials for each of the flexion and lateral bend conditions. Two separate 2 X 2 Repeated Measures ANOVAs (one for each of the flexion and lateral bend conditions) were utilized to determine main effects of stability and cost function on percent error of the compressive forces acting at L4/L5 (Figure 12). Thus, the independent variables were: 1) cost function (InterForce or SumCubed); 2) stability (constrained or unconstrained). The dependent variable was the percent error between the compressive forces predicted by the optimization model and the compressive forces found experimentally. Paired t-tests, using Bonferroni correction factors, were then run as post-hoc tests to determine the exact location of significant differences in the data. Significance level was set at  $p < 0.05$ .

<b>Cost Function</b>			
	InterForce		
	SumCubed		
		Stability constraint	No Stability constraint
		<b>Stability</b>	

Figure 12. Schematic of the 2 X 2 Repeated Measures ANOVA model used for the statistical analysis. The independent variables were cost function (InterForce or SumCubed) and Stability (constrained or unconstrained).

## Chapter 4

# RESULTS

### 4.1 Experimental Stability Values

The  $r^2$  values, representing the relationship between axis stability, and external moment are shown in Figures 13 and 14. The  $r^2$ 's resulting from the stepwise regression, and subsequent regression equations to predict stability about each axis, are as follows (n=176 for each):

#### *Flexion Moment:*

$$\text{Flexion/Extension Stability} = -12.6 + 3.50 * \text{Mom}_E - 1.25 * \text{PE}_L$$
$$r^2 = 0.88; \text{RMS Residual} = 23.5$$

$$\text{Lateral Stability} = -35.9 + 2.42 * \text{Mom}_E - 119.0 * \text{Ht}_L$$
$$r^2 = 0.33; \text{RMS Residual} = 71.5$$

$$\text{Axial Twist Stability} = -40.0 + 3.02 * \text{Mom}_E - 110.0 * \text{Ht}_L$$
$$r^2 = 0.45; \text{RMS Residual} = 67.6$$

#### *Lateral Bend Moment:*

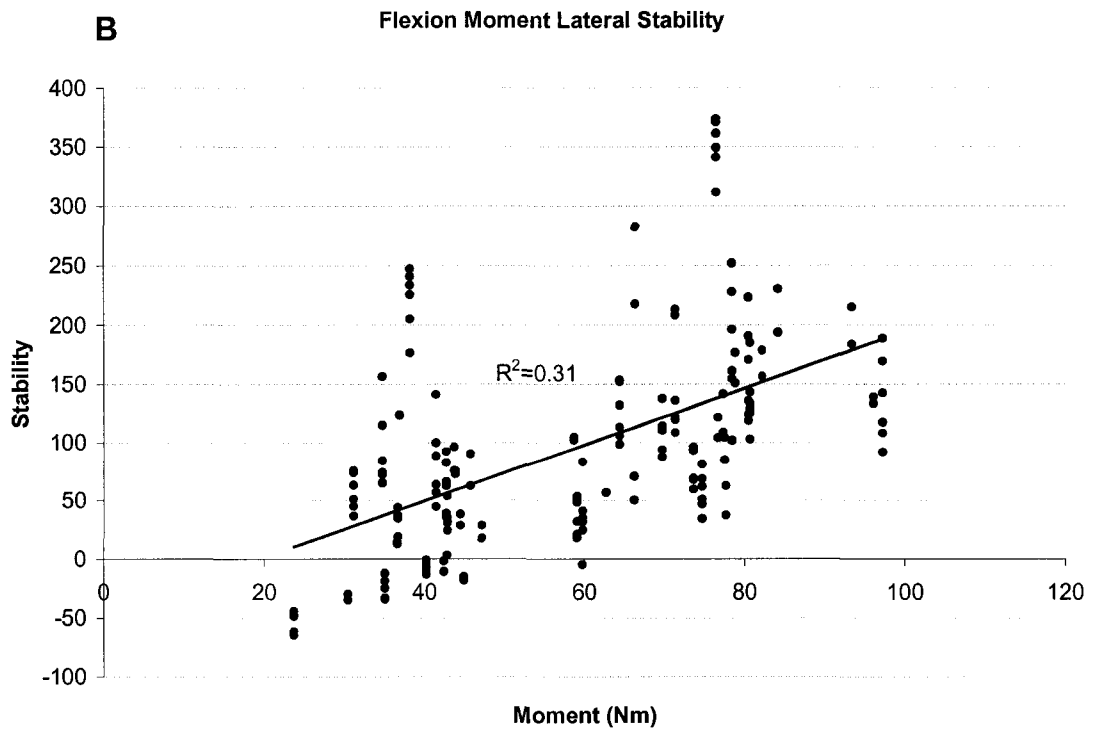
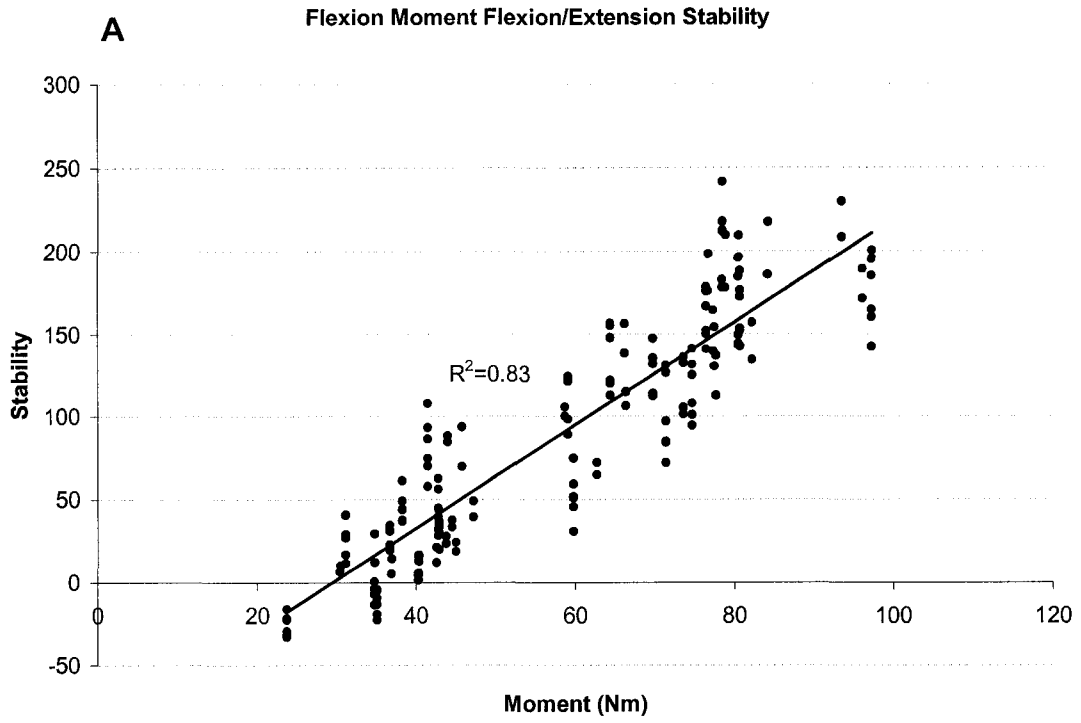
$$\text{Flexion/Extension Stability} = -43.5 + 3.22 * \text{Mom}_E - 86.1 * \text{Ht}_L - 0.804 * \text{Mass}_S$$
$$r^2 = 0.70; \text{RMS Residual} = 27.6$$

$$\text{Lateral Stability} = -924.0 + 8.82 * \text{Mom}_E + 538.0 * \text{Ht}_S - 1.07 * \text{PE}_L$$
$$r^2 = 0.70; \text{RMS Residual} = 70.8$$

$$\text{Axial Twist Stability} = -872.0 + 9.26 * \text{Mom}_E + 509.0 * \text{Ht}_S - 1.04 * \text{PE}_L$$
$$r^2 = 0.70; \text{RMS Residual} = 75.8$$

Where:  $\text{Mom}_E$  = external moment acting on the subject (Nm)  
 $\text{PE}_L$  = potential energy due to the external load (J)  
 $\text{Ht}_L$  = height, above L4/L5, of the external load (m)  
 $\text{Mass}_S$  = subject mass (kg)     $\text{Ht}_S$  = subject height (m)





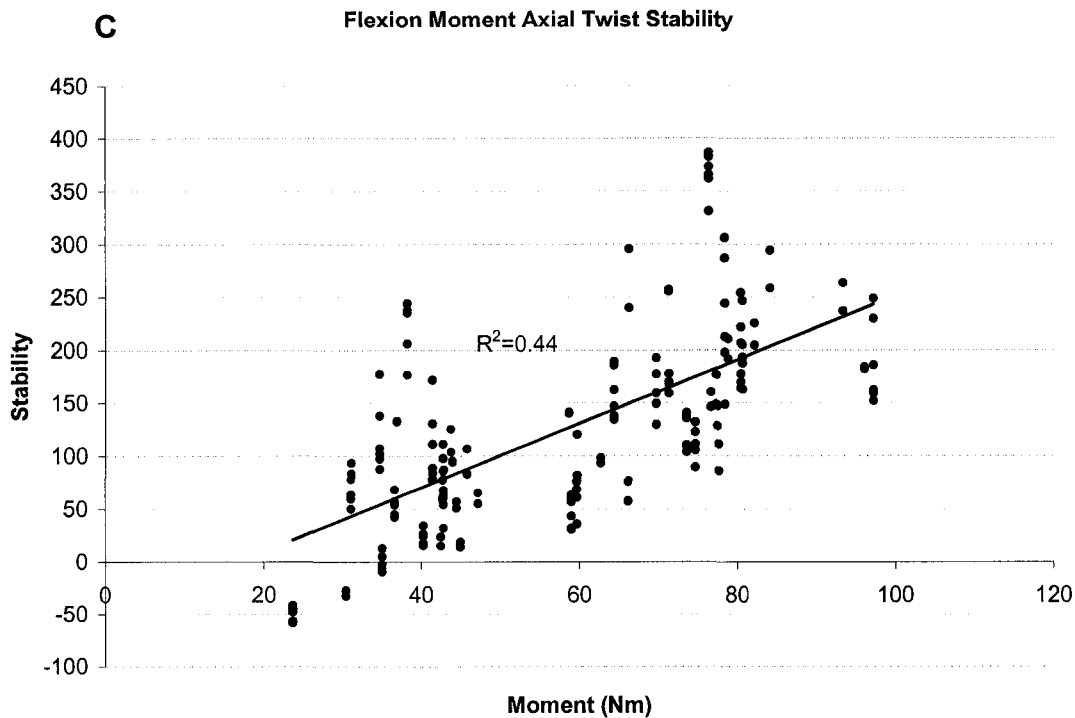
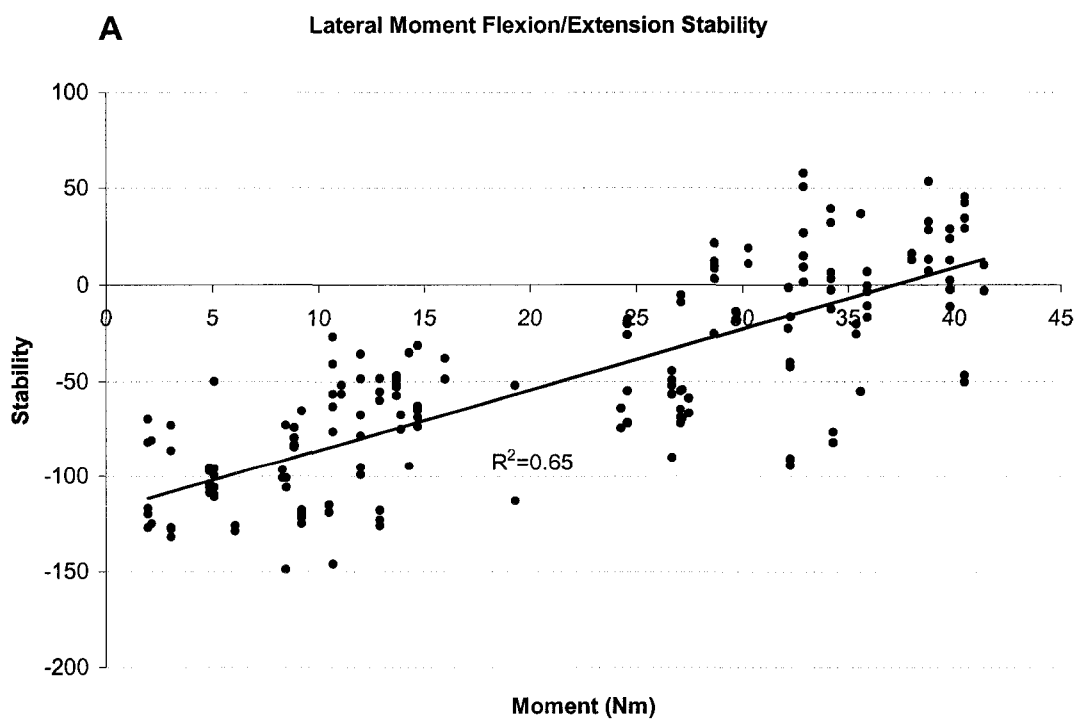


Figure 13. Relationship between external flexion moment and stability about the flexion/extension axis (A), lateral bend axis (B), and axial twist axis (C). N = 176.



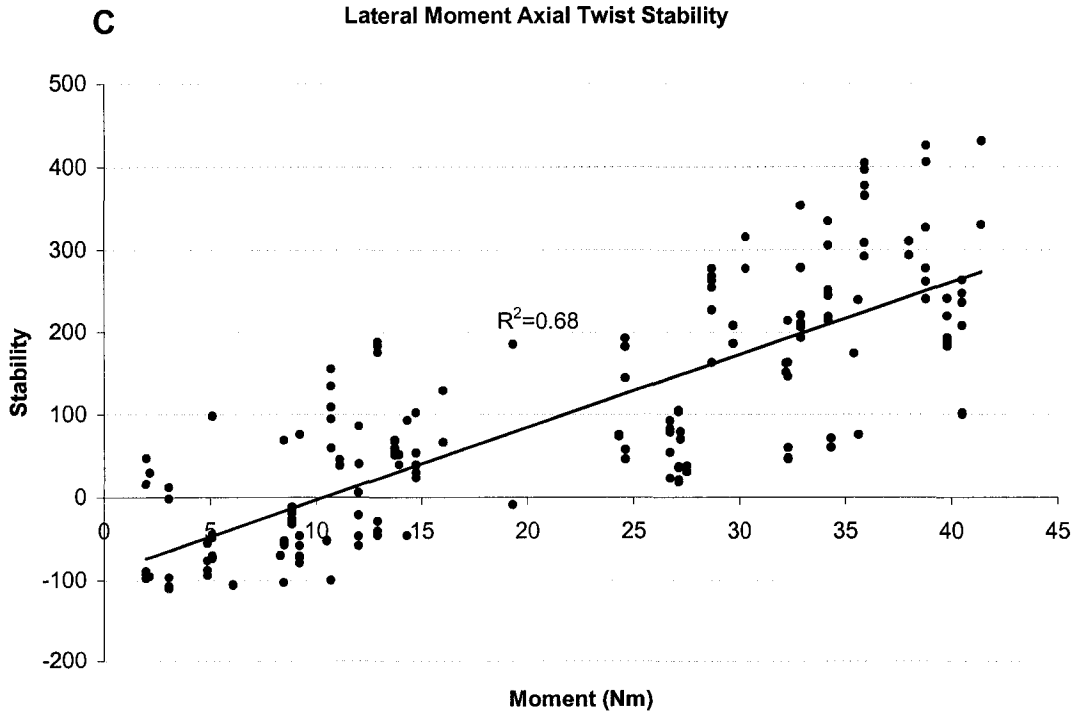
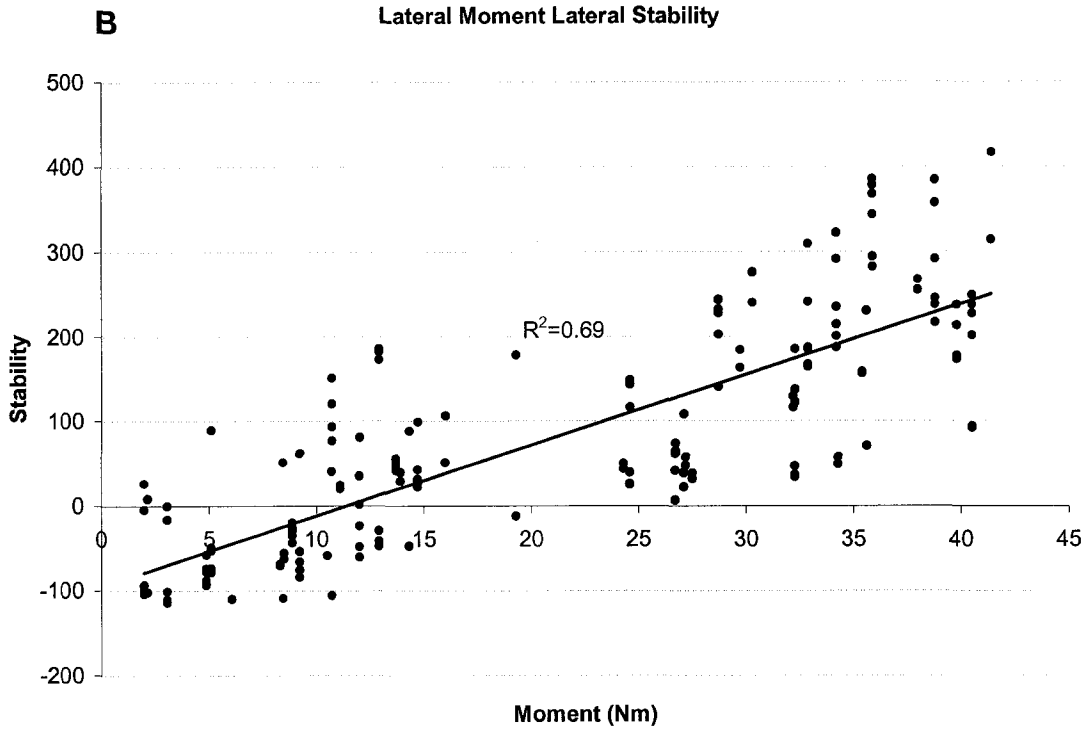


Figure 14. Relationship between external lateral bend moment and stability about the flexion/extension axis (A), lateral bend axis (B), and axial twist axis (C). N = 176.

#### 4.2 Optimization Model Performance

Comparisons were made between the static and ramped experimental data and are shown in Tables 4 and 5 for flexion and lateral bend moment conditions respectively.

**Table 4.** Average (standard error) muscle activation levels (% MVC) for static and ramped Flexion Moment trials, in which external moments were identical. Difference = Static – Ramped.

	RA	EO	IO	LES	TES	MULT	LD	QL
Static	2.2(0.2)	1.9(0.2)	6.6(0.7)	11.3(1.2)	12.5(1.3)	8.8(0.9)	2.1(0.2)	11.3(1.2)
Ramped	2.1(0.2)	1.9(0.2)	6.3(0.7)	9.6(1.0)	11.1(1.2)	7.5(0.8)	1.9(0.2)	9.6(1.0)
Difference	0.1	0.0	0.3	1.7	1.4	1.3	0.2	1.7

**Table 5.** Average (standard error) muscle activation levels (% MVC) for static and ramped Lateral Bend Moment trials, in which external moments were identical. Difference = Static – Ramped.

	RRA	REO	RIO	RLES	RTES	RMULT	RLD	RQL
Static	3.6(0.4)	2.6(0.3)	3.0(0.3)	0.0(0.0)	1.1(0.1)	0.1(0.0)	1.0(0.1)	0.7(0.1)
Ramped	4.1(0.4)	3.2(0.3)	3.3(0.4)	0.0(0.0)	0.8(0.1)	0.1(0.0)	0.9(0.1)	1.0(0.1)
Difference	-0.5	-0.6	-0.3	0.0	0.3	0.0	0.1	-0.3
	LRA	LEO	LIO	LLES	LTES	LMULT	LLD	LQL
Static	6.6(0.7)	10.8(1.1)	9.6(1.0)	4.0(0.4)	4.1(0.4)	3.3(0.4)	5.9(0.6)	5.9(0.6)
Ramped	6.5(0.7)	9.8(1.0)	9.1(1.0)	5.0(0.5)	3.6(0.4)	4.0(0.4)	4.7(0.5)	7.5(0.8)
Difference	0.1	1.0	0.5	-1.0	0.5	-0.7	1.2	-1.6

Average differences were never greater than 2 % MVC for any muscle. Thus, for the remainder of these results, only static data will be presented. It is assumed that the patterns seen in the static conditions are representative of those seen in the ramped conditions.

#### 4.2.1 Definition of Cost Functions Used in the Optimization Model

Two cost functions were tested separately in the current optimization model: 1) minimization of the sum of the cubed muscle forces (SumCubed); 2) minimization of the sum of the squared intervertebral forces at the L4-L5 disc level (InterForce)

#### 4.2.2 Flexion Moment Model

RMS errors between model predicted and experimental forces for each muscle are shown in Figure 15. Figure 16 displays the RMS errors between model predicted and experimental forces averaged across agonist antagonist, and all muscles combined, as well as for compressive force. Standard errors for data presented in line graph form are found in Appendix C Table 11.

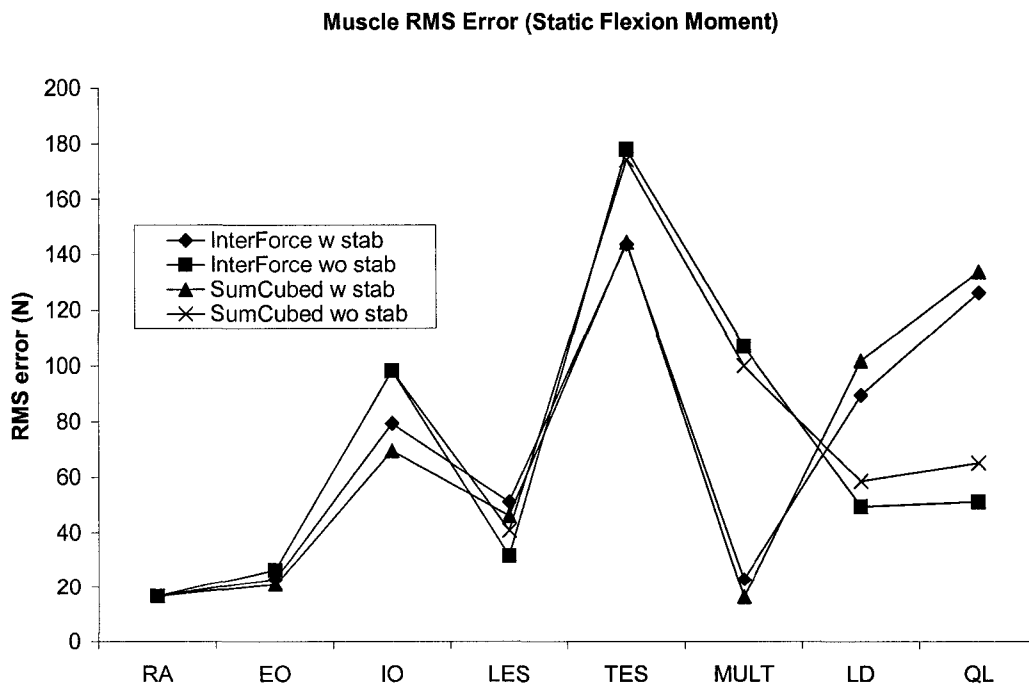


Figure 15. RMS error between model predicted and experimental muscle forces for each individual muscle.

The lowest errors in antagonist muscle force prediction occurred in the SumCubed (with stability) condition, while the highest errors resulted from the SumCubed and InterForce (without stability) conditions. The lowest errors in agonist muscle force prediction occurred in the InterForce (without stability) condition, and the highest errors occurred in the SumCubed (with stability) condition. Averaging across all muscles, the lowest errors were found with the SumCubed (with stability) cost function (RMS error = 68.6 N), followed closely by the InterForce (with stability cost function (RMS error = 69.0 N).

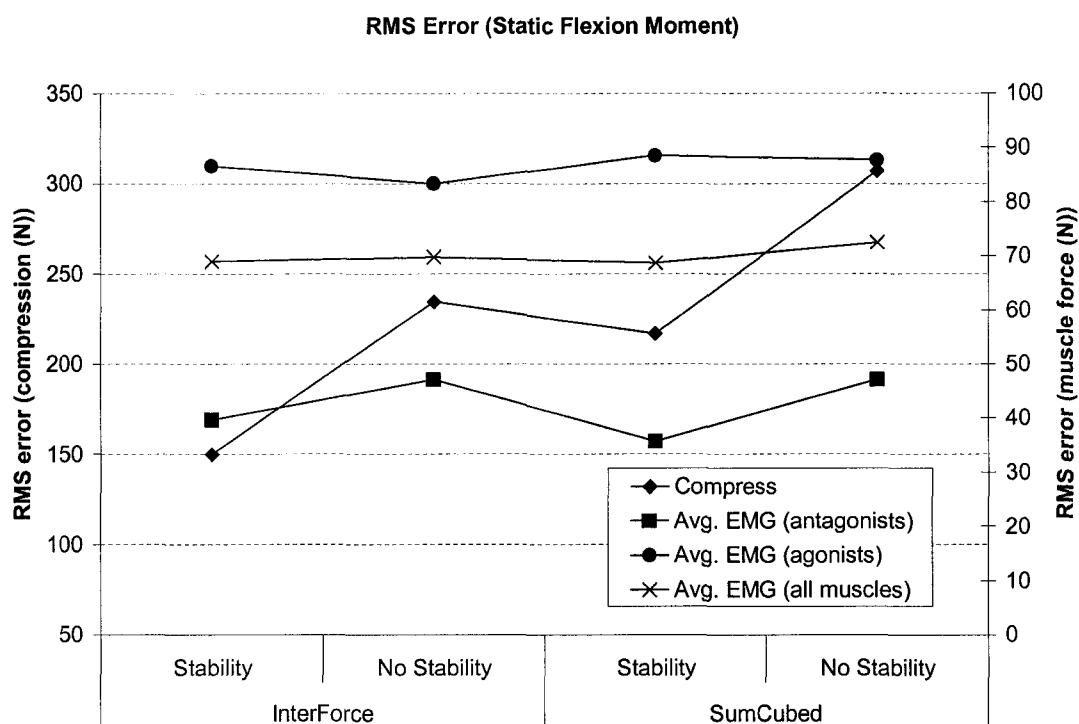


Figure 16. RMS error between model predicted and experimental compressive forces, agonist muscle forces (averaged across agonist muscles), antagonist muscle forces (averaged across antagonist muscles), and all muscle forces combined.

Muscle forces predicted by the optimization models and estimated from EMG recordings, both averaged across all trials, are shown in Figures 17 and 18 for InterForce and SumCubed cost functions respectively. Modeled compressive force predictions and experimentally found compressive forces, both averaged across all trials, are displayed in Figure 19. Actual average experimental compressive forces were found to be higher than those predicted by each of the four optimization schemes.

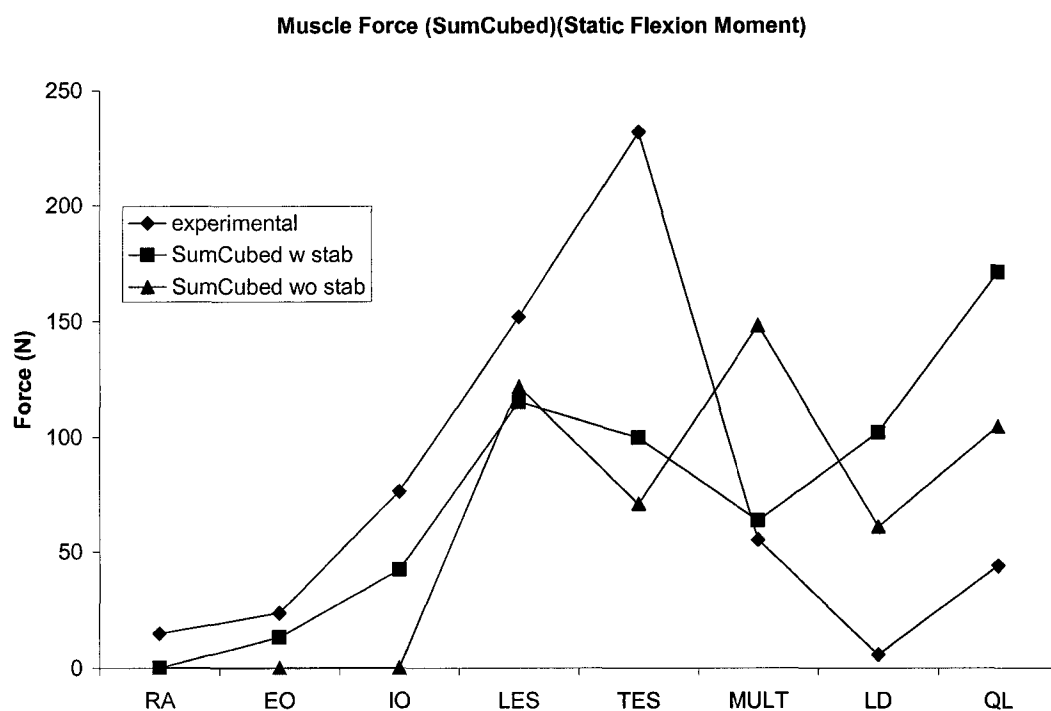


Figure 17. Model predicted muscle forces, using the InterForce cost function, and experimentally found muscle forces, both averaged across all trials, for each individual muscle.

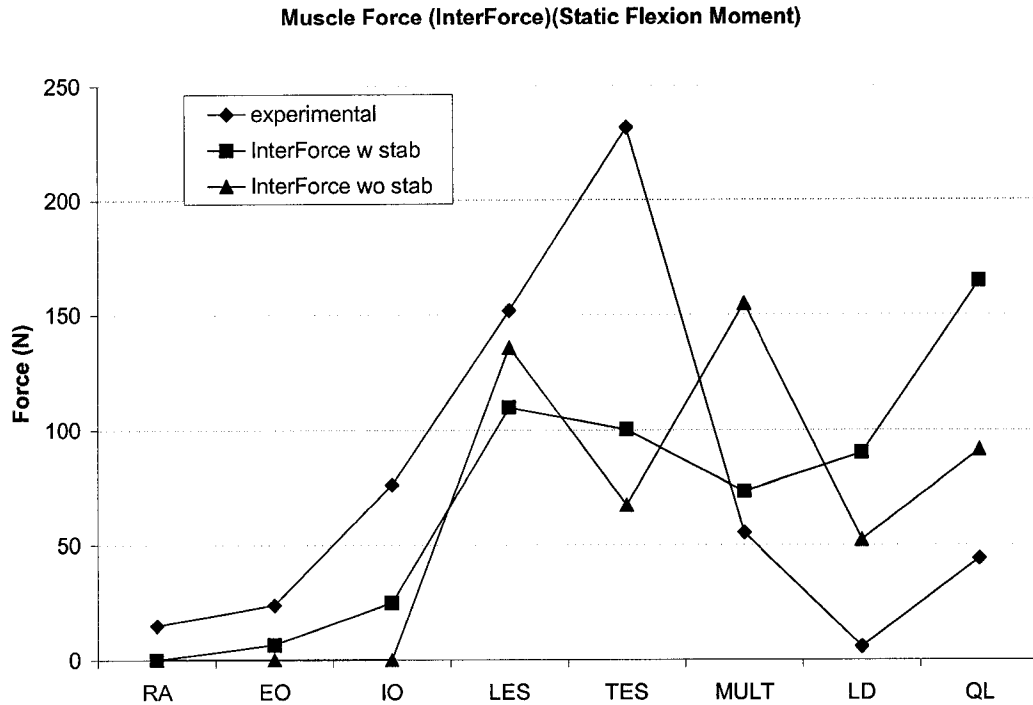


Figure 18. Model predicted muscle forces, using the SumCubed cost function, and experimentally found muscle forces, both averaged across all trials, for each individual muscle.

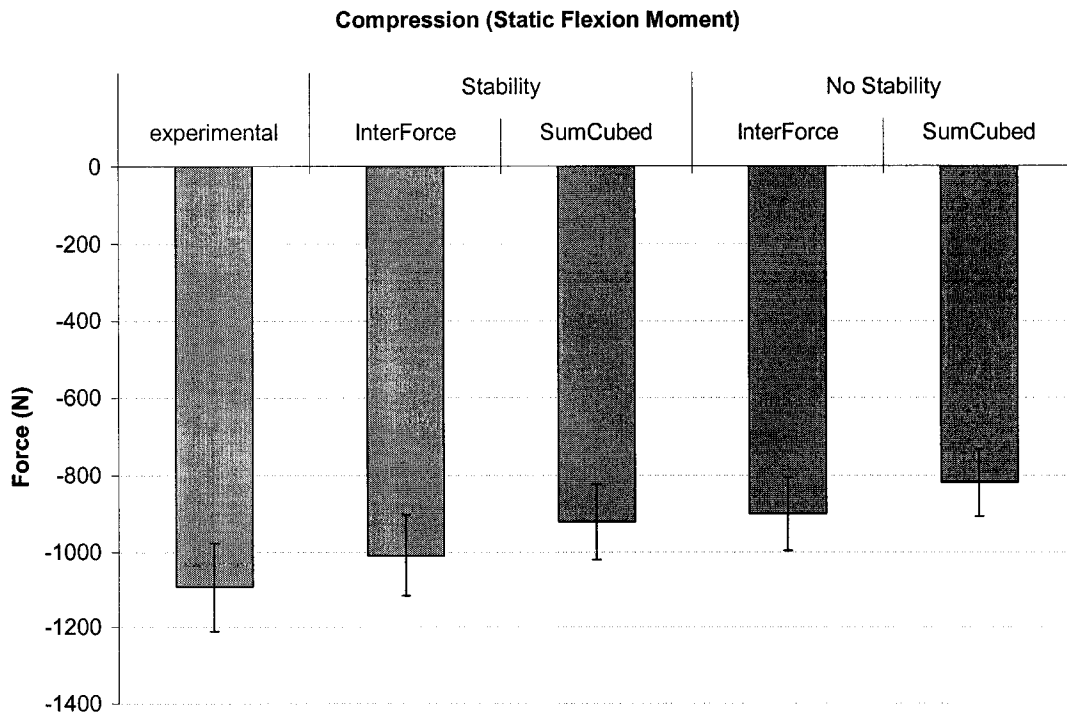
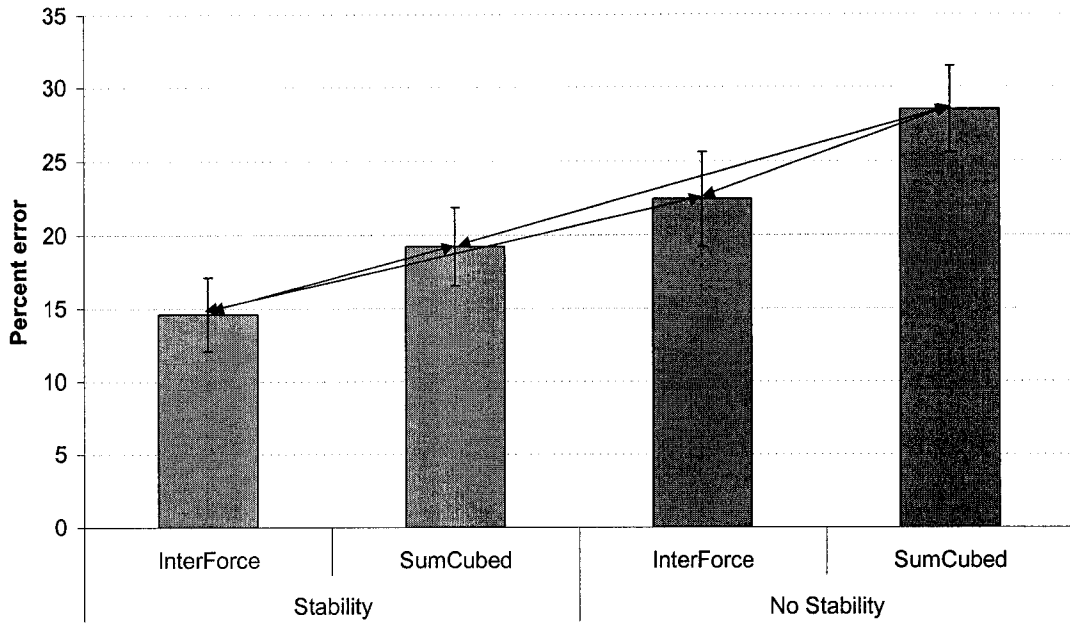


Figure 19. Model predicted and experimentally found compressive forces (N), both averaged across all trials. Standard error bars are indicated.



When collapsed across static and ramped conditions, as well as the two cost functions, the use of stability constraints in the optimization model was found to produce significantly lower errors ( $p < 0.001$ ) in the prediction of compressive force acting at L4/L5. Post hoc analyses showed that each cost function, when constraining stability levels, displayed significantly lower errors ( $p < 0.001$ ) than when not constraining stability levels. The InterForce (with stability) condition demonstrated the lowest percent error (13%). The highest error (27%) was found in the SumCubed (without stability condition). Furthermore, post hocs showed significantly lower errors for the InterForce, rather than the SumCubed criterion, both with and without stability constraints. Figure 20 presents the RMS percent errors, collapsed across static and ramped trials, as well as significant differences between modeled conditions. RMS percent errors between compressive forces predicted by each of the four optimization schemes and those found experimentally, for the Static condition alone, are displayed in Figure 21.

**Compression Percent Error (collapsed across static and ramped) (Flexion Moment)**



**Figure 20.** RMS percent error between model predicted and experimentally found compressive forces, collapsed across static and ramped conditions. Arrows indicate significant differences ( $p < 0.001$ ). Standard error bars are indicated.

**Compression Percent Error (Static Flexion Moment)**

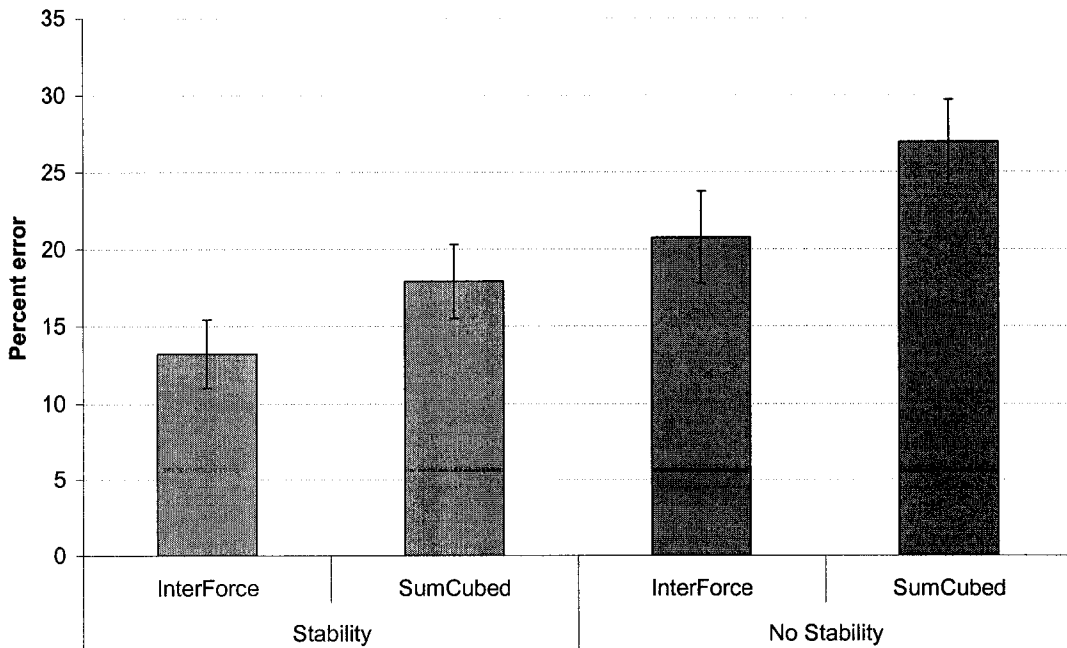


**Figure 21.** RMS percent error between model predicted and experimentally found compressive forces. Standard error bars are indicated.

Average compression levels, both experimental and modeled, did not show any functional difference between trials in which the external load was held at L4/L5 height and those in which the external load was held at a height of 50 percent of the distance between L4/L5 and shoulder (chest height) (Figure 22). Predicted compression levels are not shown for cost functions when stability was unconstrained, as without stability constraints, modeled predictions were identical regardless of external load height.

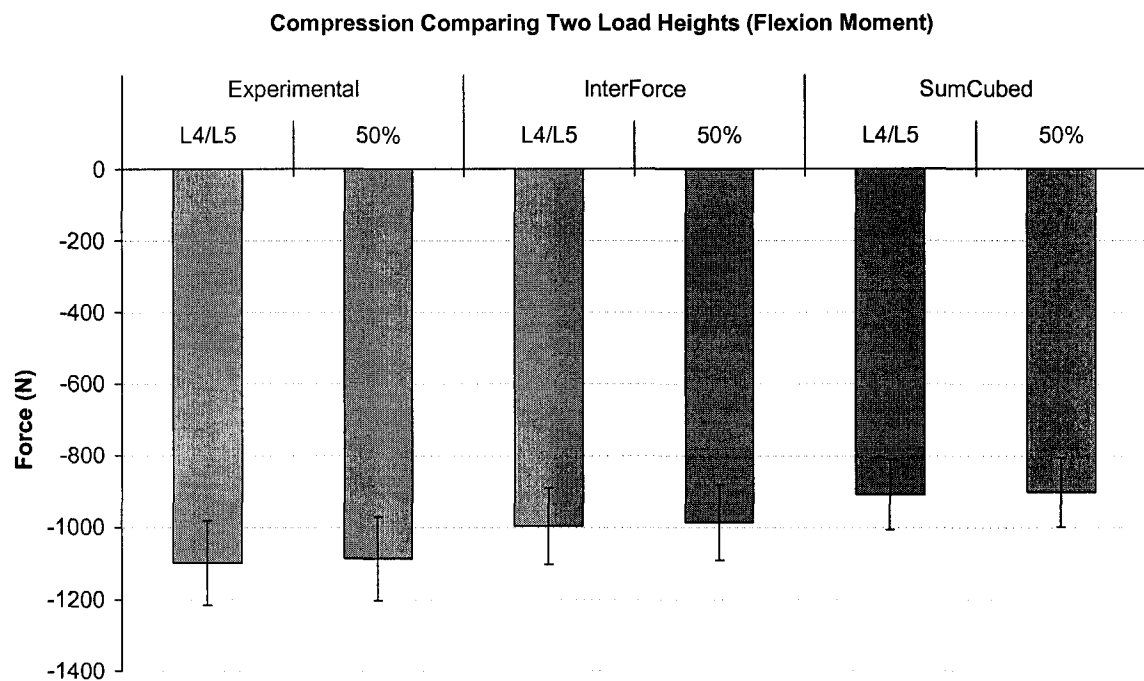


**Figure 22.** Average experimental and model predicted (with stability) compression levels, comparing the two experimental load heights: L4/L5 height and chest height. Averaged across static and ramped conditions. Standard error bars are indicated.

#### 4.2.2.1 *Stability Levels (Flexion Moment)*

Figure 23 displays the average stability values, collapsed across static and ramped conditions, for each axis, 1) determined experimentally, 2) predicted through the regression equations, and 3) found by each of the four optimization schemes.

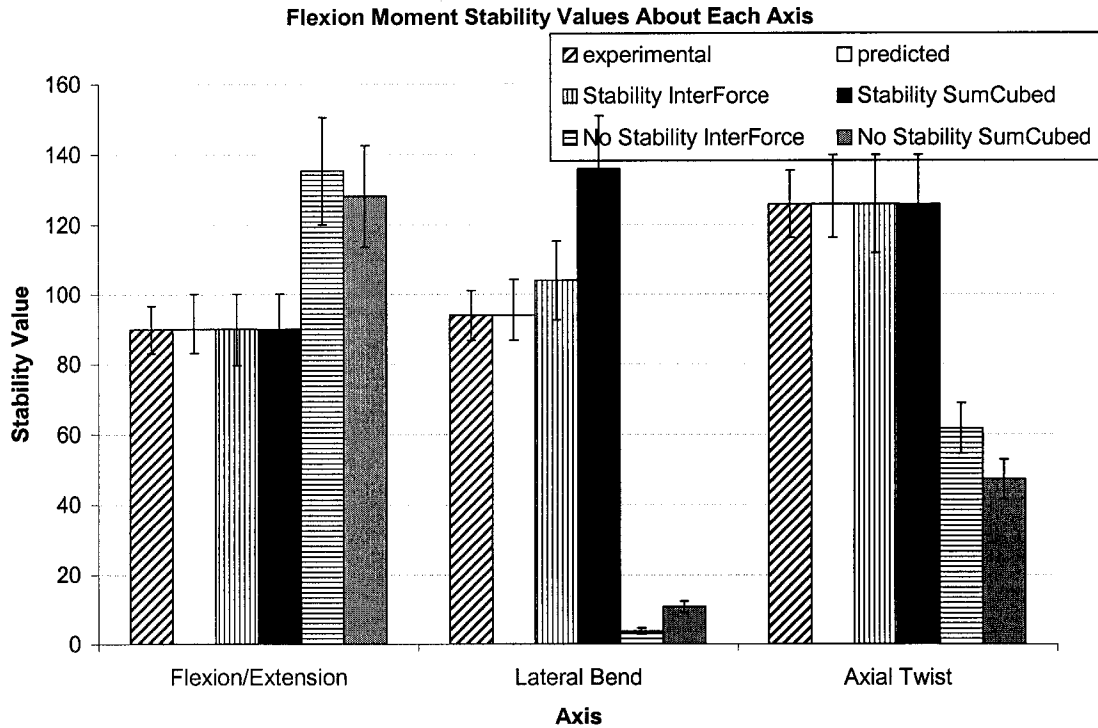


**Figure 23.** Average stability values calculated about each axis, collapsed across static and ramped conditions, for flexion moment trials. Stability values were calculated for experimental trials, predictions from regression equations, and in each of the four optimization schemes. Standard error bars are indicated.

Average stability levels, about each axis, collapsed across static and ramped conditions, were found to be higher when subjects held the external load at L4/L5 height, as compared to chest height (Figure 24).

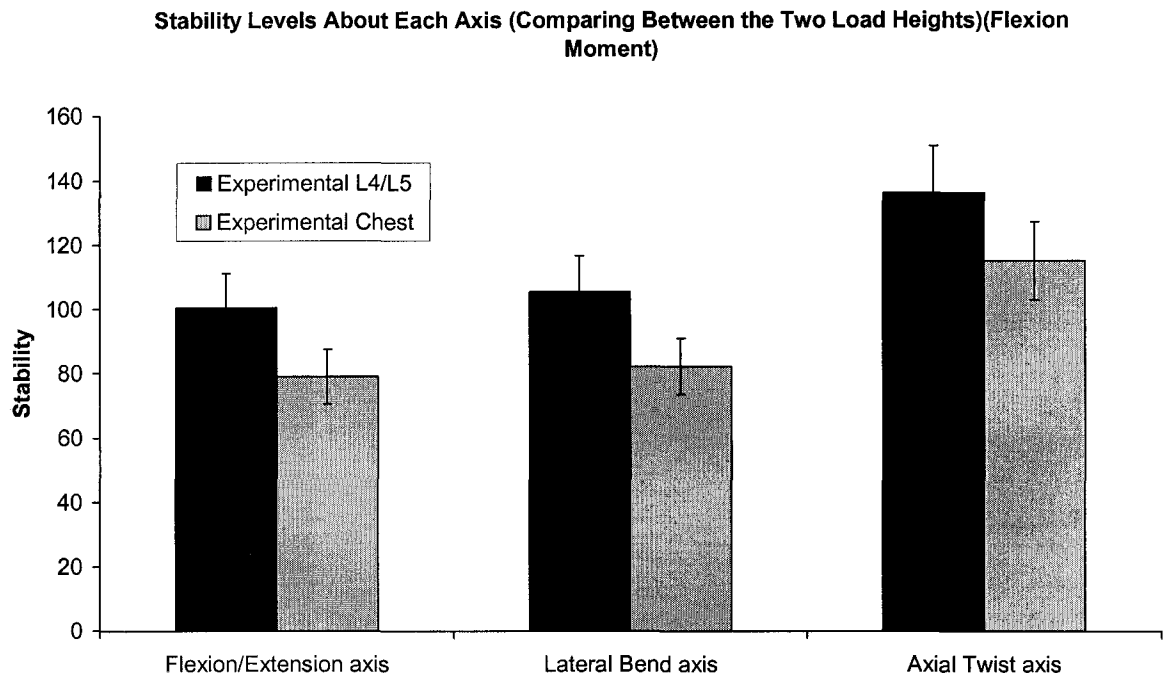
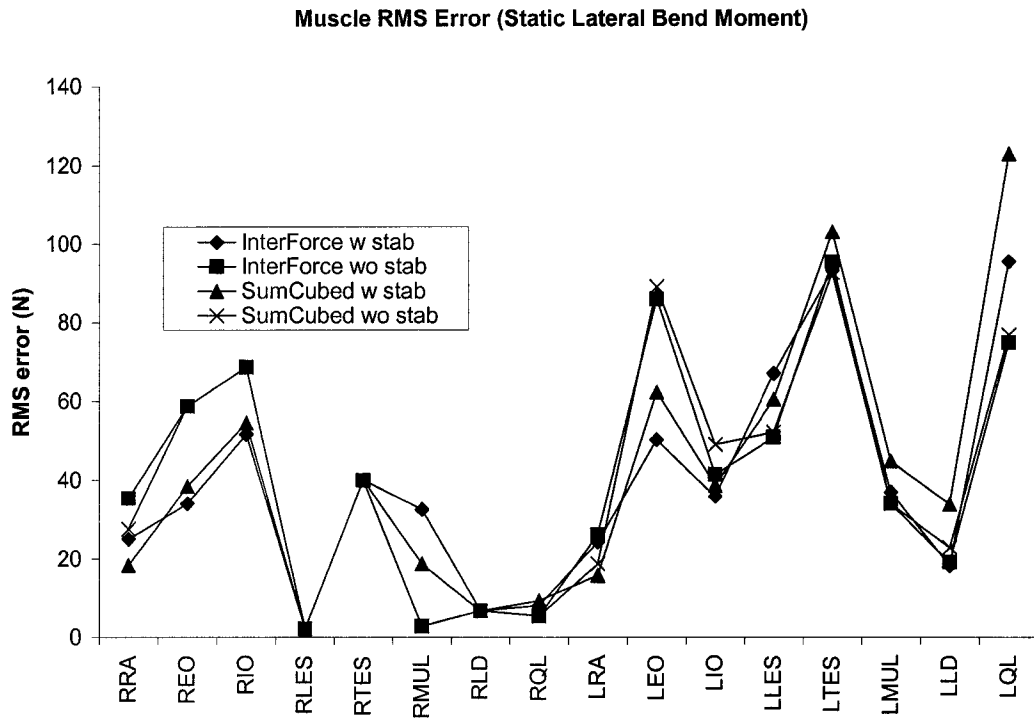


Figure 24. Average experimental stability levels, about each axis, comparing between the two external load heights: L4/L5 and chest height. Averaged across static and ramped conditions. Standard error bars are indicated.

### *Lateral Bend Moment Model*

RMS errors between model predicted and experimental forces for each muscle are shown in Figure 25. Figure 26 displays the RMS errors between model predicted and experimental forces averaged across agonist, antagonist, and all muscles combined, as well as for compressive force.



**Figure 25.** RMS error between model predicted and experimental muscle forces for each individual muscle.

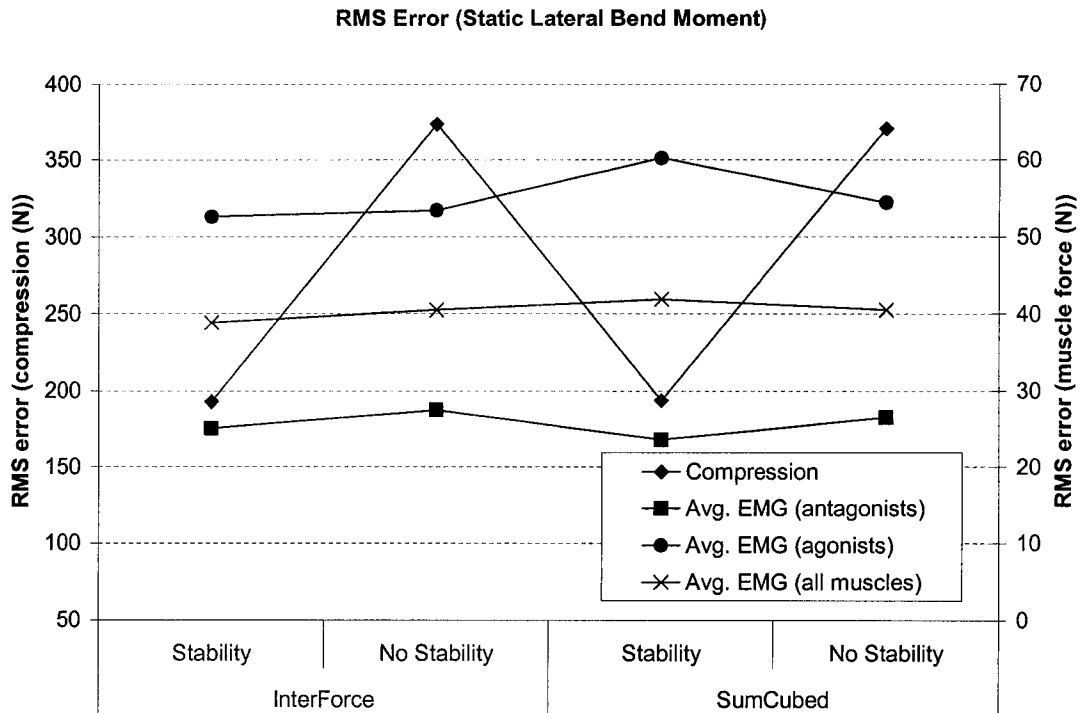


**Figure 26.** RMS error between model predicted and experimental compressive forces, agonist muscle forces (averaged across agonist muscles), and antagonist muscle forces (averaged across antagonist muscles).

The lowest RMS errors between model predicted and experimental antagonist muscle forces occurred in the SumCubed (with stability) condition, for both static and ramped data, with the highest errors occurring in the InterForce (without stability) condition. For agonist muscle force predictions, the lowest RMS errors were found in the InterForce with stability condition, while the highest errors occurred in the SumCubed with stability condition. Averaging across all muscles, the lowest errors were found with the InterForce (with stability) cost function (RMS error= 38.8).

Modeled muscle force predictions and experimentally found muscle forces, both averaged across all trials, are shown in Figures 27 and 28 for InterForce and SumCubed cost functions respectively. The only antagonist muscle to be predicted as active when not constraining stability in the model was the RRA, and this only occurred with the SumCubed cost function. The three abdominal muscles (RA, EO, IO) were predicted, by both cost functions when constraining stability, to be the most active of the antagonist muscles, which was in agreement with experimental force levels.

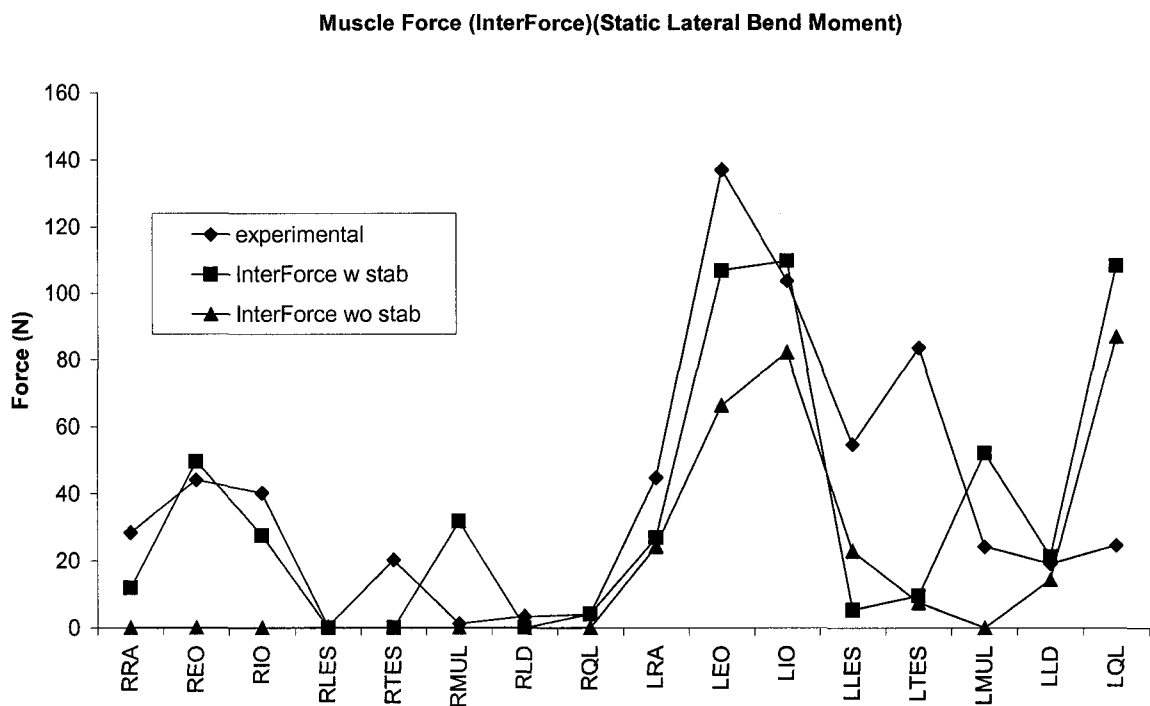
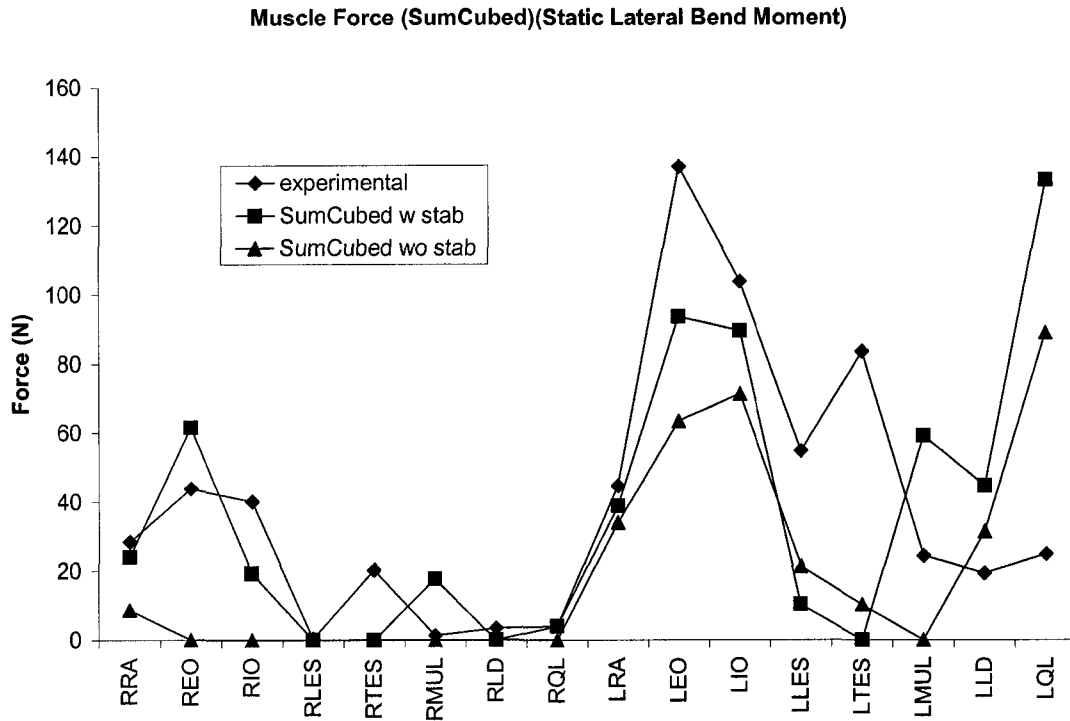


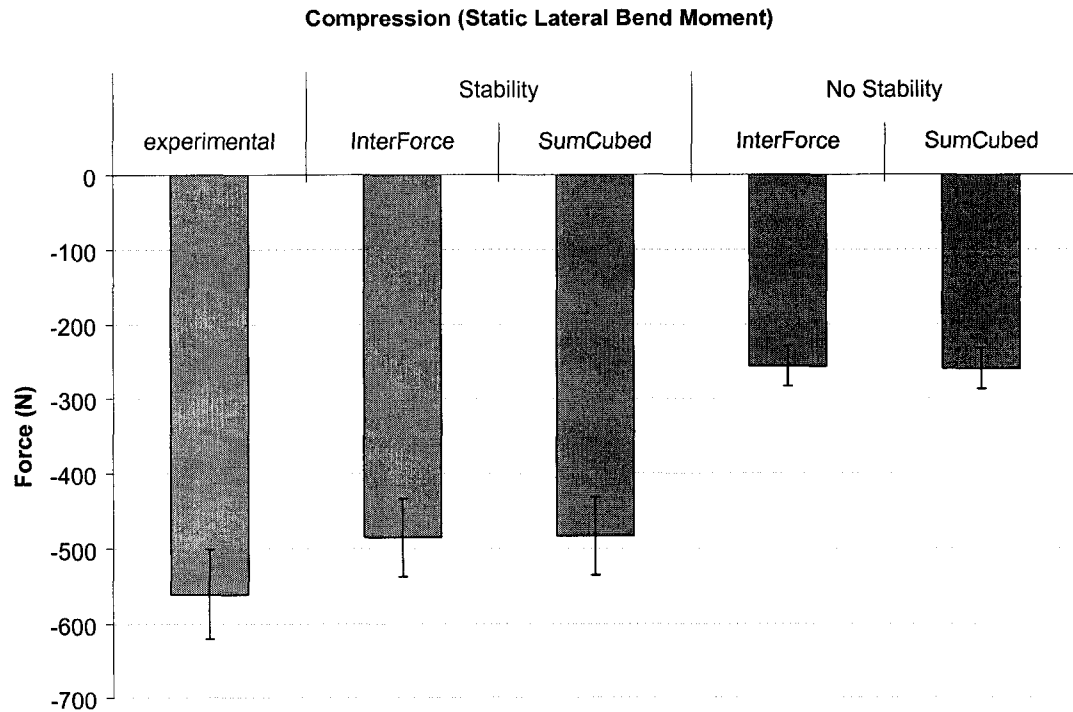
Figure 27. Model predicted muscle forces, using the InterForce cost function, and experimentally found muscle forces, both averaged across all trials, for each individual muscle.





**Figure 28.** Model predicted muscle forces, using the SumCubed cost function, and experimentally found muscle forces, both averaged across all trials, for each individual muscle.

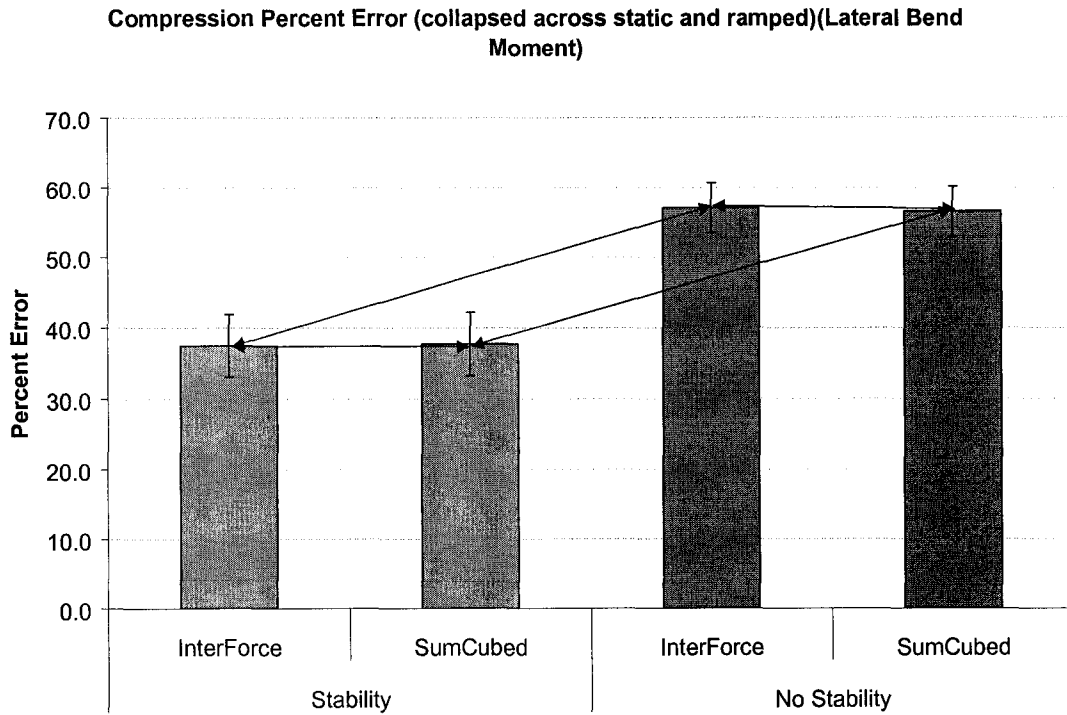
Modeled compressive force predictions and experimentally found compressive forces, both averaged across all trials, are displayed in Figure 29. Modeled compressive force predictions were found to underestimate those found experimentally in all four optimization schemes.



**Figure 29.** Model predicted and experimentally found compressive forces (N), both averaged across all trials. Standard error bars are indicated.

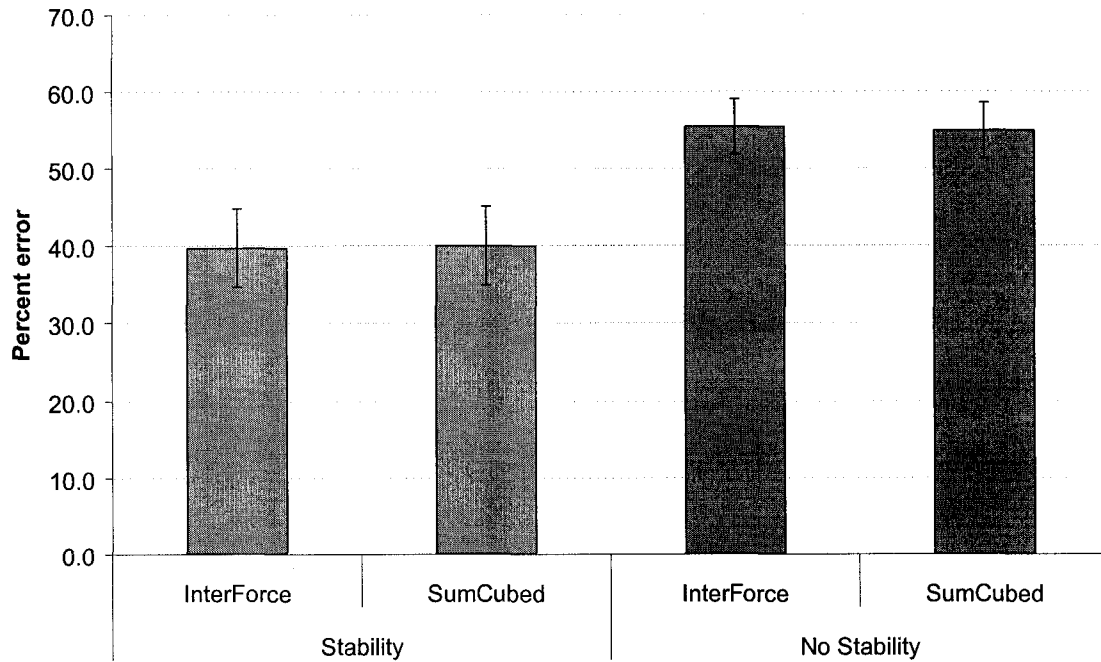
Averaged across static and ramped conditions, as well as the two cost functions, a significant main effect ( $p < 0.001$ ) was found between modeled compression predictions with and without stability constraints. Post hoc showed that, for each cost function, constraining stability resulted in significantly lower compression errors ( $p < 0.001$ ) than not constraining stability in the model. The lowest errors occurred in the InterForce with stability condition (35%). The highest errors were found in the SumCubed without stability condition (55%). Furthermore, it was found that the InterForce cost function produced significantly lower errors ( $p < 0.001$ ) than the SumCubed cost function when stability was constrained; while the SumCubed cost function produced significantly lower errors ( $p < 0.005$ ) than the InterForce cost function when stability was unconstrained.

Figure 30 shows RMS percent errors, as well as significant differences, for compressive force, averaged across static and ramped conditions. RMS percent errors, for the static condition alone, between model predicted and experimentally found compressive forces are displayed in Figure 31.



**Figure 30.** RMS percent error between model predicted and experimentally found compressive forces, collapsed across static and ramped conditions. Arrows indicate significant differences ( $p < 0.001$ ). Standard error bars are indicated.

**Compression Percent Error (Static Lateral Bend Moment)**



**Figure 31.** RMS percent error between model predicted and Static experimentally found compressive forces. Standard error bars are indicated.

Average compression levels, both experimental and modeled, did not show any functional change between trials in which the external load was held at L4/L5 height and those in which the external load was held at chest height (Figure 32). Predicted compression levels are not shown for cost functions when stability was unconstrained, as without stability constraints, modeled predictions were identical regardless of external load height.

Compression Comparing Two Load Heights (Lateral Bend Moment)

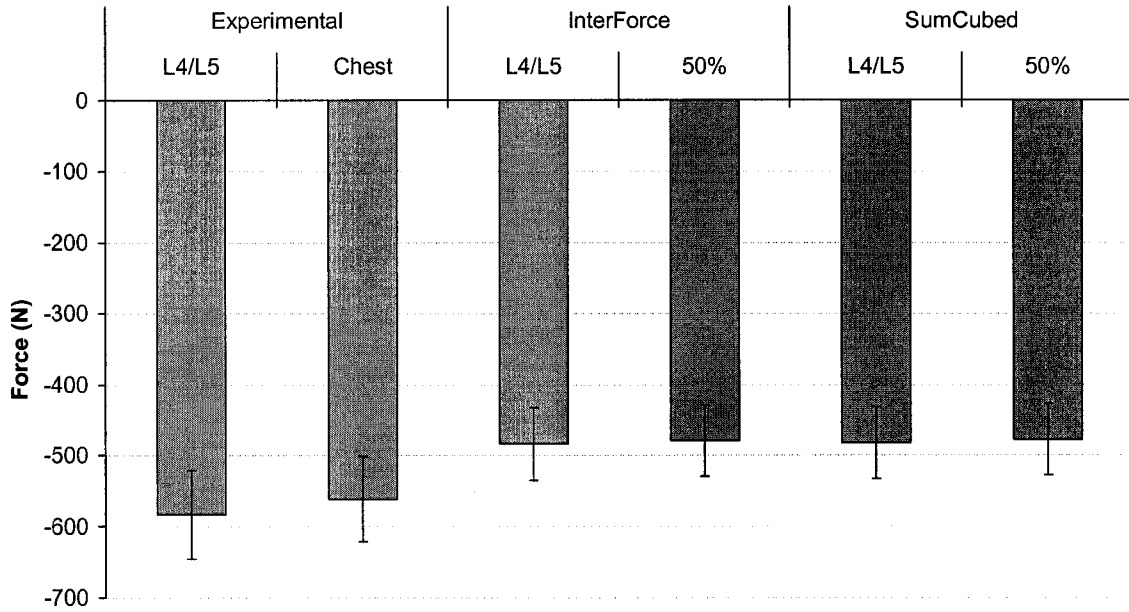
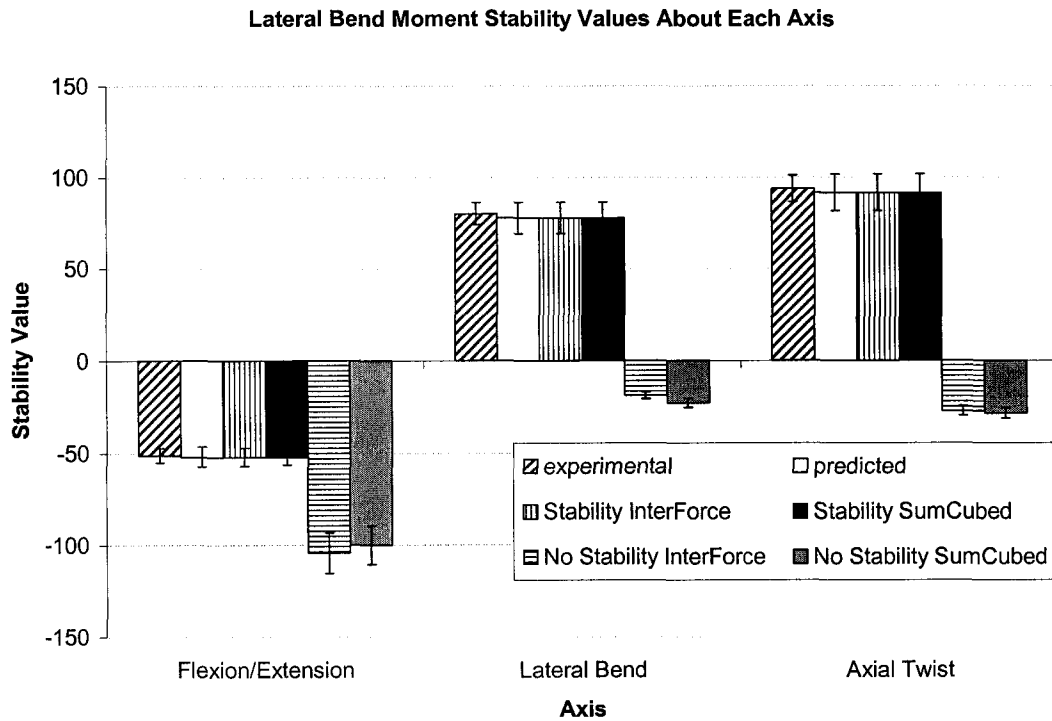


Figure 32. Average experimental and model predicted (with stability) compression levels, comparing the two experimental load heights: L4/L5 and chest height. Averaged across static and ramped conditions. Standard error bars are indicated.

#### 4.2.3.1 *StabilityLevels (Lateral Bend Moment)*

Figure 33 displays the average stability values, collapsed across static and ramped conditions, for each axis, determined experimentally, predicted through the regression equations, and found by each of the four optimization schemes.



**Figure 33.** Average stability values calculated about each axis, collapsed across static and ramped conditions, for flexion moment trials. Stability values were calculated for experimental trials, predictions from regression equations, and in each of the four optimization schemes. Standard error bars are indicated.

Average stability levels, about each axis, collapsed across static and ramped conditions, were found to be higher in trials in which the external load was held at L4/L5 height, as compared to chest height (Figure 34).

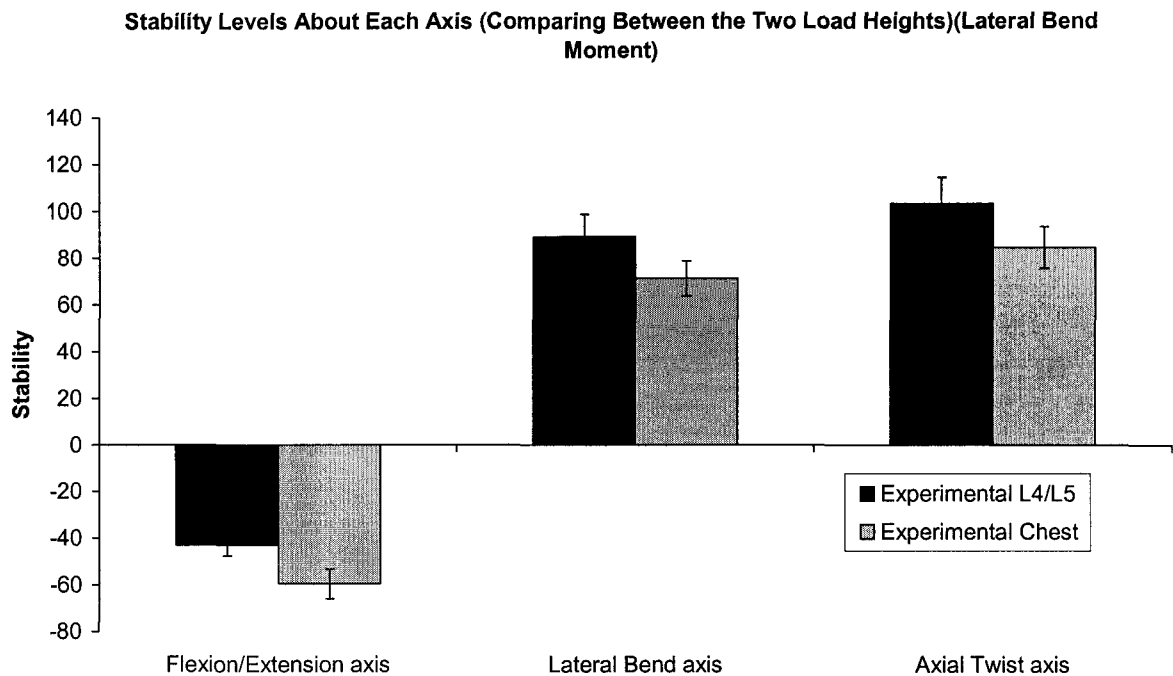


Figure 34. Average experimental stability levels, about each axis, comparing between the two external load heights: L4/L5 and chest height. Averaged across static and ramped conditions. Standard error bars are indicated.

## *Chapter 5*

### **DISCUSSION**

The purpose of this study was to demonstrate a method incorporating mechanical spine stability as a constraint in an optimization model, to improve muscle activation predictions (specifically of antagonist muscles), and subsequent estimates of spinal loading. Two cost functions were used: 1) minimization of the intervertebral force at the L4/L5 level; 2) minimization the sum of the cubed muscle forces. In both cases, employing the stability constraint succeeded in producing antagonist muscle forces and improved predictions of compressive loads on the spine. Pure antagonist muscle forces have never previously been demonstrated in optimization models of the spine. Thus, this indicates that trunk muscle recruitment patterns are, at least in part, dictated based on stabilizing the spine to an optimal level for a given loading situation.

The following discussion will break down the model performance by flexion and lateral bend simulations, and within these by agonist and antagonist muscle groups. Individual muscle and compressive force predictions will be addressed as well. Furthermore, the relevance of the findings will be discussed, as will new insights into the mechanisms of trunk muscle function.

#### **5.1 *Hypotheses Revisited***

1. *An optimal level of spinal stability exists somewhere between the maximum and minimum levels possible for a given loading situation. It is predicted that this*



*optimum level of stability will occur at a level that is marginally above the minimum possible level and will result in the lowest errors. The highest errors will be observed in the model when stability is maximized.*

Although minimum and maximum stability were not calculated for experimental trials, the true stability levels about each axis were found towards the lower end of the possible range. Only stability values predicted from regression equations generated from the experimental data were used as constraints in the optimization model, and thus the second part of this hypothesis cannot be addressed.

2. *The optimal level of spinal stability will show a positive non-linear relationship with the moment demand of the task.*

In flexion trials, the stability about the dominant (flexion/extension) axis displayed a positive  $r^2$  of 0.83 with external moment (Figure 13). Stability about the lateral bend and axial twist axes showed positive  $r^2$ s with external moment of 0.31 and 0.44 respectively. In lateral bend trials, the stability about the dominant (lateral bend) axis displayed a positive  $r^2$  of 0.69 with external moment (Figure 14). Stability about the flexion/extension and axial twist showed positive  $R^2$ s with external moment of 0.65 and 0.68 respectively. Thus, the optimal level of stability did show a positive relationship with the moment demand of the task. The high correlations, however, indicate that the relationship may be more linear, at least for the loading tasks examined here, than was hypothesized. It is possible that under more demanding conditions, the relationship would exhibit a higher degree of non-linearity, as optimal stability levels may increase to a higher degree

as the loading tasks became so difficult as to put the spine in an elevated danger of being injured.

3. *An optimization model of the spine, with a constraint being a measure of optimal spinal stability, will accurately predict and reproduce muscle recruitment patterns in the trunk. More specifically, the model will predict opposing muscle groups to be active simultaneously during the tasks examined.*

Including measures of spinal stability in the optimization model did slightly improve the overall prediction of muscle recruitment patterns in three of four cases, as compared to the optimization model without accounting for stability levels. Average RMS errors, for muscle forces averaged across all muscles, were improved with both the InterForce and SumCubed cost function in static flexion, and with the InterForce function in static lateral bend. However, including measures of spinal stability caused slightly higher errors in muscle force predictions with the SumCubed cost function in static lateral bend.

In every case, including a measure of stability as a constraint promoted the prediction of antagonistic muscle activation. In flexion, IO was activated 100 % of the time, EO 75 % of the time, while RA was never activated. In Lateral Bend, percent of trials in which antagonistic muscles were activated was as follows: RRA 100 %, REO 100 %, RIO 100 %, RLES 0 %, RTES 0 %, RMULT 100 %, RLD 1 %, RQL 36 %.

The inclusion of stability constraints in the optimization model of the spine was successful in predicting opposing muscle groups to be active simultaneously in the loading situations examined. Furthermore, a more accurate representation of

the overall muscle recruitment patterns of the trunk was observed, when compared to an optimization model in which stability was unconstrained. This indicates that constrained spinal stability levels are essential in producing realistic trunk muscle force and spine loading estimates in optimization models of the spine.

## *5.2 Model Performance*

It was found that each cost function InterForce and SumCubed, performed significantly better in the prediction of compression with the inclusion of stability constraints in the model. This indicates that the stability level about the L4/L5 joint plays a significant role in determining spinal loading, most likely through the adjustment of muscle forces.

Stokes and Gardner-Morse (2001) tested optimization cost functions while simultaneously maximizing the stability level of the entire lumbar spine, and showed a decreased ability to realistically represent trunk muscle forces and spine loading. The major difference in this study, however, was the use of “optimal” stability levels, rather than maximum levels. The “optimal” level of stability occurs far below the maximum possible in a given loading situation, and thus by forcing stability to be at a maximum, muscle and compression forces are greatly overestimated.

Lower RMS errors were found when utilizing the InterForce cost function, demonstrating that it more closely represents what the CNS is attempting to optimize in spinal muscle recruitment.

A significant interaction effect occurred between stability and cost function in the prediction of compression. This indicates that the effect of adding stability constraints to the model is significantly different between the two objective functions. It is probable that the improvements with the inclusion of stability are larger when utilizing the InterForce than the SumCubed function. This is most likely due to the lower penalty, of squaring rather than cubing muscle forces, incurred with the InterForce cost function, which may provide more room for the adjustment of muscle forces while solving for the minimized cost. Furthermore, InterForce as a whole may perform better than SumCubed due its direct consideration of the cost of high moment generation, which is neglected by SumCubed, yet clearly plays a large role in spinal loading.

A major finding of this study was the prediction of coactivity of trunk muscles, in both flexion and lateral bend conditions, when including stability as a constraint in the model. This has never before been reported in the literature for optimization modeling of the spine. In recent years, the importance of antagonistic muscle activity in maintaining stability of the spine has been greatly investigated. Numerous studies have reported coactivation of trunk muscles in a variety of loading conditions (Granata & Marras, 1995; O'Brien & Potvin, 1997; Gardner-Morse & Stokes, 1998; Krajcarski et al., 1999; Chiang & Potvin, 2001). Moreover, these researchers have theorized that this antagonistic activity functions almost exclusively as a means of stabilizing the spine. The results of the current study further reinforce this notion and shed new light into the exact mechanism of how and why trunk muscles are recruited under static loading conditions. Based on these findings, it is clear that the CNS recruits muscles, at least in part, so as to ensure optimal stability levels in the spine.

Table 8 in Appendix B details the moment and stabilizing potential, about each axis, of each right side muscle, normalized to the total potential of all right side muscles combined. Table 9 in Appendix B displays absolute stabilizing and moment potentials for each right side muscle, as well as a ratio between the two potentials. Appendix B Table 10 provides a summary, for each axis, of each individual muscle fascicle's 3-dimensional moment arm (for moment generating purposes), 2-dimensional moment arm (for stabilizing purposes), full fascicle length, and length of the fascicle vector where it crosses L4/L5.

For the purposes of this thesis, stabilizing efficiency of muscles will be inferred based on the ratios of stabilizing potential to moment potential presented in Table 9. This is based on the concept that a muscle with a high stabilizing vs. moment potential ratio is able to stabilize at a relatively high level while producing a relatively low amount of movement, and thus loading, on the spine. In other words, such muscles, when highly active, will contribute greatly to stabilizing the spine, but will not generate very high moments about the axis in question. These muscles may thus be considered primarily stabilizers in their function.

### ***5.2.1 Flexion Moment Trials***

Including a measure of stability as a constraint with each cost function significantly improved the prediction of the compressive force acting at L4/L5. Percent RMS error for the SumCubed cost function was reduced from 27 % to 18%; while error for the InterForce cost function was reduced from 21 % to 13% (Figure 21). Thus, lowest

errors occurred when including stability constraints with each cost function, with InterForce being the best predictive cost function.

Errors in predicted compressive forces found in this study, without using the stability constraints, are very comparable to those of Cholewicki et al. (1995), who showed percent RMS errors of 30 % in ramped trunk flexor moment trials when incorporating a double linear optimization scheme minimizing muscle stress followed by compression.

Average predicted compression levels were underestimated in all four optimization schemes (Figure 19). Average predicted levels were closer to those found experimentally in static compared to the ramped trial conditions.

Collapsed across static and ramped trials, stability levels in the dominant, flexion/extension axis were overestimated in optimization simulations in which stability was not constrained (Figure 23). Stability levels in the lateral bend and axial twist axes were highly underestimated under these same conditions. In fact, instability in at least one of these axes was predicted to occur in 52 % of trials with the InterForce (without stability) cost function and in 48 % of trials with the SumCubed (without stability) cost function, as compared to 3 % of trials with each cost function when stability was included as a constraint. Experimentally, instability in at least one axis actually occurred in approximately 15 % of all trials.

#### **5.2.1.1 Antagonist Muscles**

In flexion conditions, subjects resisted an external load with their hands directly anterior to their body. This produced an external moment in the anterior, or trunk

flexion, direction. Thus, trunk muscles in which activity creates anterior flexor moments, are considered to act as antagonists to the balancing of the external moment. In the current model, these muscles are the RA, EO and IO.

In both static and ramped conditions, RMS error in predicting antagonist muscle activity, with either cost function, was lower when including stability constraints (Figure 15). Lowest errors occurred with the SumCubed cost function. When not including stability constraints in the model, antagonist muscles were never predicted to be active. This is consistent with numerous studies done in the past (eg. Schultz et al., 1982; Cholewicki et al., 1995).

Following is a discussion of the stability role of each muscle monitored.

#### **5.2.1.1.1 Rectus Abdominus**

RA was never predicted to be active in any of the trials, for any of the four optimization schemes. Tables 8 and 9 show that RA, in the flexion/extension axis, has both the highest moment generating potential and the highest stabilizing potential of any of the antagonist muscles. In modeled simulations, its high moment potential may negate its stabilizing ability, as activity levels will cause a high additional anterior moment, which in turn has to be offset by additional agonist activity. Moreover, RA has very low stabilizing potential about the lateral bend and axial twist axes, which further reduces its overall efficiency as a stabilizer under the current conditions.

Experimentally, RA was the least active of the three antagonist muscles (Figures 17 and 18). This was consistent with similar studies showing RA activity of approximately 1-2 % when holding a static load anterior to the body (Brown, Haumann and Potvin, 2003; Granata et al., 2001). Furthermore, this indicates that the current

modeled representation of RA activity is highly representative of that seen experimentally, and that the theorized reasons for the absence of modeled RA activity may hold bearing in actual physiological human spine loading.

#### **5.2.1.1.2 External Oblique**

EO was predicted to be active in approximately 68 % of InterForce trials and 82 % of SumCubed trials. EO has moment and stabilizing potentials slightly lower than RA in flexion/extension, yet is far superior to RA in stabilizing about the other two axes (Tables 8 and 9). Subsequently, activating EO seems to be necessary in the majority of modeled trials, possibly because IO (with a much lower flexor moment potential) on its own cannot produce sufficient levels of stability. This is especially apparent with the SumCubed cost function, as the additional penalty of cubing the muscle forces, and thus preventing any one muscle from over-activating, seems to promote EO activation a higher percentage of the time.

Predicted RMS errors in EO force levels were improved by including stability constraints with each cost function (Figure 15). However, EO levels are still underestimated in the optimization schemes incorporating stability (Figures 19 and 20).

#### **5.2.1.1.3 Internal Oblique**

IO was predicted to be active in 100 % of the modeled trials. RMS errors in predicted IO force levels were improved, with both cost functions, by including stability as a constraint in the model (Figure 15). Its activity level was predicted to be highest amongst the antagonist muscles, which is supported by experimental findings here



(Figures 17 and 18) and elsewhere (Granata et al., 2001). IO has the lowest flexor moment potential of the three antagonist muscles (Table 8), which makes it a preferable choice to activate as it necessitates the least amount of additional agonist activity. Furthermore, its stabilizing potential, while being the lowest of the three antagonists in flexion/extension, is the second highest amongst all muscles in the lateral bend and axial twist axes (Table 8). These factors make IO an efficient stabilizer of the lateral bend and axial twist axes under the current conditions

It appears that, in conditions in which a pure anterior external moment exists, optimal stability levels in the flexion/extension axis are predominantly fulfilled by the agonist muscle forces required to balance the external moment, while the antagonist muscles (especially EO and IO) primarily function to stabilize the lateral bend and axial twist axes. This notion is supported by the observation that in optimization trials where stability levels were not constrained, stability in the flexion/extension axis was overestimated while stability in the other two axes was underestimated (Figure 23).

Overall, in flexor moment conditions, it appears that the models including stability constraints, do a far superior job in predicting antagonist muscle activity, and thus coactivation, than those models without stability constraints where antagonist activity is completely neglected. Furthermore, the model predicts muscle recruitment patterns (IO > EO > RA) that mirror experimental findings in this study and elsewhere (Granata et al., 2001).

### **5.2.1.2 Agonist Muscles**

Muscles causing extensor moments, and thus considered to be agonists under current conditions are: LES, TES, MULT, LD, and QL. All agonist muscles were predicted to be active in every trial for all four optimization schemes. Including stability constraints in the model lead to increased RMS errors in the prediction of agonist muscle forces (Figure 16).

#### **5.2.1.2.1 Lumbar Erector Spinae**

For both static and ramped trials, LES RMS errors were increased, by a relatively small amount, with the inclusion of stability as a constraint in the model (Figures 15). All four optimization schemes lead to underestimation of LES forces (Figures 17 and 18).

LES is shown to have the highest stabilizing potential (27 % of total), and the second highest antagonist moment potential (27 % of total) of all muscles in the flexion/extension axis (Table 8). The small change in error with the inclusion of stability in the model may indicate that LES, in the flexion/extension axis, acts primarily as a moment generator, and its stability contribution is a by-product of its moment balancing responsibilities. The fact that predicted LES activity decreased with the inclusion of stability constraints reinforces this notion, as it seems that LES, at the level predicted without stability constraints, produces stability levels beyond those needed under the current conditions.

Experimentally, LES is shown to be the second largest force producing muscle, behind only the TES (Figures 17 and 18). The large cross-sectional area, and thus force producing potential, of these two muscles makes this likely to be the case under

conditions with a dominant anterior moment acting on the body. Previous studies have shown these two muscles to be highly active under similar conditions (Brown et al., 2003; Haumann, 2002). In the current model, both with and without stability constraints, LES is also predicted as the second largest force generator. However, rather than TES, it falls behind QL when stability is considered and behind MULT when stability is not considered.

#### **5.2.1.2.2 Thoracic Erector Spinae**

Inclusion of stability constraints, with either cost function, created a decrease in the RMS error of predicted force levels (Figure 15). However, TES force levels were well underestimated in all four optimization schemes, producing the highest RMS errors of any muscle.

The lowest errors occurred employing the InterForce (with stability) cost function, and the highest errors occurred with the InterForce (without stability) cost function. Thus, it appears that the inclusion of stability as a constraint had a greater effect on the InterForce than on the SumCubed cost function in the ability to predict TES force levels. This may be, in part, due to the differences in LES predicted force levels. The InterForce cost function is capable of enabling higher LES force predictions due to decreased penalty of squaring rather than cubing muscle forces. Thus, the higher LES levels, without stability, cause TES levels to be lower than in the SumCubed condition, thereby creating increased errors. With stability being considered, LES is reduced, possibly for the reasons discussed in the last section, in turn raising predicted TES levels to a higher degree with the InterForce than with the SumCubed cost function.

Experimentally, TES is shown to be, by far, the largest force producing trunk muscle (Figures 17 and 18). However, with the stability constraints, it is predicted to be the third largest force producer, behind QL and LES; while without the stability constraints, it is predicted to be the fourth largest, behind MULT, LES and QL. TES is the greatest potential generator of trunk extensor moment (Table 8). Its stabilizing potential in the flexion/extension axis is behind only LES and MULT, while, of the posterior muscles, it is the greatest potential stabilizer of the axial twist axis. However, each of the three TES fascicles have a long total length ( $L$ ) and a nodal point at the L4 vertebrae level. This nodal point is, in essence, what determines the stabilizing efficiency of the muscle about a particular joint. Only the muscle vector crossing L4/L5 is considered in the calculation of the length change ( $\Delta l$ ) in the muscle work equation (equation 6), and the length ( $l$ ) in the final stability equation (equation 16). The L4 nodal points create a short  $l$  and thus make the TES a relatively inefficient stabilizing muscle, as is seen by the low ratio of stability to moment potential in Table 9.

In addition, the high moment potential of the TES most likely prevents it from being predicted as a higher, and thus more realistic, force producer. The nature of the two cost functions incorporated into this model is that they promote a balance in muscle forces rather than the domination of one or two muscles. Theoretically, high TES activity produces such a large extensor moment that other muscles are not required to contribute. Thus, by lowering TES force levels, other muscles are able to contribute to a higher degree, thereby leading to the minimization cost functions being solved.

### 5.2.2.2.3 Multifidus

RMS errors between predicted MULT force values and those found experimentally were decreased greatly by incorporating stability constraints into the model (Figure 15). In fact, MULT experienced the largest absolute improvements of any muscle.

In all four optimization schemes, for both static and ramped trials, MULT force predictions were overestimated (Figures 17 and 18). Without stability constraints, MULT was predicted to be the largest force producer of all muscles under current conditions. Including stability constraints in the model caused the predicted MULT muscle forces to decrease a large amount, resulting in the much smaller errors described earlier. The MULT muscle group is a powerful spine stabilizer in the flexion/extension axis, with the ability to produce approximately 23 % of the total stabilizing potential (Table 8). Its high activity level in optimization trials without stability constraints is most likely the major factor responsible for the overestimation of stability levels in the flexion/extension axis (Figure 23). The large changes in activation level with the incorporation of stability constraints into the model provides support for previous hypotheses that deep, intersegmental muscles play an important role in the stability of the spine (Cholewicki and McGill, 1996). However, it is interesting that, as a whole, it may be important to limit the activity of these muscles, as they may produce stability levels beyond those deemed optimal by the CNS. Future studies should examine the role of MULT under conditions in which stability is threatened to determine the exact role these muscles play in stabilizing the spine.

#### **5.2.2.2.4 Latissimus Dorsi**

RMS errors for LD prediction increased, in both static and ramped trials, with the inclusion of stability constraints in the model (Figure 15). Average predictions of LD force were overestimated in all four optimization schemes.

Experimentally, the LD was shown to be the lowest force producer of all muscles, with average forces across all trials of approximately 6 N (Figures 17 and 18). Its low cross-sectional area (of fascicles that cross L4/L5) also makes it the least capable of producing force. Furthermore, LD has the lowest L4/L5 stabilizing potential, about all three axes, of any of the muscles examined (Table 8). Much like the TES, it is a long muscle, and its second fascicle (LD2) has a nodal point at approximately the L3 vertebrae level. This makes the LD a relatively inefficient stabilizer of the L4/L5 joint (Table 9). Also, the moment generating capabilities of the LD are very minor in the flexion/extension axis (Table 8). Thus, under current external moment conditions, LD does not provide much in the way of moment generation or stabilization about the L4/L5 joint, and hence the low experimental forces. Again, however, modeled cost functions promote balance amongst muscle forces, thus leading to the overestimation of predicted LD forces.

#### **5.2.2.2.5 Quadratus Lumborum**

The inclusion of stability constraints in the model lead to increased RMS errors of QL predicted forces (Figure 15). QL forces were overestimated in each of the four optimization schemes (Figures 17 and 18).

Experimentally, QL was shown to be the second lowest force producer of all posterior muscles (Figures 17 and 18). Its activity levels were greatly overestimated in the modeled simulations, especially when stability was considered as an optimization constraint. In fact, both in static and ramped trials, QL was predicted as the largest force producing muscle. This is interesting, as Table 8 shows that QL, in the flexion/extension axis, has the lowest moment potential of the agonist muscles, and the second lowest stabilizing potential overall. However, based on its stabilizing potential-to-moment potential ratio (Table 9), QL can be considered a very efficient stabilizer about all three axes. Hence, it is capable of stabilizing without producing overly high contributions to the cost function, and therefore it is very highly activated when stability levels are constrained in the model. This seems to indicate that, based solely on the modeled results of this study, and the cost functions heretofore examined, QL is the muscle that best satisfies the relationship between spinal loading and stability. Biologically, however, this is not the case as is seen in the experimental data. This contradiction will be dealt with in detail in a later section.

### ***5.2.2 Lateral Bend Moment Trials***

The overall ability to predict compressive forces at L4/L5 was improved by incorporating stability constraints into the optimization model. Specifically, with each cost function, percent RMS errors decreased significantly when stability levels were constrained at levels predicted by the previously described regression equations (Figure 30).

Errors, when predicting compressive forces without using stability constraints (55 to 59 %), were more than double those reported by Cholewicki et al. (1995), who found an average error of 23 % for a similar task. This may be due to the problems in the lateral bend described in the limitations, especially since in Cholewicki et al. (1995), the subject's pelvis and ribcage were secured to restrict motion, and therefore may have prevented some of the unusually high antagonistic muscle forces found in the current experiment.

Average predicted compression levels were underestimated in all four optimization schemes (Figure 29). Average predicted levels, with stability constraints, were closer to those found experimentally in ramped than in static trial conditions; whereas without stability constraints, predicted levels were closer to those found in the static trials.

Collapsed across static and ramped trials, stability levels were highly underestimated (103-131%) in all three axes when stability constraints were not considered in the model (Figure 33). These underestimations directly lead to the prediction of instability in 100 % of trials in which stability was not constrained, as opposed to 86 % (InterForce) and 75 % (SumCubed) of trials in which stability was constrained. This compares to 80 % of the experimental trials in which instability occurred in at least one axis.

Agonist and antagonist muscles will next be considered separately as groups. However, addressing of individual muscles will be done bilaterally.



### 5.2.2.1 *Antagonist Muscles*

In experimental trials, external loads were held by the right hand directly to the right centerline of the body. These loads created an external lateral bend moment to the right side of the body. Thus, muscles acting to produce additional right side lateral bend moments were considered to be antagonist to the balancing of the external moment. All right side muscles in the current model fall under this blanket.

The RMS error averaged across all antagonist muscles decreased with the inclusion of stability constraints in the model (Figure 26).

Patterns of antagonistic activity agreed well with the experimental data collected for this study. The current experiment showed the three anterior muscles (RRA, REO, RIO) to be most active of all antagonist muscles under lateral bend moment conditions (Figures 27 and 28). Furthermore, with stability being constrained in the current model, the SumCubed cost function also predicted the three anterior muscles to be the most active force producers, while the InterForce cost function predicted highest activity in REO, followed by RMULT, RIO, and RRA. These modeled predictions also show agreement with experimental studies of Huang and Andersson (2001) and Zetterberg, Andersson and Schultz (1987), who both found activation levels of RA, EO and IO to be highest of all reported antagonist muscles in similar lateral bend tasks. However, as the results of the current study are reported in forces, as compared to activation levels in the other two studies, comparisons must be made with caution. Regardless, it is likely that the reason for the high activity levels of the anterior muscles is that their overall potential as flexor moment generators is far below that of posterior muscles as extensor generators

(Table 8). Thus, the abdominal muscles must achieve higher force levels in order to balance the net moment about the flexion/extension axis to zero.

When not including a stability constraint, no antagonist muscle, except RRA in the SumCubed condition, was ever predicted to be active. The predicted activity of the RRA with the SumCubed cost function is an anomaly that will be addressed in a later section.

#### **5.2.2.2 Agonist Muscles**

In conditions in which a pure right side lateral bend external moment is applied to the body, muscles that counteract said moment, by producing left side bending moments, are considered agonists to the balancing of the external moment. In the current model, all left side muscles fit this criterion.

Averaged across all agonist muscles, the inclusion of stability constraints in the optimization model improved the prediction of agonist force levels when utilizing the InterForce cost function, but decreases the predictive ability when utilizing the SumCubed cost function (Figure 26). In fact, both InterForce conditions, with and without stability constraints, produced lower errors in agonist force estimates than did either SumCubed condition. This is interesting, as it appears that the SumCubed cost function is superior in predicting antagonist muscle activity but inferior in predicting agonist muscle activity.

#### **5.2.2.3 Rectus Abdominus**

RMS errors between predicted and experimental RRA and LRA forces displayed decreases with the inclusion of stability constraints in the model (Figure 25).

Experimentally, RRA was found to be the third largest antagonist force producer (Figures 27 and 28). Its force production levels were underestimated in each of the four optimization schemes. LRA was also underestimated by each of the four optimization schemes. However, errors for this muscle were lower than its antagonist partner.

Of the three abdominal muscles, RA possesses the highest moment potential in the flexion/extension axis (Table 8), which has been identified earlier as being important under the current conditions. However, it is also both the weakest stabilizer and moment generator of the three in the lateral bend and axial twist axes (Table 8). Thus, due to the underestimation of RA force levels under lateral bend conditions, stability about the lateral bend and axial twist axes dictates muscle recruitment patterns more so than does balancing the moment about the flexion/extension axis. This makes sense when considering the high underestimation of stability levels about those two axes when running the model without constraining stability.

The most interesting finding, in regards to the RRA, was that it was predicted to be active with the SumCubed (without stability) cost function. Never before in the literature has the prediction of a muscle, acting purely as an antagonist to the external load, by an optimization model, been reported. In this case, it is most likely that the RRA is turned on in the model in an effort to balance the moment about the flexion/extension axis. As is seen in Table 8, the posterior muscles as a whole have a much greater potential to produce extensor moments than do the anterior muscles to produce flexor moments. As one of the constraints in the current model is to balance the net moment about each axis to zero, it is probable that, despite the need it creates for additional left side bending moment, the low force produced by RRA to help balance the flexor moment

produces less overall cost (based on the cubing of muscle forces) than does further increasing a left side anterior muscle.

#### **5.2.2.4 External Oblique**

Predictions of both REO and LEO force, as measured by RMS errors, are improved when stability is included as an optimization constraint in the model (Figure 25). REO is shown to be, on average, both the highest agonist and antagonist force producer in the experimental trials (Figures 27 and 28). The model, when incorporating stability constraints, does a very good job in representing this activity level, as both cost functions predict REO as the largest antagonist force producer, while the LEO is predicted as the largest and second largest overall force producer by the SumCubed and InterForce cost functions respectively.

EO is the strongest absolute stabilizer of both the lateral bend and axial twist axes at the L4/L5 level, producing 39 % and 36 % of the normalized potential about the two axes respectively (Table 8). Furthermore, its efficiency at stabilizing the lateral bend axis is highest amongst all muscles (Table 9). Consequently, both a high agonist and high antagonist EO activity level is required to adequately stabilize the spine under current conditions.

#### **5.2.2.5 Internal Oblique**

Improved predictions of both RIO and LIO force production were seen with the inclusion of stability constraints into the optimization model (Figure 25).

The RIO and LIO were shown experimentally to be the second largest force producer of the antagonist and agonist muscles respectively (Figures 27 and 28). Modeled predictions of these two muscles were highly accurate, as the RIO was predicted to be the third largest force producing antagonist in each optimization scheme, while LIO was predicted as the second largest force producer in three of the four optimization schemes. Similar to antagonist RA and EO, RIO plays an important role in the balancing of the flexion/extension moment and is, thus, required to act as a major force producer to ensure stable equilibrium. The high level of activation of the LIO is, in great part, due to its large moment generating potential (20 % of total) in the lateral bend axis (Table 8), which makes it an important muscle in counterbalancing the external load acting to the right side of the body.

Similar to EO, IO possesses a large stabilizing potential in both the lateral bend (29 % of total) and axial twist (24 % of total) axes (Table 8). Furthermore, it is an especially efficient stabilizer in the lateral bend axis, second in this respect only to the EO (Table 9). Hence, IO functions as an extremely important stabilizer under conditions of pure lateral bend moment generation.

#### **5.2.2.6 Lumbar Erector Spinae**

RLES was predicted to be inactive by each of the four optimization schemes (Figures 27 and 28). RLES forces were shown to be the lowest of any of the sixteen muscles examined experimentally, with average forces of less than 1 N. This agreed with the findings of Huang et al. (2001), who demonstrated antagonist LES activity of approximately 1 % MVC when statically holding a 20 kg load in lateral bend. This 1 %

MVC, however, would correspond to approximately 10 N of force in the current model, making their force levels slightly greater than ours.

The RMS errors for LLES prediction increased with the inclusion of stability constraints into the model (Figure 25). Furthermore, modeled LLES force predictions were highly underestimated across all conditions (Figures 27 and 28).

The LES is a powerful trunk extensor muscle, second in that respect only to the TES. It is capable of producing 27 % of the total extensor potential (Table 8). For this possible reason, it is treated by the objective functions as a costly muscle to activate under pure lateral bend moment conditions. The experimental results for the RLES demonstrate that this muscle is also treated as such by the CNS. RLES activity would produce high trunk extension forces that would have to be offset by significant abdominal muscle activation. This in turn would prove costly in terms of loading on the spine. However, the muscle's high stabilizing potential and efficiency (Table 9), particularly in the flexion/extension axis, appears to come into play in recruiting the LLES under these same conditions. As the model demonstrates decreased LLES activity when constraining stability levels, it seems the actual CNS opts for the more costly recruitment pattern of higher LLES forces. This may, in part, be a compensatory mechanism for the low activity of its right side counterpart. Moreover, the underestimation of bilateral LES no doubt contributes to stability levels in the flexion/extension axis failing to reach target levels. Thus, it seems the LES plays a role not yet well understood in stabilizing the lumbar spine.

### 5.2.2.7 Thoracic Erector Spinae

Like RLES, RTES was never predicted to be active in any of the optimization simulations (Figure 27 and 28). However, unlike RLES, RTES was found to be fairly active in experimental trials. In fact, RTES was the highest force producing posterior antagonist muscle.

In terms of LTES force prediction, incorporation of stability constraints into the model caused a decrease in RMS error when using the InterForce cost function but an increase in error when utilizing the SumCubed function (Figure 25). The differing effect of stability constraints on the two cost functions most likely stemmed, once again, from the higher cost penalty of cubing rather than squaring muscle forces in the SumCubed function. Specifically, adding stability constraints to the SumCubed optimization caused LTES force estimates to drop down to zero, whereas adding the same constraints to the InterForce function actually lead to increased LTES force predictions (Figures 27 and 28). Thus, it appears that the extremely high extensor moment potential of the TES muscle (Table 8), which would create the need for additional trunk flexor activity, forced the SumCubed objective function to deem the muscle too costly to activate. With stability constraints included in the model, overall muscle activity had to increase to achieve target stability levels, which in turn appeared to force the SumCubed cost function to shut TES off completely.

Experimentally, TES was found to be both the highest agonist and antagonist force producing trunk extensor, in both static and ramped conditions (Figures 27 and 28), and was thus well underestimated in the modeled predictions. It is possible that, due to its length spanning a number of intervertebral joints, the TES serves as an important

stabilizer at multiple spinal levels, thus, in part, accounting for its high force production. Moreover, like LES, the underestimation of TES activity bilaterally is in large part responsible for the failure to meet target stability levels in the flexion/extension axis.

#### 5.2.2.8 Multifidus

In the absence of stability constraints in the model, both RMULT and LMULT were never predicted to be active by either objective function (Figures 27 and 28). Adding stability constraints promoted the activation of both muscles beyond force levels seen experimentally.

Average RMULT forces in the experimental trials were approximately 1 N, and hence RMS errors were very low in optimization simulations in which stability was not constrained. Furthermore, while the LMULT was much more active than its right side counterpart experimentally (approximate average 24 N), the overestimated predictions with the addition of stability constraints resulted in increased errors in every optimization condition.

Unlike flexor moment trials, the addition of stability constraints in the lateral bend trials caused MULT prediction levels to increase rather than decrease. The major difference between the two conditions in this respect is that, in the lateral bend trials, agonist activity alone was not sufficient to achieve the desired stability levels about any of the three axes. Moreover, as MULT is the second most powerful stabilizer in the flexion/extension axis behind LES (Table 8), and both LES and TES force predictions were well below actual levels, it became necessary for the optimization model to



overestimate MULT force contributions in an effort to get as close as possible to target stability levels in the flexion/extension axis.

#### **5.2.2.9 Latissimus Dorsi**

RLD was predicted to be inactive by each of the four optimization schemes, thus producing identical RMS errors throughout (Figure 25). Experimentally, RLD produced an average force level of approximately 7 N in static and 6 N in ramped trials (Figures 31 and 32). Thus, the model's estimates of inactivity were not highly inaccurate.

The inclusion of stability constraints in the model resulted in increased RMS errors of LLD force predictions in every optimization condition except InterForce (Figure 25). In both static and lateral bend, average LLD forces were overestimated by all optimization schemes except InterForce (without stability).

Experimentally, LLD was found to be the lowest force producing agonist muscle (Figures 27 and 28). Furthermore, LD was shown to have little capability as either a moment generator or stabilizer about any of the three axes (Table 8). In fact, it has the least stabilizing potential of any muscle about each axis. Thus, as in the flexion moment trials, LD provides little in the way of moment generation or stabilization in lateral bend conditions.

#### **5.2.2.10 Quadratus Lumborum**

In all four optimization schemes, inclusion of stability constraints caused an increase in the RMS errors for both RQL and LQL force prediction (Figure 25). Without the constraining of stability, RQL was predicted to be inactive by both cost functions

(Figures 27 and 28). Average RQL force predictions were brought much closer to the experimental levels (4 N static) by including stability constraints in the model, but due to particular trials in which predictions were more highly overestimated, RMS errors were shown to increase slightly.

LQL force predictions were overestimated by each optimization method, with stability constraints leading to a more exaggerated overestimation (Figures 27 and 28). Experimentally, LQL was found to produce forces similar in magnitude to LMULT. However, modeled force predictions were much higher for LQL than for LMULT, both with and without stability constraints. In fact, as in the flexion moment trials, agonist QL was predicted to be the largest force producing extensor muscle. McGill, Juker and Kropf (1996b) showed QL to be more active (% MVC) than LES under lateral bend conditions, and hypothesized it to be the most active of all extensors under such conditions. However, with regards to force rather than activation, the LES, and most likely the TES, would still be more productive than the QL.

QL has a relatively low extensor moment potential (Table 8), and combined with its stabilizing efficiency (Table 9), it is chosen in the model, both in flexion and lateral bend moment conditions, as the most cost-effective muscle in both producing equilibrium and stability about the three axes. It therefore appears that QL, and to a lesser extent LD and MULT, are being chosen to activate to levels higher than those seen experimentally, at the expense of LES and TES.

It can be concluded that in lateral bend moment trials, like flexion moment trials, the inclusion of stability constraints in the current optimization model of the spine greatly

improves the prediction of antagonist muscle forces. Also, the model predicts lateral bend muscle recruitment patterns similar to those found in the current experiment as well as elsewhere (Huang et al., 2001). Finally, in both flexion and lateral bend conditions, the stability model significantly improves the prediction of spinal compressive forces as compared to the common optimization model in which spinal stability is not considered.

### **5.2.3 Examination of the Robustness of the Model**

To test the robustness of the model, two factors were incorporated into the experimental trials, both of which would not alter the external moment acting on the subject, but would potentially change the recruitment patterns of muscles in dealing with said external moment. The first of these factors was to have subjects resist loads by either holding a static force or by ramping force up and down throughout a range encompassing the different forces held statically. The second factor was to have subjects hold set load masses at set distances away from the body at two different heights: 1) L4/L5 height; 2) 50 % of the distance between L4/L5 and shoulder height (chest height).

#### **5.2.3.1 Static versus Ramped**

In flexion moment trials, RMS errors were found to be lower in static than in ramped trials for the prediction of compressive forces, as well as muscle forces, excluding LES and LD, for every optimization scheme examined. More specifically, in terms of compression, best case (InterForce with stability) percent RMS errors were 16 % in static as compared to 13 % in ramped trials.

In lateral bend moment trials, differences between static and ramped conditions showed a different pattern. RMS errors were lower in static than in ramped trials for the

prediction of compressive force, as well as RRA, LRA, REO, RIO, LLES, and LTES, while ramped showed lower errors in LEO, LIO, RTES, RLD, and RQL. RLES and RMULT were found to have essentially the same error between static and ramped data. For LMULT, errors were lower in static than ramped trials when utilizing the InterForce cost function, but higher in static than ramped when using the SumCubed cost function. Best case (InterForce with stability) percent RMS errors in compression prediction were found in ramped (35 %) as compared to static (40 %) trials.

In static (isotonic) conditions, muscle force remained at a set level throughout the duration of each trial. Thus, the CNS had ample time to adjust muscle forces to optimally stabilize the spinal joints. In ramped (anisotonic) conditions, muscle forces changed continuously throughout the duration of the trial. Muscle forces, in general, tended to be slightly higher than in static, when ramping force down, but slightly lower than in static, when ramping force up. This might indicate that the CNS stabilizes the spine in a feedback, rather than feedforward, manner. In other words, when ramping force over time, stability levels are constantly being adjusted based on incoming loading information, and thus seem to be optimal for the applied external moment present just prior to the instance being examined. In this way, during the ramp up, muscle forces, and thus stability levels, are slightly lower than those in static, and during the ramp down muscle forces and stability levels are slightly higher than in static. Thus, as would be expected, the model predicts better for static than for ramped force conditions, as in ramped conditions, stability levels have yet to adjust to optimal levels.

Throughout all conditions, inclusion of stability constraints tended to have the same effect on static as on ramped trials. Most importantly, significant improvements

were found in best case (InterForce) predictions of spinal compression both in flexion (21 to 13 % static; 24 to 16 % ramped) and lateral bend (55 to 40 % static; 59 to 35 % ramped) conditions. Thus, the addition of stability constraints improved the prediction of muscle forces and spinal loading in both static and ramped conditions. It can therefore be concluded that spine stability plays a similar role in dictating muscle recruitment patterns in both types of force generation.

#### **5.2.3.2 Two Load Heights**

In flexion trials, RMS errors in agonist and antagonist muscle activity showed very little difference between the two load heights for any of the four optimization schemes. Compression RMS errors displayed almost no difference between the two heights for the InterForce (with stability) condition, which proved to be the best, but showed reduced errors in the other three optimization conditions for the higher load height.

In lateral bend trials, average agonist, antagonist, and compression RMS errors were found to be greater with the higher load height for each optimization scheme.

An interesting finding was that, for both lateral bend and flexion moment conditions, average experimental compression forces decreased as load height increased. This pattern was mimicked exactly by the optimization simulations when incorporating stability constraints in the model (Figures 22 and 32). Of course, without stability, modeled predictions were exactly the same regardless of load height. Furthermore, in flexion trials, both modeled and experimentally, each antagonist muscle decreased its force output as load height increased. Likewise, in lateral bend, antagonist forces, in every muscle except RTES and RLD, were shown to decrease as load height increased.

Agonists, except for the TES in flexion and LEO in lateral bend, also all displayed lower forces with increasing load height. Modeled simulations predicted LES and MULT, rather than TES, to increase in flexion; and LTES, LLD and LEO to increase in lateral bend as load height increased.

These findings disagree with those of Granata and Orishimo (2001), who showed muscle activity, agonist and antagonist, to increase with increasing load height in trunk flexor moment conditions. However, EMG increases were smallest between their first two load heights (from sacrum to 20 cm above), which were most similar to the two load heights examined in the current study.

Further examination of our data uncovers that average stability levels about L4/L5 actually decreased with the higher load height. It may be possible that as load height increased from L4/L5 to chest height, the joint at which the CNS considered to be most critical transferred from a lower lumbar level to a higher level, possibly the shoulder joint. It has been shown that, in situations in which perturbations are delivered to the body, muscles act in manner to stabilize the joint closest to the perturbation (Nashner, 1982; Reitdyk, Patla, Winter, Ishac & Little, 1999; Lee & Lee, 2002). It seems reasonable then that in unperturbed situations, the CNS may prioritize stability in terms of the joints under the most demand. This may have occurred in the current study, thus leading to increased activity in the upper spine and shoulder stabilizers (TES and LD) and subsequent decrease in activity of the lower trunk muscles.

### 5.3 Insights into Stability Modeling

Average agonist RMS errors were shown to be well above those of antagonists in optimization simulations in which either stability was constrained or unconstrained (Figures 16 and 26). Lower antagonist errors are intuitively reasonable, as their experimental force levels tend to be lower than those of agonists, thus producing the likelihood of lower absolute errors. This is highly apparent when stability is not included in the model, as predictions of zero antagonistic force levels still lead to lower average errors than for agonist estimates. However, in every optimization condition, both for lateral bend and flexion moments, and with either cost function, inclusion of stability constraints improves antagonist muscle activity prediction. On the other hand, the addition of stability constraints improves overall agonist force predictions in only the static lateral bend trials when utilizing the InterForce objective function. Overall, muscle force prediction in both flexion and lateral bend moment conditions, are always improved with the consideration of stability in the model, due to the larger decrease in antagonist error compared to the increase in agonist error.

The increased error in agonist activity is still a limitation in the model that needs to be addressed. It is interesting to note that in both lateral bend and flexion moment conditions, the muscles with the two largest extensor moment potentials (TES and LES) are highly underestimated, while the muscle with the lowest extensor moment potential (QL) is highly overestimated. Furthermore, the muscle with the second lowest extensor moment potential (LD) is greatly overestimated in flexion moment trials, as well as in lateral bend trials in which stability is not constrained. As discussed earlier, the flexion/extension axis appears to be vital in the determination of muscle recruitment

patterns. First, the overall discrepancy in moment potential between flexors and extensors is the greatest of any opposing groups about any of the three axes (Table 8). Second, of any of the axes, the overall muscle stabilizing potential is lowest in flexion/extension, making it potentially the most vulnerable to instability. However, in the majority of everyday activities, and in most industrial tasks, flexion/extension is the dominant axis of movement, and thus requires higher posterior than anterior muscle activity. This, in all likelihood, makes the critical axis for instability highly task dependent.

In conditions of pure lateral bend moment, such as those tested in this study, the flexion/extension axis does become the critical axis in which buckling is most likely to occur (Figure 33). The optimization simulations in the current model, incorporating the InterForce and SumCubed objective functions, found it most difficult to achieve stability about the flexion/extension axis in lateral bend trials and, therefore, abandoned this constraint. This difficulty in stabilizing said axis arose from the high cost that would arise from the increased LES and TES forces most likely necessary to stabilize this axis. Likewise, in flexion moment trials, the lateral bend axis was deemed most difficult to stabilize and this constraint was thus abandoned. This is due to the higher EO and IO forces required to stabilize this axis, which in turn would necessitate increased LES and TES forces to balance the dominant flexion/extension axis.

The penalties incorporated into the objective functions, utilized in this model, promote balance amongst all agonist muscle forces, which clearly does not represent experimental findings. Incorporating stability constraints into the model promotes an overall better representation of trunk muscle activity, specifically by activating antagonist



muscles. This, however, results in a generally increased overestimation of the low extensor moment generating muscles (QL and LD) and more underestimation of the high extensor moment generating muscles (TES and LES). Certain exceptions do exist, as for the TES in flexion moment trials, and the LTES (InterForce) in the lateral bend trials. A possible method of improving force predictions would be to impose a larger penalty on muscles possessing lower moment potentials, thereby increasing the cost-effectiveness of choosing the larger, more dominant muscles as higher force producers. This, however, would have to be tested over a wide range of loading conditions, as the trends found for the relatively simple loading trials in this study may not hold true for more complex loading.

It must be noted that, at present, optimization models of the spine are incapable of predicting the intra-subject variability that exists in any task. Individuals have been shown to alter the manner in which they load their tissues over repetitive tasks (Potvin and Norman, 1993). As optimization models predict the same output for a given loading situation, regardless of the number of times it is performed, this biological variability cannot be accurately represented.

#### ***5.4 Insights into Spinal Stability***

Coactivation of trunk muscles is essential to providing an optimal level of stability about the spine. Without stability constraints in the optimization model, muscle force and spinal loading estimates were shown to be highly inaccurate. Forcing target stability levels to be met clearly resulted in a better representation of the overall trunk muscle function. This may indicate that optimal stability levels maintain a higher place,

compared with moment equilibrium, in the hierarchy of dictating trunk muscle activation patterns in static, unperturbed postures. Of course, as the spine is perturbed, equilibrium may take a temporarily more prominent role in this theoretical framework. In such cases, agonist muscles take on the dominant role of initiating the restoration of equilibrium, in order to prevent significant damage to the body. Agonists have repeatedly been shown to act prior to antagonists in response to a sudden perturbation of the spine (Nashner, Woollacott & Tuman, 1979; Diener, Dichgans, Bootz & Bacher, 1984; Hodges & Richardson, 1997; Brown et al., 2003), and by definition, act as prime movers of a joint. Thus, agonists may be thought of as moment generators with antagonists serving as stabilizers. In examining whole-body postural control, Hodges, Gurfinkel, Brugmagne, Smith and Cordo (2002) describe a “multi-joint kinetic chain”, similar to the hierarchy described above, which is organized in concert by stability and mobility. Based on these thoughts, and assuming a most influential role of spine stability in unthreatened postures, the CNS may recruit muscles in the form of a cause-and-effect manner:

1. Optimal stability levels in the CNS, as in the model, require antagonist muscle forces to act as a catalyst for achieving desired stability levels.
2. Antagonist activation levels dictate the agonist forces required to counteract the additional disequilibrating moments supplied by the antagonists. These forces, in turn, function together to achieve an optimal stability level. As was seen in the flexion moment condition in the current study, antagonist activity does not necessarily require all agonists to achieve higher force levels, and thus higher stability levels. Modeled stability levels in the flexion/extension axis decreased as antagonists became active, thereby displaying that optimal levels of stability most

likely exist well below the maximum level possible under simple loading conditions, and that the CNS works to maintain these optimal levels in an effort to establish a beneficial relationship between spinal loading and stability.

3. Combined antagonist and agonist muscle forces lead directly to loading of the spine.

Of course, in more complex loading situations, in which external moments occur about more than one axis, differentiation between muscles functioning as agonists and antagonists becomes more difficult. It is quite possible that under such circumstances, stability takes on a more complex and vital role, as trade-offs must occur between stability and equilibrium about multiple joints at once. Thus, muscles may play both agonist and antagonist roles at the same time, thereby acting in conjunction as stabilizers (antagonists) and moment generators (agonists).

In the course of the modeling in this study, particular muscles were demonstrated to be affected more than others by the inclusion of stability constraints in the optimization simulations. EO and IO, with their high percentage of total lateral bend and axial twist stabilizing potential, as well as their important flexor moment potential, were highly activated in response to stability. The QL, although producing high forces under purely moment constraint conditions, showed further increases with the inclusion of stability constraints in the model. MULT may have proven to be the most interesting muscle in its adjustment to stability, as it increased its agonist and antagonist activity a great deal in lateral bend conditions, yet decreased its activity in flexion conditions. Both the QL and MULT are considered to be deep trunk muscles. Andersson, Oddsson, Grundstrom, Nilsson and Thorstensson (1996) found QL and the deep lateral erector spinae to increase

activation levels under conditions in which the spine was considered to require higher levels of lateral stability. Clearly, deep spinal muscles play a significant role in maintaining stability levels in the spine, however, this role is not yet fully understood. LES and TES were the two muscles that displayed relatively little change in predicted force levels in response to stability constraints in the current model. These muscles have long been considered prime movers rather than stabilizers of the spine (Bergmark, 1989). However, due to their long length and large size, they are capable of providing significant amounts of stability to a large number of spinal joints, and thus should be considered critical in maintaining stability levels in the spine (Crisco and Panjabi, 1991; Cholewicki and McGill, 1996). Finally, the importance of a wide number of muscles activating, as opposed to a single muscle or two, to provide optimal stability levels about the spine, has been demonstrated here and elsewhere (Cholewicki and Van Vliet IV, 2002).

As mentioned earlier, optimal stability levels most likely exist well below the maximum levels possible for a given loading situation, and thus, absolute stabilizing potential does not play as important a part in determining muscle recruitment patterns as does a muscle's potential relationship between spinal loading and stability. It is this association that, in all likelihood, plays the most vital role in preventing tissue damage and injury. Thus, further examination of this relationship is required, as it is likely that, rather than a minimization of cost, the CNS attempts to optimize this relationship in dictating muscle recruitment.

## 5.5 Limitations

### 5.5.1 Lateral Bend Experimental Data

The lateral bend experimental data were initially run through the same gain adjustment protocol as the flexion data as a means of obtaining an initial sense of the data. A high number of trials (77 of 88 static; 75 of 88 ramped) required gain values that fell outside of the physiologic range of 30 to 100 N/cm<sup>2</sup> (McGill and Norman, 1987; Reid and Costigan, 1987), with the majority of values falling above 100 N/cm<sup>2</sup>. Similarly high gain values have been reported elsewhere in the literature (Marras and Sommerich, 1991b). However, in that particular study, a biomechanical model, consisting of a limited number of muscles was utilized, thereby creating the need for such high gains for the few muscles that were included.

In the current study, the most likely reason for the necessity of high gain values was the nature of the application of the external load to the subject. Subjects held the applied moment-generating load in their right hand, either at L4/L5 level or at a height of 50% of the distance between L4/L5 and shoulder. Under these circumstances, certain right side muscles demonstrated higher than expected levels of activation. The right TES and LD, in particular, often showed higher activation levels than their left side counterparts. It is possible that holding the loads in the hand at such distances and heights, away from the body, caused overly high demands on the shoulder, thus creating the need for additional right side muscular activation. The LD muscle crosses the shoulder joint and, thus, it is hypothesized that it is functioning here as a stabilizer of said joint under these conditions. The TES findings appear to be more confounding, as it is not directly capable of stabilizing the shoulder joint. Haumann (2002) made similar

findings of higher right side than left side TES activation in asymmetric (right side) sudden loading of the hands. It is possible that the TES electrode location makes it vulnerable to cross-talk from the trapezius muscle, which may act to stabilize the scapula in situations of high moment demand at the shoulder.

Balancing the moments about each axis using the hybrid method, described in the Methodology section, required a *PercentRMSchange* in muscle activations of 28% for static trials and 29% for ramped trials. Both of these values are far below the value of 43% required in lateral bend conditions by Cholewicki, McGill and Norman (1995). It is, however, thought that the *PercentRMSchange* would have fallen well below even 23%, had a different experimental protocol been used to generate the external moment. Muscle activations in certain muscles, particularly the right side TES, and to a lesser extent the right side LES, were often adjusted to, or near, zero with right TES being reduced by as much as approximately 30% MVC. Furthermore, left side muscles, particularly IO, were on occasion increased by as much as approximately 25% MVC. However, on the whole, the majority of muscles required very minor adjustments, and final adjusted activation patterns agree closely with a similar experiment by Huang and Andersson (2001).

#### 5.5.2 Use of Regression Equations

For the purposes of the prediction of stability constraints in the optimization simulations, regression equations were developed from the same experimental data to which they were later applied. This study in no way suggests that these equations, and thus these stability predictions, can be generalized to a wider variety of tasks and/or population. These predictions were used simply to demonstrate the potential to predict

antagonistic muscle activity, and thus improve overall muscle force and spine load estimates by incorporating a measure of stability as a constraint in an optimization model.

In flexion moment simulations, stability constraints were satisfied about the flexion/extension and axial twist axes, but not about the lateral bend axis. With the InterForce cost function, lateral bend stability was overestimated by an average of approximately 10 %, while with the SumCubed cost function lateral bend stability was overestimated by an average of approximately 45 %. In lateral bend moment simulations, stability constraints were satisfied about the lateral bend and axial twist axes, but not the flexion/extension axis. With the InterForce cost function, flexion/extension stability was underestimated by an average of approximately 103%, while, with the SumCubed cost function, flexion/extension stability was underestimated by an average of approximately 95 %. With improved understanding of the relationship between external loading factors and spine stability, predictions of stability levels under various loading conditions will improve, thereby increasing the likelihood that constraints about all three axes would be satisfied in a similar model, and that predicted muscle patterns would exact a more realistic look. Thus, future studies should attempt to quantify, over a wide range of loading situations and populations, the relationship between external loading factors, such as moment, and spine stability.

### 5.5.3 Stability Measures

The stability values presented in this thesis represent only the stability due to the modeled system (muscles, passive tissues and external loads), and are not a definitive measure of the true overall stability of the system. In fact, instability values occurred in a

high number of experimental trials (13 of 88 static flex; 12 of 88 ramped flex; 72 of 88 static lateral bend; 68 of 88 ramped lateral bend). Other muscles, such as the psoas major and transversus abdominis (TrA), along with intra-abdominal pressure (IAP), have the potential to stabilize the lumbar spine. In particular, the transversus abdominis has recently been identified as a possibly important spinal stabilizer (Hodges and Richardson, 1997; Hodges, Cresswell and Thorstensson, 1999; Grenier and McGill, 2002).

Incorporating these other potential stabilizing sources in the model would no doubt increase stability levels, possibly reducing the occurrence of instability values in the experimental data. To what degree these sources would contribute to stability is a source of much debate. Contrary to an early report citing the potential stabilizing role of the psoas major (Nachemson, 1986), recent work in this lab has shown this muscle to have a relatively minor stabilizing potential about each axis at the L4/L5 level (Brown and Potvin, 2003). Also, IAP has often been hypothesized to simply exist as a by-product of abdominal muscle activity and to have little or no potential to stabilize the spine on its own (Marras and Mirka, 1996; Cholewicki, Juluru and McGill, 1999a; Cholewicki, Juluru, Radebold, Panjabi, and McGill, 1999b). Recent work by Hodges, Cresswell, Daggfeldt and Thorstensson (2001), however, has demonstrated that IAP may have the potential to provide a larger stabilizing contribution than previously thought. Finally, the role of TrA in spine stability is still not well understood and requires further study.

The instability measured in experimental trials may, however, be an accurate reflection of the actual state of the L4/L5 joint under current loading conditions. Cholewicki and McGill (1996), reported instability in a high number of instances for subjects in upright standing while holding various loads. This falls in line with the



neutral zone theory (Panjabi, 1992b), which states that highest levels of instability occur when the vertebral joint is in a neutral posture, where trunk muscles are at their least active.

Regardless, the purpose of this thesis was simply to present the notion that stability is an important element in dictating recruitment patterns in trunk muscles, and that incorporating a measure of stability into models of the spine allows for better representation of the system and subsequently an improved prediction of all forces within. Moreover, the stability values presented here are thought to provide a fair representation of the nature of spinal stability under the tested conditions.

## **5.6 Conclusions**

1. The current model, by incorporating measures of stability as constraints about each anatomical axis, served two major functions that have never before been shown in optimization models of the spine:
  - i) the ability to predict pure muscle coactivation through the activation of muscles acting in purely antagonistic roles
  - ii) sensitivity to inter-individual differences through the incorporation of subject mass, height, and external load height into the stability calculation
2. The model, when constraining stability to optimal levels about each axis, significantly improves the prediction of compressive forces acting on the spine. This is true under both pure flexor moment and pure lateral bend moment conditions.

3. The cost function of minimizing the sum of the squared intervertebral forces at the L4/L5 level better represents the CNS objective in determining trunk muscle recruitment than does the cost function of minimizing the sum of the cubed muscle forces.
4. Optimal stability levels exist far below the maximum levels for a given loading situation. Furthermore, the CNS controls a majority of trunk muscles to levels above or below those that would result in equilibrium at a minimum loading and/or metabolic cost.
5. Stability of the spine requires a combination of all trunk muscle forces acting together to achieve levels deemed optimal by the CNS. No one muscle is predominant through all possible loading conditions. Rather, the function of each muscle is highly dependent on the loading situation to which the spine is subject.
6. Antagonist muscle forces are necessary to optimally stabilize the spine. Absence of these forces creates an increased likelihood of instability by decreasing the level of stability in at least the critical axis for a given loading situation.

### **5.7 Recommendations for Future Research**

First, this model should be tested under more complex loading conditions. In situations of loading in which external moments are applied to more than one axis simultaneously, muscles no longer take on purely agonistic or antagonistic roles and, in turn it, is highly likely that optimal stability levels will rise. The model would then have to balance external moments about multiple axes while targeting higher stability levels.

This may result in the muscles underestimated in the current model to increase force magnitude predictions to more realistic levels.

In determining muscle force patterns, the CNS most likely optimizes multiple criteria in concert with spine stability. Thus, different and more complex objective functions should be tested in the model. Multiple cost functions can be tested together in sequence, or by assigning weighting to the different components in an effort to determine and then utilize the best function under various loading conditions. More simply, as discussed earlier, different penalties may be assigned to muscles based on their moment generating capabilities.

The exact role of different muscles in stabilizing the spine is not yet fully understood. Consequently, further in vivo work needs to be done to test various muscles under different loading conditions, especially those in which stability is threatened, to see how and which muscles adjust in response to these changes. Modeling studies can also be performed in which particular muscles are constrained at preset force levels to determine how other muscles respond to reestablish stability and/or equilibrium. This will help shed new light onto the relationship between different muscles and muscle groups in this respect.

Further work needs to be done in the modeling of stability in the spinal system. The stabilizing effect of intra-abdominal pressure, the thoracolumbar fascia, and other trunk muscles, such as the transversus abdominis, should eventually be incorporated into models such as the one presented in this study. Also, the relationship between stability and moment demand, at various spine levels, needs to be investigated in order to gain a

better understanding of injury mechanisms and possible stabilizing deficiencies in people with chronic low back pain and/or deformities.

The current model should be expanded to encompass each of the six lumbar joints, the corresponding musculature, and stability measures at each disc level. This will allow for a more realistic representation of the human lumbar spine. Furthermore, this will enable the examination of trunk muscle function and stability levels in varying degrees of spine flexion, as well as dynamic analyses of loading tasks.

Finally, to achieve a full understanding of the development and progression of spinal injury, mathematical stability analyses should be conducted to, in essence, dissect the spine and determine the initial location, and hence cause, of instability and buckling in the spine. Post-buckling modes need also be investigated to determine the reason and location for damage occurring in particular tissues. These analyses then need to be compared to in vivo and in vitro studies dealing with the nature of spine instability and buckling.

## REFERENCES

- Anderson, C. K., Chaffin, D. B., Herrin, G. D., Matthews, L. S. (1985). A biomechanical model of the lumbosacral joint during lifting activities. Journal of Biomechanics, 18, 8, 571-584.
- Andersson, E. A., Oddsson, L. I. E., Grundstrom, H., Nilsson, J., Thorstensson, A. (1996). EMG activities of the quadratus lumborum and erector spinae muscles during flexion-relaxation and other motor tasks. Clinical Biomechanics, 11, 7, 392-400.
- Andersson, G. B. J., Murphy, R. W., Ortengren, R., Nachemson, A. L. (1979). The influence of backrest inclination and lumbar support on lumbar lordosis. Spine, 4, 1, 52-58.
- Bean, J. C., Chaffin, D. B. (1988). Biomechanical model calculation of muscle contraction forces: a double linear programming method. Journal of Biomechanics, 21, 1, 59-66.
- Bergmark, A. (1989). Stability of the lumbar spine: a study in mechanical engineering. Acta Orthopaedica Scandinavica Supplementum, 60, 230, 3- 52.
- Bigland-Ritchie, B. (1981). EMG/force relations and fatigue of human voluntary contractions. Exercise Sport Science Review, 9, 75-117.
- Brown, S. H. M., Haumann, M. L., Potvin, J. R. (2003). The response of leg and trunk muscles to sudden unloading of the hands: implications for balance and stability. Clinical Biomechanics, In Press.
- Brown, S. H. M., Potvin, J. R. (2003). Stabilizing potential of trunk muscles. To be presented at: Proceedings of the American Society of Biomechanics, Toledo, Ohio.
- Caillet, R. (1981). Low Back Pain Syndrome. F.A. Francis Co., Philadelphia.
- Chaffin, D. B. (1969). A computerized biomechanical model-development of and use in studying gross body actions. Journal of Biomechanics, 2, 429-441.
- Chaffin, D. B., Andersson, G. B. J. (1984). Occupational Biomechanics. New York: Wiley.
- Chiang, J, Potvin, J. R. (2001). The in vivo dynamic response of the human spine to rapid lateral bend perturbation: effects of preload and step input magnitude. Spine, 26, 13, 1457-1464.
- Cholewicki, J., McGill, S. M., Norman, R. W. (1991). Lumbar spine load during the lifting of extremely heavy weights. Med. Sci. Sports Exercise, 23, 1179-1186.

- Cholewicki, J., McGill, S. M. (1994). EMG assisted optimization: a hybrid approach for estimating muscle forces in an indeterminate biomechanical model. Journal of Biomechanics, 27, 10, 1287-1289.
- Cholewicki, J., McGill, S. M., Norman, R. W. (1995). Comparison of muscle forces and joint load from an optimization and EMG assisted lumbar spine model: towards development of a hybrid approach. Journal of Biomechanics, 28, 3, 321-331.
- Cholewicki, J., McGill, S. M., (1996). Mechanical stability of the in vivo lumbar spine: implications for injury and chronic low back pain. Clinical Biomechanics, 11, 1, 1-15.
- Cholewicki, J., Panjabi, M. M., Khachatryan, A. (1997). Stabilizing function of trunk flexor-extensor muscles around a neutral posture. Spine, 22, 19, 2207-2212.
- Cholewicki, J., Juluru, K., McGill, S. M. (1999a). Intra-abdominal pressure mechanism for stabilizing the lumbar spine. Journal of Biomechanics, 32, 13-17.
- Cholewicki, J., Juluru, K., Radebold, A., Panjabi, M. M., McGill, S. M. (1999b). Lumbar spine stability can be augmented with an abdominal belt and/or increased intra-abdominal pressure. European Spine Journal, 8, 388-395.
- Cholewicki, J., Van Vliet IV, J. J. (2002). Relative contribution of trunk muscles to the stability of the lumbar spine during isometric exertions. Clinical Biomechanics, 17, 99-105.
- Crisco, J. J., Panjabi, M. M. (1991). The intersegmental and multisegmental muscles of the lumbar spine: a biomechanical model comparing lateral stabilizing potential. Spine, 16, 7, 793-799.
- Crisco, J. J., Panjabi, M. M. (1992). Euler stability of the human ligamentous lumbar spine. Part 1: theory. Clinical Biomechanics, 7, 19-26.
- Crisco, J. J., Panjabi, M. M., Yamamoto, I., Oxland, T. R. (1992). Euler stability of the human ligamentous lumbar spine. Part 2: experiment. Clinical Biomechanics, 7, 27-32.
- Crowninshield, R. D., Brand, R. A. (1981). A physiologically based criterion of muscle force prediction in locomotion. Journal of Biomechanics, 14, 11, 793-801.
- DeLuca, C.J. (1995). Surface electromyography detection and recording. NeuroMuscular Research Center. <http://nmrc.bu.edu/nmrc/detect/emg>.
- Diener, H. C., Dichgans, J., Bootz, F., Bacher, M. Early stabilization of human posture after a sudden disturbance: influence of rate and amplitude of displacement. Experimental Brain Research, 56, 126-134.

- Gajdosik, R. L. (2001). Passive extensibility of skeletal muscle: review of the literature with clinical implications. Clinical Biomechanics, 16, 87-101.
- Gardner-Morse, M. G., Stokes, I. A. F. (1998). The effects of abdominal muscle coactivation on lumbar spine stability. Spine, 23, 1, 86-91.
- Granata, K. P., Marras, W. S. (1995). The influence of trunk muscle coactivity on dynamic spinal loads. Spine, 20, 8, 913-919.
- Granata, K. P., Marras, W. S. (2000). Cost-benefit of muscle cocontraction in protecting against spinal instability. Spine, 25, 11, 1398-1404.
- Granata, K. P., Orishimo, K. F. (2001). Response of trunk muscle coactivation to changes in spinal stability. Journal of Biomechanics, 34, 1117-1123.
- Granata, K. P., Wilson, S. E. (2001). Trunk posture and spinal stability. Clinical Biomechanics, 16, 650-659.
- Grenier, S. G., McGill, S. M. (2002). The role of transversus abdominis in spine stability. Proceedings of the IV World Congress of Biomechanics, Calgary, Alberta.
- Haumann, M. L. (2002). The Control of Whole-Body Equilibrium and Trunk Stability During Sudden Hand Loading. Unpublished Masters Thesis. University of Windsor, Windsor, Ontario, Canada.
- Hodges, P. W., Richardson, C. A. (1997). Feedforward contraction of transversus abdominis is not influenced by the direction of arm movement. Experimental Brain Research, 114, 362-370.
- Hodges, P., Cresswell, A., Thorstensson, A. (1999). Preparatory trunk motion accompanies rapid upper limb movement. Experimental Brain Research, 124, 69-79.
- Hodges, P. W., Cresswell, A. G., Daggfeldt, K., Thorstensson, A. (2001). In vivo measurement of the effect of intra-abdominal pressure on the human spine. Journal of Biomechanics, 34, 347-353.
- Hodges, P. W., Gurfinkel, V. S., Brumagne, S., Smith, T. C., Cordo, P. C. (2002). Coexistence of stability and mobility in postural control: evidence from postural compensation for reparation. Experimental Brain Research, 144, 293-302.
- Huang, Q. M., Andersson, E. (2001). Intramuscular myoelectric activity and selective coactivation of trunk muscles during lateral flexion with and without load. Spine, 26, 13, 1465-1472.
- Hughes, R. E. (2000). Effect of optimization criterion on spinal force estimates during asymmetric lifting. Journal of Biomechanics, 33, 225-229.

- Hunt, G. W., Thompson, J. M. T. (1973). A General Theory of Elastic Stability. London, New York: Wiley.
- Krajcarski, S. R., Potvin, J. R., Chiang, J. (1999). The in vivo dynamic response of the spine to perturbations causing rapid flexion: effects of pre-load and step input magnitude. Clinical Biomechanics, 14, 54-62.
- Lavender, S. A., Tsuang, Y. H., Andersson, G. B. J., Hafezi, A., Shin, C. C. (1992). Trunk muscle cocontraction: the effects of moment direction and moment magnitude. Journal of Orthopaedic Research, 10, 691-700.
- Lavender, S., Trafimow, J., Anderson, G. B. J., Mayer, R. S., Chen, I. (1994). Trunk muscle activation: the effects of torso flexion, moment direction, and moment magnitude. Spine, 19, 7, 771-778.
- Leamon, T. B., (1994). Research to reality: a critical review of the validity of various criteria for the prevention of occupationally induced low back pain disability. Ergonomics, 37, 12, 1959-1974.
- Lee, Y. H., Lee, T. H. (2002). Muscle response while holding an unstable load. Clinical Biomechanics, 17, 250-256.
- Marras, W. S., Sommerich, C. M. (1991a). A three-dimensional motion model of loads on the lumbar spine: I. Model structure. Human Factors, 33, 2, 123-137.
- Marras, W. S., Sommerich, C. M. (1991b). A three-dimensional motion model of loads on the lumbar spine: II. Model validation. Human Factors, 33, 2, 139-149.
- Marras, W. S., Mirka, G. A. (1996). Intra-abdominal pressure during trunk extension motions. Clinical Biomechanics, 11, 5, 267-274.
- McGill, S. M., Norman, R. W. (1986). Partitioning of the L4/L5 dynamic moment into disc, ligamentous and muscular components during lifting. Spine, 11, 666-678.
- McGill, S. M., Norman, R. W. (1987). Effects of an anatomically detailed erector spinae model on L4/L5 disc compression and shear. Journal of Biomechanics, 20, 6, 591-600.
- McGill, S. M. (1991). Electromyographic activity of the abdominal and low back musculature during the generation of isometric and dynamic axial trunk torque: implications for lumbar mechanics. Journal of Orthopaedic Research, 9, 91-103.
- McGill, S. M. (1992). A myoelectrically based dynamic three-dimensional model to predict loads on lumbar spine tissues during lateral bending. Journal of Biomechanics, 25, 4, 395-414.



- McGill, S., Seguin J., Bennett, G. (1994). Passive stiffness of the lumbar torso in flexion, extension, lateral bending, and axial rotation: effect of belt wearing and breath holding. Spine, 19, 6, 696-704.
- McGill, S., Juker, D., Kropf, P. (1996a). Appropriately placed surface EMG electrodes reflect deep muscle activity (psoas, quadratus lumborum, abdominal wall) in the lumbar spine. Journal of Biomechanics, 29, 11, 1503-1507.
- McGill, S., Juker, D., Kropf, P. (1996b). Quantitative intramuscular myoelectric activity of quadratus lumborum during a wide variety of tasks. Clinical Biomechanics, 11, 3, 170-172.
- Mital, A., Pennathur, A. (1999). Musculoskeletal overexertion injuries in the United States: mitigating the problem through ergonomics and engineering interventions. Journal of Occupational Rehabilitation, 9, 2, 115-149.
- Morris, J. M., Lucas, D. B., Bresler, B. (1961). Role of the trunk in stability of the spine. J. Bone Jt. Surg., 43, 3, 327-351.
- Nachemson, A. (1986). The possible importance of the psoas muscle for stabilization of the lumbar spine. Acta. Orthop. Scand., 39, 47.
- Nashner, L. M., Woollacott, M., Tuma, G. (1979). Organization of rapid responses to postural and locomotor-like perturbations of standing man. Experimental Brain Research, 36, 463-476.
- Nashner, L. M. (1982). Adaptations of human movement to altered environments. Trends in Neuroscience, 62, 356-361.
- O'Brien, P. R., Potvin, J. R. (1997). Fatigue-related EMG responses of trunk muscles to a prolonged, isometric twist exertion. Clinical Biomechanics, 12, 5, 306-313.
- Panjabi, M. M. (1992a). The stabilizing system of the spine. Part 1: function, dysfunction, adaptation, and enhancement. Journal of Spinal Disorders, 5, 4, 383-389.
- Panjabi, M. M. (1992b). The stabilizing system of the spine. Part 2: neutral zone and instability hypothesis. Journal of Spinal Disorders, 5, 4, 390-397.
- Pope, M. H., Andersson, G. B. J., Broman, H., Svensson, M., Zetterberg, C. (1986). Electromyographic studies of the lumbar trunk musculature during the development of axial torques. Journal of Orthopaedic Research, 4, 288-297.
- Pope, M. H., Svensson, M., Andersson, G. B. J., Broman, H., Zetterberg, C. (1987). The role of prerotation of the trunk in axial twisting efforts. Spine, 12, 10, 1041-1045.

- Potvin, J. R., McGill, S. M., Norman, R. W. (1991). Trunk muscle and lumbar ligament contributions to dynamic lifts with varying degrees of trunk flexion. Spine, 16, 9, 1099-1107.
- Potvin, J. R., Norman, R. W. (1993). Quantification of erector spinae muscle fatigue during prolonged, dynamic lifting tasks. European Journal of Applied Physiology, 67, 76-82.
- Potvin, J.R., Norman, R.W., McGill, S.M. (1996). Mechanically corrected EMG for the continuous estimation of erector spinae muscle loading during repetitive lifting. European Journal of Applied Physiology, 74, 119-132.
- Reid, J.G., Costigan, P.A. (1987). Trunk muscle balance and muscular force. Spine, 12, 783-786.
- Rietdyk, S., Patla, A. E., Winter, D. A., Ishac, M. G., Little, C. E. (1999). Balance recovery from medio-lateral perturbations of the upper body during standing. Journal of Biomechanics, 32, 1149-1158.
- Schultz, A. B., Andersson, G. B. J., Haderspeck, K., Ortengren, R., Nordin, M., Bjork, R. (1982). Analysis and measurement of lumbar loads in tasks involving bends and twists. Journal of Biomechanics, 15, 9, 669-675.
- Schultz, A. B., Haderspeck, K., Warwick, D., Portillo, D. (1983). Use of lumbar trunk muscles in isometric performance of mechanically complex standing tasks. Journal of Orthopaedic Research, 1, 77-91.
- Stokes, I. A. F., Gardner-Morse, M. (2001). Lumbar spinal muscle activation synergies predicted by multi-criteria cost function. Journal of Biomechanics, 34, 733-740.
- Stone, R. J., Stone, J. A. (1990). Atlas of the Skeletal Muscles. Wm. C. Brown Publishers.
- Thelen, D. G., Schultz, A. B., Ashton-Miller, J. A. (1995). Co-contraction of lumbar muscles during the development of time-varying triaxial moments. Journal of Orthopaedic Research, 13, 390-398.
- Tortora, G. J. (1995). Principles of Human Anatomy 7<sup>th</sup> ed. Harper Collins College Publishers.
- Waters, T. R., Putz-Anderson, V., Garg, A., Fine, L. J. (1993). Revised NIOSH equation for the design and evaluation of manual lifting tasks. Ergonomics, 36, 7, 749-776.
- White, A. A., Panjabi, M. (1990). Clinical Biomechanics of the Spine. J. B. Lippincott Co., Toronto.

Zetterberg, C., Andersson, G. B. J., Schultz, A. B. (1987). The activity of individual trunk muscles during heavy physical loading. Spine, 12, 10, 1035-1040.

# Appendix A

## Information and Consent Form

**Project Title:** A Biomechanical Model of the Lumbar Spine to Predict Trunk Muscle Forces: Optimizing the Relationship Between Spinal Stability and Spinal Loading.

**Researchers:** Stephen Brown, Masters student; Jim Potvin, Professor.

### Study Details:

The purpose of the experimental portion of this study is to validate the use of stability constraints in an optimization model of the spine. For all trials, subjects will be asked to stand in an upright posture with feet separated by approximately shoulder width. Participants will perform a number of trials in which they statically hold a load in either a pure anterior or pure lateral bend trunk moment position. Each of these trials will last approximately two seconds. Various load masses and moment arms will be tested under these conditions. Furthermore, participants will be required to perform eight trials in which they isometrically ramp force up and down through pre-set levels in either a pure anterior or pure lateral bend trunk moment position. These trials will last approximately ten seconds each. External loads will range from 3.2 to 13.8 kg in flexion and from 2.3 to 9.1 kg in lateral bend. Participants will be instrumented with EMG electrodes over 14 trunk muscles bilaterally. Furthermore, subjects will be videotaped for the purposes of video digitization and analysis. The entire data collection session should last approximately one hour. Muscle stiffness may result after the collection, but should be no more than may be experienced after any unaccustomed physical activity.

### Consent of Subject:

I have read and fully understand the information provided in this consent form, and voluntarily agree to participate in the described research project. I also acknowledge that I do not suffer from chronic low back pain or other low back injuries. The purpose and methods of the experiment have been fully described to me by the above-mentioned researchers. I am aware that I may report what I consider violations of my welfare to the Office of Human Research, University of Windsor, and may withdraw as a subject from the experiment for any reason at any time. I understand that my personal identity will remain confidential throughout my participation in this study. I am mindful of my right to ask for feedback on the results at the end of the study. With full knowledge of the foregoing, I agree, of my own free will, to participate in this study.

\_\_\_\_\_ Signature of Participant \_\_\_\_\_ Date

\_\_\_\_\_ Signature of Witness \_\_\_\_\_ Date

## **Appendix B**

**Table 6.** Anatomical model coordinates: cross-sectional areas, origins, insertions, and first nodal points crossing L4/L5. (Cholewicki and McGill, 1996)

Muscle	Cross-sectional area (cm <sup>2</sup> )	Origin					Insertion						
		bony landmark	X	Y	Z	bony landmark	X	Y	Z	nodal point	X	Y	Z
RA	10.0	Pelvis	18.4	5.0	3.0	Rib	19.0	35.0	7.0				
EO1	10.0	Pelvis	12.8	18.6	13.0	Rib	6.0	30.0	12.5				
EO2	9.0	Pelvis	19.0	5.0	0	Rib	12.5	31.5	10.5	L4	18.7	21.2	5.2
IO1	9.0	Pelvis	9.0	21.5	12.5	Rib	15.0	29.0	7.0				
IO2	8.0	Pelvis	16.0	16.0	12.0	Rib	19.0	38.0	0	L4	18.8	24.2	5.6
LES1	6.0	Pelvis	2.4	17.8	6.0	L4	7.4	23.4	4.0				
LES2	5.7	Pelvis	2.4	17.8	6.0	L3	6.9	26.6	3.0				
LES3	5.0	Pelvis	2.4	17.8	6.0	L2	5.9	29.8	2.7	L4	2.5	22.3	5.0
LES4	4.0	Pelvis	2.4	17.8	6.0	L1	4.4	32.8	2.6	L4	2.5	22.3	5.0
TES1	11.0	Pelvis	1.4	16.6	6.8	Rib	1.6	39.0	8.4	L4	2.5	22.3	7.4
TES2	16.8	Pelvis	1.4	16.5	3.3	Rib	2.0	44.0	5.0	L4	2.5	22.3	3.8
TES3	0.7	L5	4.0	20.4	0.2	Rib	2.0	53.5	2.0	L4	2.5	22.3	1.5
MULT1	2.9	Pelvis	2.0	13.8	1.5	L4	4.1	21.5	0.5				
MULT2	2.4	Pelvis	2.6	18.0	3.6	L3	4.0	24.0	0.5				
MULT3	1.5	Pelvis	2.6	18.0	3.6	L2	3.2	26.9	0.5				
MULT4	0.9	Pelvis	2.6	18.0	3.6	L1	2.2	30.2	0.5				
MULT5	0.8	L5	5.8	19.1	1.5	L3	4.0	24.0	0.5				
MULT6	0.6	L5	5.8	19.1	1.5	L2	3.2	26.9	0.5				
MULT7	0.6	L5	5.8	19.1	1.5	L1	2.2	30.2	0.5				
LD1	2.0	Pelvis	4.8	21.5	6.0	Rib	9.0	47.0	12.0				
LD2	2.0	Pelvis	3.6	19.2	3.0	Rib	9.0	47.0	12.0	Rib	3.6	24.2	6.5
QL1	2.0	Pelvis	6.0	21.4	9.0	Rib	7.2	23.8	4.4				
QL2	1.0	Pelvis	6.0	21.4	9.0	L1	6.2	26.8	3.8				
QL3	1.0	Pelvis	6.0	21.4	9.0	L2	5.2	30.0	3.8				
QL4	1.0	Pelvis	6.0	21.4	9.0	L3	4.0	33.0	3.6				
QL5	1.0	Pelvis	6.0	21.4	9.0	L4	3.5	25.5	7.2				
L4-L5			10.6	21.1	0								

**Table 7.** Additional nodal points for the three TES fascicles. (Cholewicki and McGill, 1996).

Muscle	Bony land-mark	X	Y	Z
TES1	L3	2.0	25.2	7.6
TES1	L2	1.4	27.9	7.8
TES1	L1	0.2	31.0	8.0
TES2	L3	2.0	25.2	3.9
TES2	L2	1.4	27.9	4.1
TES2	L1	0.2	31.0	4.3
TES3	L3	2.0	25.2	1.5
TES3	L2	1.4	27.9	1.5
TES3	L1	0.2	31.0	1.5
TES3	Rib	0.2	34.0	1.5

**Table 8.** Moment and stabilizing potentials of each muscle, about each axis, normalized (as percents) to the total potential of all muscles combined about each axis. Agonist and antagonist moment potentials are considered separately. Antagonist muscles are bolded and are considered as follows: flexion/extension (muscles causing flexor moments); lateral bend (muscles causing left side bending moments); axial twist (muscles causing left side twist moments). Numbers in columns for individual muscles (ie. RA) are in % of total potential. Numbers in columns for agonist and antagonist totals are in Nm.

Muscle	Normalized Moment Potential			Normalized Stabilizing Potential		
	Flexion/ Extension	Lateral Bend	Axial Twist	Flexion/ Extension	Lateral Bend	Axial Twist
RA	<b>42.9</b>	8.0	7.3	9.5	2.5	4.7
EO	<b>40.2</b>	24.2	66.4	8.1	39.0	35.9
IO	<b>16.9</b>	19.8	<b>62.6</b>	5.5	28.6	23.8
LES	27.2	14.2	2.2	27.4	12.2	5.2
TES	49.7	21.8	<b>29.9</b>	19.2	6.4	13.6
MUL	13.4	2.2	12.4	23.3	0.9	7.9
LD	4.9	2.9	<b>7.5</b>	1.7	0.9	2.3
QL	4.8	7.0	11.6	5.5	9.5	6.5
Agonist Total	231.3	320.0	66.8	1037.4	1524.5	1700.1
Antagonist Total	<b>-93.9</b>	<b>0.0</b>	<b>-83.5</b>			

Table 9. Moment and stabilizing potentials, and a ratio of stabilizing potential to moment potential, for each individual muscle about each of the three anatomical axes.

Muscle	Moment Potential			Stabilizing Potential			Ratio (Stab Potential : Mom Potential)		
	Flexion/ Extension	Lateral Bend	Axial Twist	Flexion/ Extension	Lateral Bend	Axial Twist	Flexion/ Extension	Lateral Bend	Axial Twist
RA	-40.2	25.5	4.9	98.0	38.6	79.5	2.4	1.5	16.4
EO	-37.7	77.5	44.4	83.6	594.1	610.7	2.2	7.7	13.8
IO	-15.9	63.4	-52.2	56.6	435.7	404.0	3.6	6.9	7.7
LES	62.9	45.4	1.5	284.0	186.5	88.7	4.5	4.1	59.0
TES	115.0	69.6	-25.0	199.4	97.6	231.4	1.7	1.4	9.3
MUL	30.9	7.0	8.3	241.6	13.5	134.7	7.8	1.9	16.2
LD	11.4	9.2	-6.3	17.5	13.4	39.9	1.5	1.5	6.4
QL	11.2	22.3	7.8	56.7	145.1	111.2	5.1	6.5	14.3



**Table 10.** Individual muscle fascicle 3-dimensional moment arm (3-D r)(for moment generating purposes), 2-dimensional moment arm (2-D r)(for stabilizing purposes), full fascicle length (L) and length of the fascicle vector where it crosses L4/L5 (l).

Muscle	Flexion/Extension				Lateral Bend				Axial Twist			
	3-D r	2-D r	L	l	3-D r	2-D r	L	l	3-D r	2-D r	L	l
RA	-0.08	-0.08	0.30	0.30	0.05	0.05	0.30	0.30	-0.07	0.01	0.04	0.04
EO1	-0.01	-0.01	0.13	0.13	0.13	0.11	0.11	0.11	-0.13	0.07	0.07	0.07
EO2	-0.08	-0.08	0.28	0.16	0.05	0.05	0.29	0.17	-0.08	0.03	0.13	0.05
IO1	0.01	0.01	0.10	0.10	0.10	0.09	0.09	0.09	0.08	-0.06	0.08	0.08
IO2	-0.07	-0.05	0.23	0.09	0.06	0.06	0.25	0.10	0.10	-0.06	0.13	0.07
LES1	0.04	0.04	0.08	0.08	0.05	0.03	0.06	0.06	0.03	-0.02	0.05	0.05
LES2	0.06	0.06	0.10	0.10	0.05	0.04	0.09	0.09	0.00	0.00	0.05	0.05
LES3	0.08	0.08	0.13	0.05	0.05	0.05	0.13	0.05	-0.08	0.02	0.05	0.01
LES4	0.08	0.08	0.15	0.05	0.05	0.05	0.15	0.05	-0.08	0.02	0.04	0.01
TES1	0.08	0.08	0.23	0.06	0.07	0.07	0.23	0.06	0.10	-0.02	0.05	0.01
TES2	0.08	0.08	0.28	0.06	0.04	0.04	0.28	0.06	0.07	-0.01	0.06	0.01
TES3	0.06	0.05	0.34	0.02	0.01	0.00	0.34	0.02	0.04	-0.03	0.06	0.02
MUL1	0.06	0.06	0.08	0.08	0.01	0.01	0.08	0.08	-0.02	0.01	0.02	0.02
MUL2	0.07	0.06	0.06	0.06	0.02	0.02	0.07	0.07	-0.06	0.03	0.03	0.03
MUL3	0.08	0.07	0.09	0.09	0.02	0.02	0.09	0.09	-0.07	0.02	0.03	0.03
MUL4	0.08	0.08	0.12	0.12	0.03	0.03	0.13	0.13	-0.08	0.02	0.03	0.03
MUL5	0.05	0.05	0.05	0.05	0.01	0.01	0.05	0.05	-0.04	0.01	0.02	0.02
MUL6	0.05	0.05	0.08	0.08	0.01	0.01	0.08	0.08	-0.03	0.01	0.03	0.03
MUL7	0.05	0.05	0.12	0.12	0.01	0.01	0.11	0.11	-0.03	0.01	0.04	0.04
LD1	0.06	0.06	0.26	0.26	0.06	0.06	0.26	0.26	0.08	-0.02	0.07	0.07
LD2	0.07	0.06	0.28	0.05	0.04	0.04	0.30	0.06	0.07	-0.04	0.11	0.04
QL1	0.04	0.04	0.14	0.14	0.09	0.09	0.14	0.14	-0.10	0.02	0.03	0.03
QL2	0.05	0.03	0.05	0.05	0.07	0.07	0.08	0.07	-0.04	0.03	0.05	0.05
QL3	0.05	0.04	0.09	0.09	0.08	0.08	0.10	0.10	-0.06	0.03	0.05	0.05
QL4	0.04	0.04	0.12	0.12	0.08	0.08	0.13	0.13	-0.07	0.03	0.06	0.06
QL5	0.04	0.02	0.03	0.03	0.04	0.04	0.05	0.05	-0.02	0.02	0.05	0.05

## **Appendix C**

**Table 11.** Standard errors (N) for individual muscle forces for the Flexion Moment conditions.

Condition	Muscle							
	RA	EO	IO	LES	TES	MULT	LD	QL
Experimental	1.6	2.5	8.1	16.2	24.7	5.9	0.6	4.7
InterForce (with stability)	0.0	0.7	2.6	11.7	10.7	7.8	9.6	17.6
InterForce (without stability)	0.0	1.4	4.5	12.3	10.6	6.8	10.9	18.2
SumCubed (with stability)	0.0	0.0	0.0	14.5	7.2	16.5	5.6	9.7
SumCubed (without stability)	0.0	0.0	0.0	13.0	7.5	15.8	6.5	11.1

**Table 12.** Standard errors (N) for the RMS errors between model predicted and experimentally determined muscle forces for the Flexion Moment conditions.

Condition	Muscle							
	RA	EO	IO	LES	TES	MULT	LD	QL
InterForce (with stability)	2.4	3.4	17.7	7.8	14.5	3.5	4.1	6.6
InterForce (without stability)	2.4	3.0	16.9	7.5	14.6	2.2	4.5	6.8
SumCubed (with stability)	2.4	3.5	19.0	5.4	15.8	6.8	2.3	3.6
SumCubed (without stability)	2.4	3.5	19.0	7.2	15.7	6.6	2.6	4.1

**Table 13.** Standard errors for individual muscle forces for the Lateral Bend Moment conditions.

Condition	Muscle															
	RRA	REO	RIO	RLES	RTES	RMULT	RLD	RQL	LRA	LEO	LIO	LLES	LTES	LMULT	LLD	LQL
Experimental	3.0	4.7	4.3	0.0	2.2	0.1	0.4	0.4	4.8	14.6	11.1	5.8	8.9	2.6	2.1	2.6
InterForce (with stability)	1.3	5.3	2.9	0.0	0.0	3.4	0.0	0.4	2.9	11.4	11.7	0.6	1.0	5.6	2.3	11.5
InterForce (without stability)	2.6	6.6	2.1	0.0	0.0	1.9	0.0	0.4	4.1	10.0	9.5	1.1	0.0	6.3	4.8	14.2
SumCubed (with stability)	0.0	0.0	0.0	0.0	0.0	0.0	0.0	0.0	2.6	7.1	8.8	2.4	0.8	0.0	1.5	9.3
SumCubed (without stability)	0.9	0.0	0.0	0.0	0.0	0.0	0.0	0.0	3.6	6.8	7.6	2.3	1.1	0.0	3.3	9.5

**Table 14.** Standard errors for the RMS errors between model predicted and experimentally determined muscle forces for the Lateral Bend Moment conditions.

Condition	Muscle															
	RRA	REO	RIO	RLES	RTES	RMULT	RLD	RQL	LRA	LEO	LIO	LLES	LTES	LMULT	LLD	LQL
InterForce (with stability)	4.0	3.7	10.9	0.6	9.7	1.6	1.7	1.3	3.8	9.4	3.4	10.9	13.8	5.2	3.0	5.6
InterForce (without stability)	3.0	4.5	12.5	0.6	9.7	2.5	1.7	1.5	2.5	10.4	7.4	10.2	14.1	6.0	3.6	6.8
SumCubed (with stability)	5.0	8.8	15.7	0.6	9.7	0.7	1.7	0.9	3.9	10.5	8.5	9.6	13.9	6.2	3.9	6.1
SumCubed (without stability)	4.5	8.8	15.7	0.6	9.7	0.7	1.7	0.9	3.3	10.6	9.8	9.8	13.8	6.2	2.9	6.2

## VITA AUCTORIS

NAME: Stephen H. M. Brown

PLACE OF BIRTH: Windsor, Ontario

YEAR OF BIRTH: 1978

EDUCATION: F. J. Brennan High School, Windsor  
1991-1996

University of Windsor, Windsor, Ontario  
1996-2000 B.H.K. (Honours Movement Science)

University of Windsor, Windsor, Ontario  
2000-2003 M.H.K.